DARK MATTER DISTRIBUTIONS IN THE CENTRAL REGION OF LATE TYPE NGC3256 AND NGC4321 GALAXIES

ISRAA ABDULQASIM MOHAMMED ALI

FACULTY OF SCIENCE
UNIVERSITY OF MALAYA
KUALA LUMPUR

2018

DARK MATTER DISTRIBUTIONS IN THE CENTRAL REGION OF LATE TYPE NGC3256 AND NGC4321 GALAXIES

ISRAA ABDULQASIM MOHAMMED ALI

THESIS SUBMITTED IN FULFILMENT OF THE REQUIREMENTS FOR THE DEGREE OF DOCTOR OF PHILOSOPHY

DEPARTMENT OF PHYSICS
FACULTY OF SCIENCE
UNIVERSITY OF MALAYA
KUALA LUMPUR

2018

UNIVERSITY OF MALAYA

ORIGINAL LITERARY WORK DECLARATION

Name of Candidate: **ISRAA ABDULQASIM MOHAMMED ALI**

Matric No.: **SHC130106**

Name of Degree: **DOCTOR OF PHILOSOPHY**

Title of Project Paper/Research Report/Dissertation/Thesis ("this Work"):

DARK MATTER DISTRIBUTIONS IN THE CENTRAL REGION OF LATE TYPE NGC3256 AND NGC4321 GALAXIES

Field of Study: **RADIO ASTRONOMY**

I do solemnly and sincerely declare that:

(1) I am the sole author/writer of this Work;
(2) This Work is original;
(3) Any use of any work in which copyright exists was done by way of fair dealing and for permitted purposes and any excerpt or extract from, or reference to or reproduction of any copyright work has been disclosed expressly and sufficiently and the title of the Work and its authorship have been acknowledged in this Work;
(4) I do not have any actual knowledge nor do I ought reasonably to know that the making of this work constitutes an infringement of any copyright work;
(5) I hereby assign all and every rights in the copyright to this Work to the University of Malaya ("UM"), who henceforth shall be owner of the copyright in this Work and that any reproduction or use in any form or by any means whatsoever is prohibited without the written consent of UM having been first had and obtained;
(6) I am fully aware that if in the course of making this Work I have infringed any copyright whether intentionally or otherwise, I may be subject to legal action or any other action as may be determined by UM.

Candidate's Signature Date:

Subscribed and solemnly declared before,

Witness's Signature Date:

Name:
Designation:

DARK MATTER DISTRIBUTIONS IN THE CENTRAL REGION OF LATE TYPE NGC3256 AND NGC4321 GALAXIES

ABSTRACT

The distribution of the unseen matter (also known as the dark matter) in the galaxies defines their formation, evolution and dynamics. The mass distribution of a few galaxies is studied using the CO observations of Atacama Large Millimeter/sub-millimeter Array (ALMA) and the near Infrared (near-IR) data of the Two Micron All Sky Survey (2MASS). The dark matter has been investigated for the late type galaxies and active galaxies. Results indicate a vast amount of invisible dynamical mass ($10^9 M_\odot$) in the central region of the galaxy, which cannot be explained by the molecular and stellar masses within this region. The expected mass of the supermassive black hole (SMBH) in the galaxy is much smaller than its dynamical mass and it is inferred from the SMBH-bulge relation and other suitable ways. The mass of the SMBH cannot significantly contribute to the dynamical mass. The invisible mass is likely caused by dark matter, which might have a cuspy dark matter profile. In addition to the dark matter investigation in this thesis, the alternative of the dark matter (i.e.Modified Newtonian Dynamics (MOND)) is also looked into. The latter could not explain the dark matter because of the relative strong acceleration in the central region of galaxies. This study might also thus pose a challenge to the MOND models.

Keywords: Cosmology, dark matter, galaxies.

TABURAN JIRIM GELAP DI KAWASAN PUSAT GALAKSI NGC3256 DAN NGC4321

ABSTRAK

Taburan jirim ghaib (atau lebih dikenali sebagai jirim gelap) dalam galaksi memberi takrifan kepada pembentukan, evolusi dan pergerakan galaksi tersebut. Taburan jisim dalam galaksi aktif dikaji dengan menggunakan data cerapan radio dari Atacama Large millimeter/sub-milimter Array dan data Inframerah jarak dekat (near-IR) dari Two Micron All Sky Survey (2MASS). Jirim gelap dalam galaksi spiral berkategori 'late type' dikaji dalam tesis ini. Hasil kajian menunjukkan jumlah jisim ghaib berdinamik yang besar ($10^9 M_\odot$) di kawasan tengah galaksi, yang tidak boleh dirungkaikan dengan jisim gas dan bintang di kawasan tersebut. Jangkaan jisim bagi lohong hitam berjisim besar (SMBH) dalam galaksi ini ialah amat kecil apabila dibanding dengan jisim dinamiknya dan ianya dianggar berdasarkan hubungan 'SMBH-bulge' dan kaedah lain yang bersesuaian dalam penganggaran SMBH. Jisim SMBH ini tidak menyumbang secara sinifikan kepada jisim berdinamik. Jisim ghaib ini berkemungkinan besar adalah daripada jirim gelap, yang mungkin mempunyai profil 'cuspy'. Selain daripada kajian kami mengenai jirim gelap, alternatif seperti 'Modified Newtanian Dynamics (MOND)' turut dikaji. Namun, MOND didapati tidak mampu menerangkan jirim gelap kerana pecutan yaug agak kuat di kawasan tengah galaksi. Kajian ini berkemungkinan memberi cabaran kepada model MOND.

Kata kunci: Kosmologi, jirim gelap, galaksi.

ACKNOWLEDGEMENTS

In the Name of Allah, the Beneficent, the Merciful.

First and foremost, thanks to Allah who has given me this opportunity, the strengths as well as enabling me to complete this thesis writing after all the difficulties and challenges. My deepest thanks to the head of the Department of Physics, the academic staff at the Faculty of Science, University of Malaya for their encouragement and especially my supervisors Assoc. Prof. Dr. Zamri Zainal Abidin and Prof. Hwang Chrong-Yuan. I would also like to thank the entire ALMA staff for their help in the data reduction of NGC 3256 and NGC 4321. This work makes use of the following ALMA data: ADS/JAO.ALMA #2011.0.00525.S. ALMA and ADS/JAO.ALMAA# 2011.0.00004.SV. ALMA. ALMA is a partnership of ESO (representing its member states), NSF (USA) and NINS (Japan), together with NRC (Canada), NSC and ASIAA (Taiwan), and KASI (Republic of Korea), in cooperation with the Republic of Chile. The Joint ALMA Observatory is operated by ESO, AUI/NRAO and NAOJ. I am particularly grateful to all my friends at the Radio Cosmology Research Lab for their support, friendship, and physics discussions. I thank Norsiah, Kiew, Abbas, Danial and Dr. Chrisphin Karthick for their worthy contributions. I would also like to thank Prof. Zainol Abidin Ibrahim for being a great mentor. I thank all my colleagues in UM. I also warmly reach out to all my friends from Malaysia. Last but not least, I offer my thanks to my family for their support and encouragement through my entire life. I know even if I wrote thousands and thousands of pages trying to thank them. All that I am, and all that I will ever be, I owe to them.

Israa Abdulqasim Mohammed Ali

KL-02:10 am, 16/07/2017

TABLE OF CONTENTS

LIST OF FIGURES

LIST OF TABLES

LIST OF SYMBOLS AND ABBREVIATIONS

M_{gas}	:	gas mass.
ΛCDM	:	ΛCold Dark Matter.
χ^2_{red}	:	reduced χ^2.
$\mathrm{M_{HI}}$	:	neutral hydrogen mass.
M_*	:	stellar mass.
$\mathrm{M_{dyn}}$	:	dynamical mass.
$\mathrm{X_{CO}}$	:	CO-to-H_2 conversion factor.
v_{obs}	:	observed radial velocity.
v_r	:	radial component of the rotation velocity on the line of sight.
2MASS	:	Two Micron All Sky Survey.
ACA	:	Compact Array.
ACS	:	Advanced Camera for Surveys.
AGN	:	active galactic nuclei.
AIPS	:	Astronomical Image Processing System.
ALMA	:	Atacama Large Millimeter/sub-millimeter Array.
ASIAA	:	Academia Sinica Institute of Astronomy and Astrophysics.
ASTRON	:	Netherlands Institute for Radio Astronomy.
CASA	:	Common Astronomy Software Applications.
CASS	:	CSIRO division for Astronomy and Space Science.
CMB	:	Cosmic Microwave Background.
CO	:	Carbon monoxide.
Dec.	:	Declination.
ESO	:	European Southern Observatory.
HDM	:	hot dark matter.

HI	:	neutral hydrogen.
HLIRGs	:	Hyper-LIRGs.
HST	:	Hubble Space Telescope.
IR	:	Infrared.
IRAC	:	Infrared Array Camera.
IRAF	:	Image Reduction and Analysis Facility.
IRAS	:	Infrared Astronomical Satellite.
IRS	:	Infrared Spectrograph.
ISM	:	interstellar medium.
LIRGs	:	Luminous Infrared Galaxies.
M/L	:	mass-to-light ratio.
M31	:	Andromeda galaxy.
M33	:	Triangulum galaxy.
MACHO	:	Massive Astrophysical Compact Halo Object.
MIPS	:	Multiband Imaging Photometer for Spitzer.
MOND	:	Modified Newtonian Dynamics.
NAOJ	:	National Astronomical Observatory of Japan.
NED	:	NASA/IPAC Extragalactic Database.
NFW	:	Navarro-Frenk-White.
NIR	:	near-infrared.
NRAO	:	National Radio Astronomical Observatory.
OrCA	:	Origins in Cosmology and Astrophysics.
OVVs	:	optically-violent variable.
PA	:	position angle.
PV	:	Position-Velocity.
Quasars	:	Quasi-stellar radio sources.
R.A.	:	Right Ascension.

SI	:	International System.
SMA	:	Submillimeter Array.
SMBH	:	supermassive black hole.
TPA	:	Total Power Array.
ULIRGs	:	Ultra LIRGs.
VLA	:	Very Large Array.
WDM	:	warm dark matter.
WFPC2	:	Wide Field and Planetary Camera 2.
WIMPs	:	Weakly Interacting Massive Particles.
WMAP	:	Wilkinson Microwave Anisotropy Probe.
XSC	:	2MASS All-Sky Extended Source Catalog.

LIST OF APPENDICES

CHAPTER 1: INTRODUCTION

1.1 Background

The understanding of dark matter is one of the most important problems in modern physics. It is known that excess gravity is caused by invisible matter. The first to suggest the existence of dark matter was Dutch astronomer Jan Oort in 1932. He studied the motion of the stars in the Milky Way galaxy and found that the stars were moving much faster than expected (Oort, 1932).

In standard ΛCold Dark Matter (ΛCDM) cosmology, about 84% of the mass of the Universe is made up of dark matter, which dominates gravitational evolution on large scales (Cattaneo et al., 2014). Dark matter plays a crucial role not only to explain the dynamics of stars and galaxies, but also the origin and formation of large-scale structures and the temperature anisotropies of the Cosmic Microwave Background (CMB). Dark matter does not emit radiation in the electromagnetic spectrum. It is completely invisible, and it also does not emit, absorb or reflect light on any frequency. In fact, it does not interact with ordinary matter at all, and hence it is very difficult to detect. Different expainations of missing mass (also known as dark matter or unseen matter) have been studied, and they have reached the same conclusion: that the mass of all those galaxies is larger than that of the visible mass (Oort, 1932; Zwicky, 1933; Rubin & Ford, 1970).

The nature of the basic constituents of dark matter is still unknown, and currently remains one of the greatest mysteries in science. There are various hypotheses with regard to the nature of the dark matter particles. Basically, dark matter can be described in terms of a quantum field theory. However, the types of matter can be divided into two categories: baryonic and non-baryonic forms. The baryonic matter covers the Massive Astrophysical Compact Halo Object (MACHO) which includes black holes or neutron stars as well as brown dwarfs and unassociated planets. Faint stars (white dwarfs and very faint red dwarfs) have also been proposed as MACHO candidates. This term was first used by the astrophysicist Kim Griest. Meanwhile, non-baryonic (elementary particles) dark matter can be divided into three classes: hot dark matter (HDM), warm dark matter (WDM) and cold dark matter (CDM). The mean velocities of the particles at the time they decoupled from the thermal bath determine the category they belong to (Primack & Gross, 2001).

The usual suspects for non-baryonic dark matter include Weakly Interacting Massive Particles (WIMPs). They are somewhat like neutrinos, but are much heavier with mass 10 GeV to 1000 GeV. This is predicted in supersymmetric theories, so they are a form of CDM (Dodelson et al., 1996). The second attractive possibility is that it behaves like cold dark matter: an axion of mass 10^{-6} eV to 10^{-4} eV, which is needed to solve a small problem in the standard model of particle physics. The third interesting possibility is that one of the three neutrino species has a mass between 5 eV and 30 eV. Neutrinos move very fast and are referred to as hot dark matter. Candidates in between hot and cold are called warm dark matter.

The interest in measuring the rotation curves of spiral galaxies is that they give a direct measure of the radial distribution of the total gravitating mass. In the early 1970s, Vera Rubin and her collaborators found that most of the rotation curve data for spiral galaxies came from optical observations which did not extend beyond the luminous inner regions (Rubin et al., 1980). At that time, the optical observations seemed consistent with the distribution of luminous matter. With the availability of radio observations like the Westerbork Radio Synthesis Telescope in the Netherlands, it finally became possible to measure the distribution and dynamics of neutral hydrogen (HI) in spiral galaxies (e.g., Bosma (1981a)). It was soon found that the HI in many spirals extended far beyond the starlight, and that HI rotation curves in such galaxies often showed nearly constant rotational velocity out to the radial limits of the data.

As dark matter particles have not yet been observed, the existence of dark matter remains theoretical. Alternative gravity theories, such as Modified Newtonian Dynamics (MOND), claim to explain the observed gravitational fields without resorting to any mysterious dark matter. In these alternative theories, gravity behaves differently on cosmological distance scales from smaller distances. If Einstein's Theory of Gravity is incomplete, then there might be no missing matter, only ordinary matter that gives rise to gravitational fields that look different from what we expect.

In this thesis, we try to estimate the mass distributions of NGC 3256 and NGC 4321 using data from the Atacama Large Millimeter and sub-millimeter Array (ALMA) and the Two Micron All Sky Survey (2MASS). On the other hand, this study also attempts to test the MOND framework, the alternative to the dark matter. Our focus will be looking into how well MOND is able to explain the mass discrepancy in the central regions of galaxies. In the next subsection, we will touch on dark matter, evidence for dark matter, galaxies, starburst galaxies, active galactic nuclei, luminous infrared galaxies and molecules in Astronomy.

1.2 Dark Matter

The cosmological principle in modern physical cosmology is the notion that the distribution of matter in the universe is homogeneous and isotropic (Bennett et al., 2014). From the Wilkinson Microwave Anisotropy Probe (WMAP) mission of microwave background observation, the universe is flat, $\Omega = 1 = \Omega_M + \Omega_\Lambda$, where Ω_Λ is the contribution of vacuum energy (Ellis, 2003). From there it follows that the mean energy density in the universe is equal to the critical density (within a 0.5% margin of error). This is equivalent to a mass density of 9.9×10^{-30} g/cm^3, which is equivalent to only 5.9 protons per cubic meter. The age of the Universe is estimated to be 13.5 Gyr. The Hubble constant that

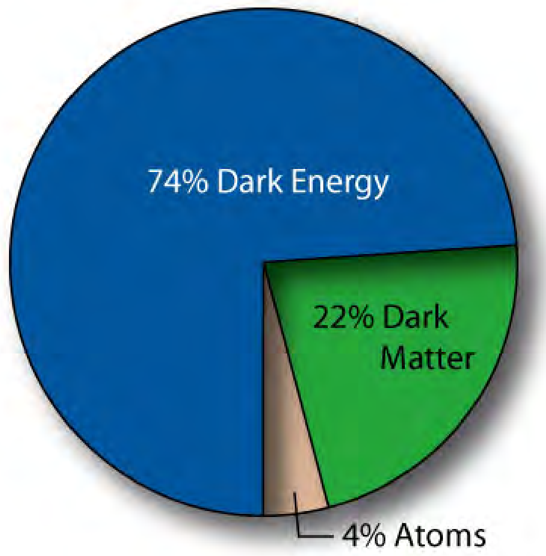

Figure 1.1: The composition of the Universe by the WMAP data.

gives the rate of expansion is about 72 km s^{-1} Mpc^{-1}. From the latest astrophysical measurements we know that the Universe consists of 4% Baryons, 22% Cold Dark Matter, and 74% Dark Energy; see Figure 1.1. The WMAP data shows that its contents include 4% atoms, the building blocks of stars and planets. Dark matter comprises 22% of the universe. 74% of the universe is composed of dark energy that acts as a sort of anti-gravity. This energy, distinct from dark matter, is responsible for the present-day acceleration of universal expansion.

The value for Ω_M has slightly changed from the first year results from WMAP observations to the third year WMAP data, i.e., Ω_M from 0.29 ± 0.07 to 0.234 ± 0.035(Reiprich, 2006). It turns out that dark matter plays an important role in structures on a wide range of scales ranging from faint satellite galaxies to the largest known structures of the Universe. Dark matter however, also presents a veritable problem for particle physics.

1.2.1 Evidence for Dark Matter

There is much evidence for the existence of dark matter, although it has not been directly detected. A main evidence for dark matter (matter with a much larger mass-to-light

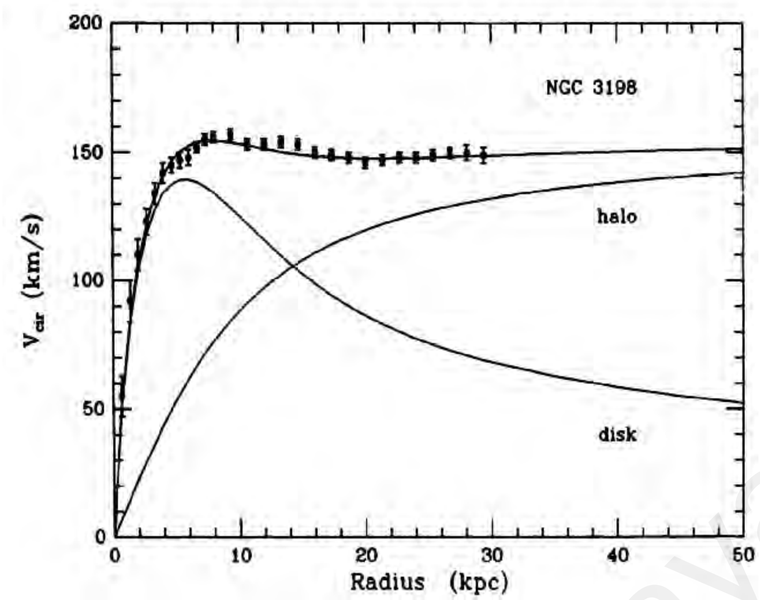

Figure 1.2: Roation Curve of NGC 3198. The points indicate the observed rotation curve. The solid curves are the contribution from disk and gas. This figure is taken from Origins in Cosmology and Astrophysics (OrCA).

ratio (M/L) than usual) comes from measuring the rotation curves of galaxies, that is the variation of rotational velocity of stars with distance (R) from the galactic centre. On the other hand, most of the luminous mass of spiral galaxies is found to be concentrated in the central bulge. According to the Newtonian gravity, the rotational velocity of stars should increase up to a certain radius R_{lum} that contains most of the luminous matter, and drop off as the square root of 1/R in the outer parts. For example, there was a flattening in the rotation curve of Andromeda galaxy (M31) beyond R_{lum} (Rubin & Ford, 1970). This implies that this galaxy (M31) contains mass with a distribution different from the distribution of luminous matter. In Figure 1.2, experimental data can be seen from the galaxy NGC3198 with a fitted curve which does not decrease with the distance but is instead constant. This is the discrepancy which is solved by postulating the existence of dark matter.

Another important observational evidence of dark matter comes from studying a distant system, e.g., a galaxy cluster. One way to estimate the mass of a galaxy cluster is through an effect called "gravitational lensing" (Bartelmann & Schneider, 2001). This makes use of the bending of light from a massive object like a quasar, by the gravitational potential in between the source and the observer, as given by Einstein's Theory of General Relativity. In this method, the distortion of light can give the total mass of the cluster by measuring the distortion of light. Many clusters have been subjected to this method and it is estimated that a large fraction of the mass of the clusters is composed of dark matter. The left panel of Figure 1.3 shows the Hubble Space Telescope (HST) image of the galaxy cluster Abell 1689. The gravitational lensing effects are shown by the lensing arcs in the image. The estimated dark matter distribution is shown in blue.

One direct observational evidence for dark matter comes from the Bullet Cluster, comprising of two clusters of galaxies passing through each other (Harvey et al., 2015). When two galaxy clusters pass each other, their visible matter collides and slow down. On the other hand, the dark matter components of the two clusters pass each other without interacting nor do they slow down. A separation occurs between the dark matter and ordinary matter components. This separation was detected by comparing the X-ray images of the luminous matter taken with the Chandra X-ray Observatory with measurements of the cluster's total mass from gravitational lensing observations. In this case, it is possible to determine the locations of both the dark and luminous matter. Finding indicate that that two large clumps of dark matter were moving away from the center of collision at high speeds, while the two smaller clumps of ordinary luminous matter were moving at slower speeds behind them (see the right panel of Figure 1.3)

1.3 Galaxies

Galaxies are generally defined as baryonic condensates in dark matter potential troughs and have been recognized since 1920. Galaxies are huge assemblies of stars, dust and gas which are held together only by their mutual gravitational attraction. The galaxy in which

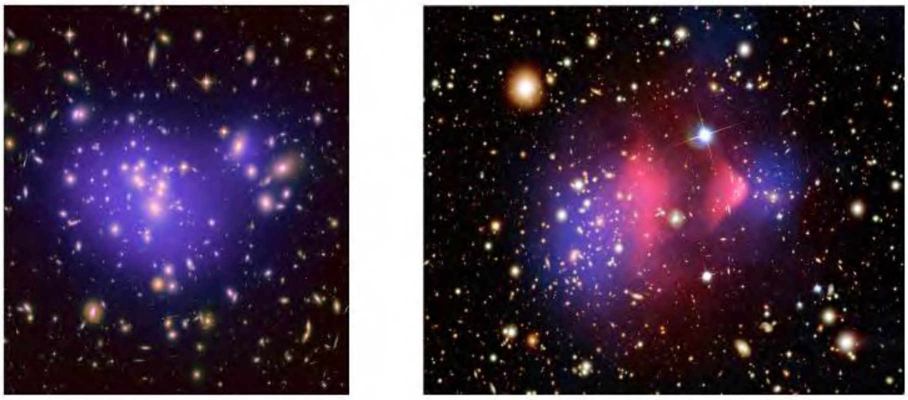

Figure 1.3: Left: HST image of Abell 1689. The existence of dark matter can be inferred from its gravitational effects. Right: Separation of dark matter (see blue color) from luminous matter (red) in the Bullet Cluster.

we reside, the Milky Way Galaxy, is host to about 10^{11} stars. The observed motion of stars, in our and other spiral galaxies, does not slow down, as expected in accordance with Keplerian behaviour ($v \propto 1/\sqrt{R}$) at larger radial distances, and implies the presence of a larger body of mass. We infer from these so-called rotation curve measurements that our Galaxy consists of 10 times more matter, i.e., the so called dark matter (Schneider, 2014).

The number of stars in a galaxy can range from several million in a dwarf elliptical, to over a trillion stars in a massive elliptical, with varying amounts of gas, dust and dark matter. Also, galaxies have varying ranges of luminosities and masses, from 3×10^5 $L_\odot$ and 10^7 $M_\odot$ for a dwarf galaxy to 10^{12} $L_\odot$ and 10^{12} $M_\odot$ for the supergiant galaxy correspondingly.

Hubble's scheme of classification of galaxies (Hubble, 1926, 1936) was the first step to understanding the nature of galaxies based on morphology. Galaxies are morphologically classified, in agreement with the Hubble sequence, as ellipticals, lenticular, spirals and irregulars (Figure 1.4). This sequence was originally conceived as an evolutionary sequence in which elliptical galaxies (early types) evolved into spiral galaxies (late types). In this study we are using only spiral galaxies, although other types of galaxies will be mentioned.

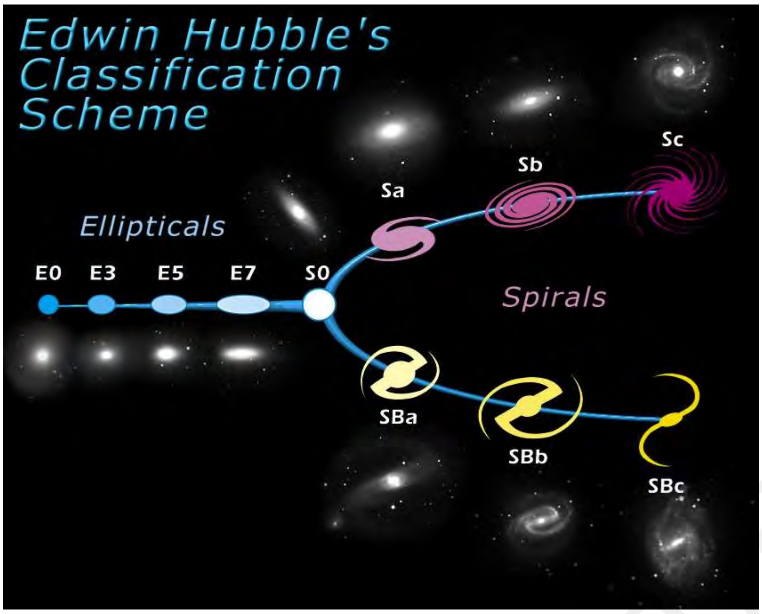

Figure 1.4: The galaxy classification scheme by Edwin Hubble. Image Credit: Space Telescope Science Institute.

- Spiral Galaxies. Most of the observed galaxies have a spiral structure. Spirals come in two types: normal and barred. For a normal type, spiral arms start from the nuclear bulge. A barred spiral has its arms appear at the end of a bar crossing the nucleus itself. Within these two groups several subtypes can be distinguished according to their overall shape: Sa, Sb, Sc for normal spirals and SBa, SBb, SBc for barred spirals, although intermediate types also exist (Hubble, 1926). Spiral galaxies are characterised by a flattened disk of stars, gas and dust, in which the most recent star formation occurs in the arms extending outwards from a densely-packed central concentration of stars, also known as the bulge (Sandage & Bedke, 1994). Most of the stars in the spiral arms are young. There are also objects such interstellar clouds, concentrated near the plane of symmetry of the galaxy. Spiral galaxies contain a larger fraction of young blue (hot) stars, and have relatively high star formation rates (Drexler, 2006) because of proportionally larger amounts of available gas. Recently, the study of the structure of spiral galaxies has become one of the essential astronomical advances for understanding the universe. One of the more accepted theories today argues that the spiral arms in these galaxies are "density waves", in the sense that the individual stars in the spiral arms are not fixed in position.

- Elliptical Galaxies. Elliptical galaxies are spherical or ellipsoidal stellar systems consisting almost entirely of old stars. Their gas reservoir from which new stars can be formed is getting exhausted leading to a low star formation rate (Singh, 2015). A larg elliptical contains many globular clusters. In all these respects, ellipticals resemble the nucleus and stellar halo components of spiral galaxies. Elliptical galaxies are denoted as En, where n is a number ranging from 0 to 7. For an elliptical galaxy with observed axial ratio b/a (a is the semi-major axis, and b is the semi-minor axis), n = 10 (1-b/a). Thus, circular elliptical galaxies are denoted E0, and ellipticals with highly elongated forms are E7 (Schneider, 2014). In contrast to spirals, ellipticals have a low angular momentum and high velocity dispersion (Kent, 1990). Their light distribution is rather smooth and featureless and their typically larger mass and size as well as their spherical or ellipsoidal shape bear witness to a history of interactions and mergers with other galaxies.

- Lenticular Galaxies. The S0 galaxies or lenticular galaxies are in between ellipticals and spirals in terms of morphology. Like spirals they have a central bulge surrounded by a flat disc but no spiral arms (Schneider, 2014). They form a transitional type between ellipticals and spirals. They lack extensive gas and dust, and often found in regions of space that are fairly densely populated with galaxies (like ellipticals). They also have a thin and fast-rotating stellar disc in addition to the central elliptical bulge (like spirals), although the disc lacks any spiral arms or extensive dust lanes (Kalinova Dimitrova, 2014).

- Irregular Galaxies. These galaxies do not fit well into the standard classification of spirals, lenticulars, or ellipticals. They have amorphous shape without any kind of symmetry. In comparison to spirals or ellipticals, they are less luminous with less well defined spiral structure. These galaxies are extremely gas-rich, with interstellar gas masses could be above 30% of their stellar masses. The circular speeds of Irregular galaxies are linear functions of their radii with maximum speeds of around 50 – 70 km s^{-1} near the edge of the disc. This rotation profile is very different from those of spirals, where the circular velocity is nearly flat and much higher (300 – 400 km s^{-1})(Binney & Tremaine, 1998).

1.3.1 Starburst Galaxies

Starburst galaxies are galaxies that are observed to be forming stars at an unusually fast rate (about 10^3 times greater than in a normal galaxy). Generally, a starburst galaxy maintains a high rate of star formation for 10^8 – 10^9 years (Carroll & Ostlie, 2007). Although the mechanism is still poorly understood, it is thought that most starburst galaxies generally are in a state of interacting or merging with one another, one of the most famous examples being the Antennae galaxies, see Figure 1.5, or, due to the presence of a galactic bar, there is an accumulation of substantial amounts of gas and dust in the central regions of the galaxy (Martig & Bournaud, 2008). On the other hand, a study by Bergvall et al. (2003) showed that interaction or merger might be a necessary criterion for creating a starburst galaxy, but definitely not a sufficient criterion. Most studies found only a modest increase of star formation in the interacting galaxies.

Starburst galaxies emit copious amounts of ultraviolet radiation which are absorbed by the surrounding dust, and re-radiated at infrared wavelengths, making starburst galaxies among the most luminous infrared objects in the Universe .

Figure 1.5: The Antennae Galaxies from the NASA/ESA HST. Hubble has released images of these stunning galaxies twice before, once using observations from its Wide Field and Planetary Camera 2 (WFPC2) in 1997, and again in 2006 from the Advanced Camera for Surveys (ACS).

1.3.2 Active Galactic Nuclei

At the centres of active galaxies are active galactic nuclei (AGN). It is from these that huge amounts of energy, detected by astronomers, are emitted. It is accepted now that their activity comes from gas in the galaxy being pulled onto a supermassive black hole at the galaxy's centre. Some feed from an "accretion disk", first formulated by von Weizsäcker (1948), which is formed from hot material orbiting close to the black hole, usually consisting of dust and gas ripped from the interstellar medium (ISM) and from nearby stars. The material loses angular momentum and falls into the black hole through processes such as disk viscosity, outflows and magnetic field effects (Shakura & Sunyaev, 1973; Xie & Yuan, 2008; Gan et al., 2009). The gravitational potential energy of the material which is falling onto the black hole is converted into kinetic energy. This in turn causes particles in the infalling material to collide and head up through friction, thus converting kinetic into thermal energy. The huge amount of heat this produces causes the intense radiation.

AGNs can outshine their host galaxies by several orders of magnitude. They are among the brightest objects in the universe in one or more wavebands. Whether a galaxy hosts an AGN or not is typically determined by the properties of its spectrum, such as the existence of strong radio emission, or the luminosity of its nucleus (Schneider, 2014).

The emission of active galaxies commonly covers all wavelengths, such as the nuclear optical continuum and infrared emission, broad and narrow optical emission lines, radio and X-ray continuum emission, and X-ray line emission. There are many different kinds of active galaxies: Seyfert Is and IIs, LINERs, radio galaxies, quasars, and blazars.

- Seyfert galaxies. This is the first distinct class of AGN identified (Seyfert, 1943). They can be divided into two forms, Seyfert Is and Seyfert IIs, depending on their viewing angle (Khachikian & Weedman, 1974). Seyfert Is show both broad and narrow emission lines, in a manner similar to quasars, while all the emission lines in Seyfert IIs are narrow. Seyfert Is are also more likely to have X-ray emission from the nucleus while Seyfert IIs oftentimes absorb the X-ray in their high column density tori. In both cases the galaxy has a bright, dominant nucleus. It is the optical spectrum of this nucleus that determines the difference between the two forms. The host galaxy of Seyfert-type AGNs are typically spirals.

- Quasi-stellar radio sources (Quasars). About 10% of quasars are radio-loud. These are the most luminous AGNs, and are typically very distant. Their optical luminosities are greater than that of their host galaxy. Quasars show strong optical continuum emission, broad and narrow emission lines, and strong X-ray emission, together with nuclear and often extended radio emission.

- Radio-quiet quasars/QSOs. These are very similar to Seyfert I galaxies but are more luminous. They can be hosted by spirals, irregulars or ellipticals. There exists a host-mass quasar-bulge correlation (Macchetto, 2000), which is why the most luminous quasars inhabit the most massive ellipticals. They show strong optical continuum emission, X-ray continuum emission, and broad and narrow optical emission lines (Shapley, 1943).

- Radio galaxies. Mostly hosted by (giant) ellipticals, these galaxies have luminosities up to 10^{47}ergs^{-1}. They show nuclear and extended radio emission and have rather heterogeneous AGN properties, but there are no strong narrow or broad emission lines (Anderson, 2015). However existing emission lines may be excited by a different mechanism. Objects with high excitation (narrow-line radio galaxies) have emission line spectra similar to those of Seyfert IIs.

- Blazars. They are among the brightest, most energetic and bizarre objects in the universe. They are divided into two types: BL Lacertae object (BL Lac, firstly detected by Cuno Hoffmeister in 1929), and an optically-violent variable (OVVs). In the unified AGN picture (Urry & Padovani, 1995), the line-of-sight to these objects is aligned to their relativistic jet. The very similar OVVs are highly variable quasars. Their visible light output can change by 50% in a day. As opposed to BL Lacs, OVVs have stronger broad emission lines.

- LINERs. Galaxies with a low-ionisation nuclear emission line region (LINERs) (Anderson, 2015) have historically been added to the AGN family. The continuum emission of LINER nuclei is weaker, but they have strong low-ionisation emission lines. LINER galaxies are very common. About one third of the galaxies in the local universe are LINERs. Most spiral galaxies show weak LINER activity. It is not

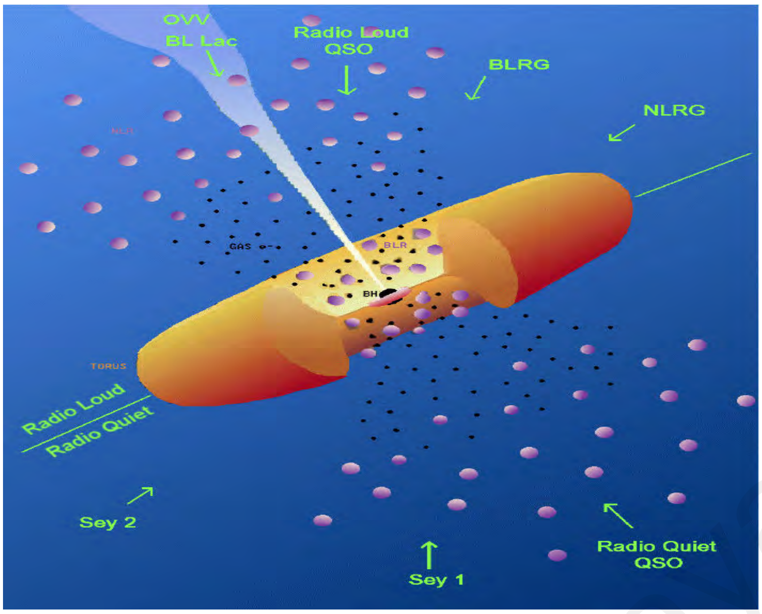

Figure 1.6: The unified picture of AGNs. This schematic shows the different types of AGN classifications.

clear in all cases if the observed emission originates from the nucleus of the galaxy or if it is associated with other emission regions, such as starburst emission.

As with the starburst galaxies, many of the AGN galaxies have companion galaxies with which they interact. For example, these companions might supply the central black hole with fuel to power the AGN (Carroll & Ostlie, 2007). Figure 1.6 shows a unified illustration of all AGN species.

1.3.3 Luminous Infrared Galaxies

In the local universe, galaxies with an infrared luminosity > 10^{11} $L_{\odot}$, are called Luminous Infrared Galaxies (LIRGs). Beyond the LIRGs are the Ultra LIRGs (ULIRGs) with infrared luminosities above 10^{12} $L_{\odot}$, and the Hyper-LIRGs (HLIRGs) above 10^{13} $L_{\odot}$. Both LIRGs and ULIRGs will be collectively referred to as U(LIRGs). Luminous Infrared Galaxies play an important role in the star formation history of the Universe.

These galaxies' bolometric emission is strongly dominated by their infrared components (Sanders & Mirabel, 1996). This does not indicate that the strong IR luminosity is powered by an AGN or a starburst event. Some research has been proposed U(LIRGs) as a third possible classification of an active galaxy, along with starburst and AGN (Condon et al., 1991; Borne et al., 1999). The studies of Sanders et al. (1988) and Kim et al. (1995) provide evidence that the fraction of AGNs increases with the luminosity of the host galaxy. Studies of U(LIRGs) in the local universe have found that a large fraction are merging and interacting systems (e.g., (Kim et al., 2002)).

In most cases, the energy source of the strong IR radiation is unknown. However, (U)LIRG might be useful at least as an interim classification, until more data can be accumulated.

1.4 Molecules in Astronomy

Molecules are an important aspect of our universe. The most abundant molecule in the universe is molecular hydrogen, H_2 (Fraser et al., 2002). Since it has no dipole moment and no rotational transitions, molecular hydrogen cannot be detected by radio/mm spectroscopy. However, hot H_2 gas with $T \gtrsim 100$ K shows vibrational transitions in the IR spectrum.

In the interstellar medium, about 150 different molecules have been found in space, with most of them identified by their rotational and/or vibrational spectra. For this work, the molecule chosen is CO.

- Carbon monoxide (CO) is the molecule that is most easily detected in the mm-spectrum and the best tracer of molecular hydrogen, since it is the most abundant molecule with a weak dipole moment. It is the second most abundant molecule in the universe after H_2 (Mashian et al., 2013). H_2 is difficult to study directly, and therefore astronomers have used CO as a proxy for molecular hydrogen. It is thus used instead of H_2 to trace cold molecular gas, since the CO (1-0) transition is triggered mostly by collisions between CO and H_2. Many works have been done to determine the conversion factor between CO (1-0) intensity and H_2 density. A more extensive discussion of the use of CO as a tracer of H_2 can be found in Scoville and Sanders (1987).

1.5 Problem Statement

The nearby environments of spiral galaxies with starburst and active galactic nuclei will be examined in order to test the dark matter distribution. Many studies have been undertaken to address this question. Most of them were based on different radiation wavelengths (HI, Hα, etc), which each possess their own shortcomings for analysis in the outer region of galaxies, but there is no accurate study in the centre regions of galaxies. To accomplish this, CO lines will be the most appropriate tool to investigate the central kinematics of spiral galaxies, if the angular resolution is sufficiently high. CO molecular lines are useful to derive accurate rotation curves in the central regions of spiral galaxies, because of the high concentration in the center as well as for negligible extinction. The validity on dark matter is tested by considering the alternative solution known as MOND. It will be seen whether MOND can explain the dark matter distribution in the central regions of galaxies.

1.6 Scope and Objectives of the Research

The scope of this research covers the investigation of dark matter in the central regions of spiral galaxies, namely, NGC 3256 and NGC 4321. This type of galaxies is believed to be dark matter-dominated. The underlying theme of this thesis is mainly from six main objectives below:

1. To determine the projected rotation curves analysis for our sources. It is based on the position-velocity diagram using CO observations of the interferometer of radio telescope ALMA.

2. To determine the dynamical (total) mass. This is inferred from spiral galaxy rotation curves of NGC3256 and NGC4321.

3. To deduce the molecular gas mass using ALMA database. This is based on the integrated flux density and conversion factor.

4. To determine the stellar mass within the central regions of our samples using the near-infrared (NIR) data of 2MASS.

5. To estimate dust mass using the Infrared (IR) data of the Infrared Astronomical Satellite (IRAS) and Spitzer images.

6. To test the dark matter in these galaxies with MONDs framework.

   Throughout this thesis the common units of measurements used are the International System (SI) unit and non-SI units (Astronomical unit).

1.7 Thesis Organization

This thesis is the outcome of the several years of PhD work, combined with the scientific collaborations stated in our list of publications. In the first part of this thesis, we are studying the rotation curve of NGC 3256 from ALMA observations. In order to investigate the dark matter distribution in that galaxy, we proposed the following method: subtracting the other masses of that galaxy (gas mass, stellar mass, etc) from the total mass giving its dark matter mass. Then in the second part of this work, we used another data from ALMA for NGC 4321. The last part of this study is where we consider the alternative to dark matter, i.e. MOND.

The thesis is organized as follows.

- **Chapter 2** gives information on past studies and current knowledge pertaining to this study.

- **Chapter 3** gives the main method of estimating the mass of dark matter using radio and IR data.

- **Chapter 4** introduces the NGC 3256 and its properties. We estimated the projected rotation curve.We then obtained the total mass and other masses of the galaxy. We also presented the results from the MOND theory. It is found that there is a huge amount of invisible dynamical mass in the central region of the galaxy.

- In **Chapter 5** gives the projected rotation curve for another galaxy, i.e. NGC 4321. We calculate the gas mass of this galaxy from ALMA and VLA data. All derived masses in this chapter are obtained by using the same way as the previous chapter. We show that the invisible mass is likely caused by dark matter in the central region of the galaxy

- In **Chapter 6** we finally outline our conclusions and future works.

CHAPTER 2: LITERATURE REVIEW

2.1 Introduction

We are still confronting one of the biggest mysteries of the universe. It is generally accepted that the universe contains much more matter than what can be observed directly from their emission or absorption properties. It is well known that there has been no accurate study on the nature of dark matter. This chapter deals principally with the early studies of dark matter in Section 2.2, and the modern study in Section 2.3, from a minor observation to an intensive study of dark matter.

2.2 Early History of Dark Matter

The possibility of an invisible matter which interacts gravitationally but is not seen via electromagnetic radiation has been considered since 1915 at least. The name "dark matter" to denote invisible matter was coined by Jacobus Kapteyn in 1922 in his studies on the motion of stars in the Milky Way (Kapteyn, 1922). He found that the amount of dark matter in the Solar neighbourhood was small. His was the first attempt to derive the total density of matter in the Solar vicinity. In the same year, Jeans (1922) counted "about three dark stars in the universe for every bright star", while Trimble (1995) pointed out that this statement closely matches the range of dark matter density. A decade later, Jan Oort in 1932 concluded that the total local density of our galaxy disk from dynamical data could exceed the density of visible stellar populations by a factor of 2. This result meant that the amount of dark matter in the Solar vicinity should be approximately equal to the amount of visible matter (Oort, 1932). This was the first claim of evidence of dark matter.

The first clear discovery of dark matter was referred to as (Zwicky, 1933), who estimated the radial velocities of eight galaxies in the Coma cluster and found large velocities of (1019 ± 360) km s^{-1}, which was due to the luminous matter in the galaxies. A step further, Zwicky used the virial theorem to the Coma cluster to show that the observed total mass density was significantly much more than the expected mass density from the luminous matter. His conclusion was that some kind of unseen matter in the clusters was about ten to twenty times the mass of the gas and galaxies together. Although Zwicky's data was of low quality, Colless and Dunn (1996) showed that the core principle result of his result survives. Smith (1936) repeated the analysis for the nearby Virgo cluster. Once again, the radial velocities of 30 galaxies indicated an unexpectedly high mass.

The discrepancy between the high galaxy masses calculated from the virial mass of the clusters, and the low masses calculated from the very inner rotation curves for five galaxies, troubled Hubble (1936). "The discrepancy seems to be real and is important," he wrote. It is not surprising that these early absorption line rotation curves extended only over the brightest nuclear regions, and were poor indicators of galaxy mass. Several decades would pass before the cluster dark matter would be associated with the flat rotation curves derived for individual galaxies.

Six years after Zwicky's research, Babcock (1939) used long-slit spectra to measure the rotation of the Andromeda galaxy M31, which showed that the rotational velocity in the outer regions was higher than expected from the stellar mass, indicating either strong dust absorption or a high mass-to-light ratio in that region. Oort (1940) noted that "... the distribution of mass [in NGC 3115] appears to bear almost no relation to that of the light." His conclusion, "The strongly condensed luminous system appears embedded in a large more or less homogeneous mass of great density," was a clear statement of the puzzle that would grip astronomers again in the 1970s. However, it seemed to have impressed few in 1940 and in the decades following. A similar result was found for M31 by Roberts (1966) using the National Radio Astronomy Observatory large 300-foot telescope. He studied the rotation and surface brightness, and concluded that the local value of mass-to-luminosity could be estimated to be 250 at large radii.

There were two possibilities to interpret flat rotation curves of galaxies. The first was to define the observed rotation velocity with the circular velocity for a very high local M/L. For this case, it was suggested that in the outer regions of galaxies low-mass dwarf stars dominated (Oort, 1940). The second possibility was there existed non-circular motions which distorted the rotation velocity. From rotation velocities, masses of individual galaxies were used to investigate dark matter.

A quarter of a century later, Kahn and Woltjer (1959) compared the mass of the Local Group of galaxies, in which the Milky Way and the Andromeda galaxy were the dominating members, with that expected from the luminous matter in these two objects. They found that the mass of the Local Group contained an appreciable amount of dark matter. From a historical perspective, this was a contemporary formulation of Zwicky's virial cluster problem. Another earlier work on dark matter can be found in Karachentsev (1966). Ostriker (1999) had re-confirmed Zwicky's finding for the total mass.

2.3 Modern Study of Dark Matter Research

The eventual acceptance of a hypothesis of 'dark matter' is often understood as an example of the accumulation of unequivocal evidence: two results from different branches of astronomy: high velocity dispersions in clusters and flat rotation curves in galaxies. It indicated unexpectedly large galaxy masses, and only by the early 1970s had enough evidence been accumulated to accept the existence of a preponderance of yet-unobserved matter.

Radio astronomy had emerged as a major tool for exploring the galactic and extragalactic phenomena in 1970. Through the Westerbork Synthesis Radio Telescope, observations of the 21-cm line from HI traced the mass distribution of many spiral galaxies. HI-derived galaxy rotational curves extended to almost twice the optical radius of the galaxy and demonstrated flat profiles. However, radio observations demonstrated that the rotational evidence for dark matter grew stronger in M31. They also concluded that the mass-to-light ratio had to exceed 200 in the outer parts (e.g., Rubin et al. (1980); Roberts and Whitehurst (1975)). Freeman (1970) using 21-cm velocity maps pointed out that spiral galaxies NGC 300 and the Triangulum galaxy (M33) contained a large fraction of dark matter. A similar result for other large disk galaxies was found by Einasto et al. (1974). The majority of astronomers was convinced that dark matter existed, but did not constrain its spatial distribution. At the same time, Ostriker and Peebles (1973) proposed that galactic disks would be unstable because they might be surrounded by massive, spherical halo components. This dark halo extended beyond the visible disk and increased the mass-to-light ratio in the outer regions of the galaxies. Hence, dark matter had become a well-recognized concept. Many independent estimations of the rotation curve of galaxies in the outer parts of galaxies confirmed the presence of dark halos around galaxies (Rubin et al., 1978).

The nature of dark matter around galaxies was still not clear. The first suggestions of dark matter candidates were ionized gas (Field, 1972) in the baryonic category, which contributed most of the mass to the matter familiar to us from everyday life. Also considered were very faint, low-mass stars (Napier & Guthrie, 1975) and collapsed objects, like stellar black holes (Thorstensen & Partridge, 1975). On the other hand, Cowsik and McClelland (1973) seemed to have been the first to propose a non-baryonic particle, the neutrino, as a candidate for dark matter.

Extensive reviews of mass distributions have been done by Bosma (1981a, 1981b) from HI rotation curves of 25 galaxies. He found that most spiral galaxies stayed more or less flat out to the largest observed radius, which exceeded the optical radius of these objects. Bosma mentioned in his study that the M/L ratio had to increase with r, and that there still must be substantial amounts of mass at the last measured point of the rotation curve. Another evidence for dark matter was provided by spiral galaxies. The optical rotation curves of Sc, Sb and Sa galaxies extended to slightly less than the optical radius and suggested the existence of a significant non-luminous matter component beyond the optical galaxy (see Rubin et al. (1978); Rubin et al. (1980)). This work later led to a series of research on rotation curves which was contemporary, and HI data extended it even further. In the early 80s, when everybody thought that dark halos were necessary to explain the flatness of rotation curves, Dekel and Shlosman (1983) demonstrated that the optical rotation curves had no need for dark halos, a conclusion corroborated by many more optical rotation curves, e.g., Kent (1986); Athanassoula et al. (1987) as reported in Palunas and Williams (2000). As a rule, HI data extended at least twice as far as the "easy visible disk", and far enough to establish the discrepancy between the expected and the observed rotation curve, but optical (Hα) data usually did not extend far enough to reach this conclusion.

Modern simulations have suggested the universe is dominated by dark matter (Springel et al., 2005). Galactic evolution seems to be driven by the formation of the dark matter halos. For instance, gas in dark matter halo cools and condenses in the center of the halo, but the exact mechanism for the hierarchical assembling of the stellar masses is still undiscovered (White & Rees, 1978). The observed stellar mass is calculated from the luminosity of the galaxy times the value of the M/L ratio coming from stellar populations (Sánchez-Blázquez et al., 2007). The dynamical mass is constructed from the velocity and velocity dispersion fields of the galaxies. Then the remaining of the estimated stellar mass and the dynamical mass would give the dark matter mass.

The dark matter density profiles in the inner parts of galaxies are still controversial. In earlier studies, most researchers assumed constant density distribution 'cores' in the center of galaxies. However, CDM simulations of structure formation and galaxy evolution predicted that dark matter haloes had ‘cusp’ dark matter distributions with density increasing steeply at small radii, $\rho \propto r^{\alpha}$, from $\alpha \approx$ -1 to 1.5 (Navarro et al., 1997, 2004; De Blok & Bosma, 2002; De Naray et al., 2008), while some researchers have suggested that observed rotation curves of dwarf galaxies were flat central dark matter density profiles (cores) (Burkert, 1995; Borriello & Salucci, 2001; Gentile et al., 2004; Oh et al., 2008; Hashim et al., 2015; Oh et al., 2015). Others have suggested that the inconsistency might be due to systematic effects and that observed rotation curves were still consistent with central density cusps (Swaters et al., 2003). It may be necessary to reconsider our understanding in terms of the processes of galaxy formation and evolution and the nature of dark matter, if the discrepancies between the predicted and the observed rotation curves persist. An example that illustrates the disagreement between the dark matter models can be seen in Figure 2.1, from the work of Gentile et al. (2005). However, this issue is still controversial. Different studies find cusps and cores to be consistent with the data, depending on the method that is assumed (e.g., Breddels and Helmi (2013)).

Dark matter is still a complex problem. It is known to be the dominant component in the outer regions of galaxies and in galactic clusters. However, its behavior in the central part of galaxies is worth investigating. In the most recent study, dark matter in the inner region of the Milky Way was studied by (Iocco et al., 2015). They measured the motion of stars and gas, and compared the measured rotation curve with that expected using baryonic mass distribution. They argued that the observed rotation curve could be explained, and that large amounts of dark matter existed. According to previous studies, evidence for dark matter was compelling in dwarfs, spiral galaxies, galaxy clusters as well as at cosmological scales. However, detecting dark matter may be easier to do on the outer region of the Milky Way, although it has been historically difficult to pin down dark matter contribution to the

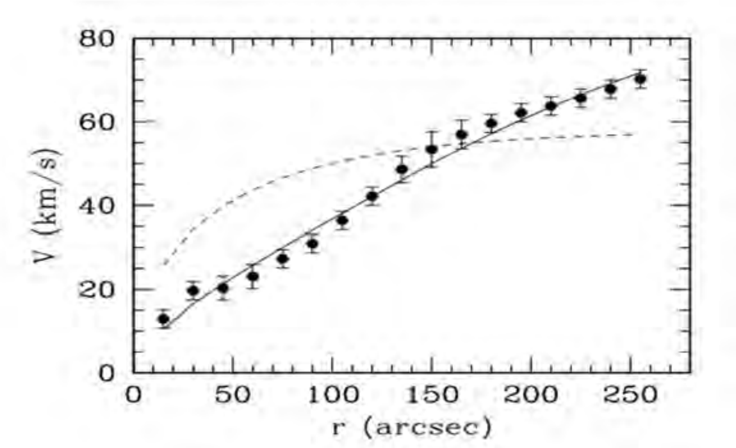

Figure 2.1: Mass models for DDO 47: the solid line is the fit with the Burkert halo, and the dotted line is the Navarro-Frenk-White (NFW) fit. Taken from Gentile et al. (2005).

total mass density in the Milky Way, particularly in the innermost regions of the Galaxy.

2.4 MOND

Despite the wide acceptance of dark matter by the researchers in Astrophysics, an attempt to come up with an alternative to dark matter as the solution for the rotation curve problem has been studied in the past decades. It is appears that alternative proxies could generate better rotation curves. This is to say that Newton's law of gravity is invalid at the galactic scale. Therefore, there is an alternative for the dark matter, that is by modifying the laws of gravity (Scarpa et al., 2006). This discovery could affect the way we think about the Universe as dramatically as Copernicus' assertion did to the notion that the earth moved around the sun.

Milgrom in 1983 proposed a novel paradigm which can be interpreted as reflecting non-Newtonian as well as nonlinear character of gravity already at the nonrelativistic level. He called the scheme Modified Newtonian Dynamics. In MOND theory, rotation curves naturally become flat at large radii and MOND has proven remarkably successful in explaining the shape of rotation curves without any unseen matter (De Blok & McGaugh, 1998; Sanders & McGaugh, 2002; Sanders & Noordermeer, 2007). On the other hand, the

MOND fares less well on larger scales of galaxy clusters, such as rich clusters that consist of dozens of bright galaxies and hundreds of fainter ones (Sanders, 2003; Clowe et al., 2006). The predictions MOND makes for rich clusters are off by a factor of 2. MOND also suffers from some considerable problems. The most serious drawback is that MOND lacks a satisfactory theoretical basis and was not much more than an empirical fitting formula (Noordermeer, 2006).

Furthermore, we examine the MOND framework against our sources. The detailed discussions of the MOND will be presented in Chapters 4 and 5. We will know whether the dark matter in the central regions of our sources is preferred solution of the rotation curve problem or whether MOND is valid.

2.4.1 MOND: Basic Equations

One alternative to the alleged ”dark” matter is Milgrom’s Modified Newtonian Dyanmics (Milgrom, 1983a), also referred to as MOND. Before MOND many theoreticians already toyed with the idea that a change in the $1/r^2$ force law at large length scales can serve as an explanation for the mass discrepancy. But as Milgrom first realized, any modification attached to a length scale would cause the larger galaxies to exhibit the larger discrepancy. Milgrom hence suggested to rather introduce a universal acceleration scale and modifying Newton’s second law of motion, respectively:

$$F_N = m\mu(\frac{a}{a_0})a, \tag{2.1}$$

where F_N is the Newtonian force and $\mu(x)$ is the "interpolating function". The exact form of the interpolating function is still yet to be determined, but it should have the approximations:

$$\mu(x) = \begin{cases} x, & for \quad x \ll 1 \\ 1, & for \quad x \gg 1 \end{cases} \tag{2.2}$$

From the above equation, i.e., Equation 4.2, $\mu(x) \approx x$ represents the deep MOND regime when x $\gg$1. Otherwise, it is under the Newton regime.

Even though MOND has been introduced as a modification to accelerations it can also be re-interpreted as a modification to the law of gravity. In the non-relativistic and weak-field approximation, a galaxy with a baryonic matter density distribution ρ, the acceleration of stars and the Newtonian gravitational potential ϕ are assumed to satisfy the modified Poisson equation (Bekenstein & Milgrom, 1984) below,

$$\nabla . \left[\mu\left(\frac{\nabla\Phi}{a_0}\right)\nabla\,\Phi\right] = 4\pi G\rho \tag{2.3}$$

In brief, for symmetric mass distribution, the MOND acceleration, g related to Newtonian acceleration g_N through the following relation (Milgrom, 1983a):

$$\mu(\frac{a}{a_0})a = g_N, \tag{2.4}$$

where MOND is formulated from the nonrelativistic formulation. From Equation 4.4, $a_0 \approx 1.2 \times 10^{-10}$ m s^{-2}. g_N is the conventional gravitational acceleration (Newtonian) and a is the true gravitational acceleration of a particle, (a = $|\mathbf{a}|$) with respect to some fundamental frame. Here, $x = \frac{|a|}{a_0}$, the ratio of the acceleration to a_0, is a measure of modified gravity.

There are several suggestions for the interpolating functions. For this, this study adopted the following form of the function form, which is the most commonly used interpolating

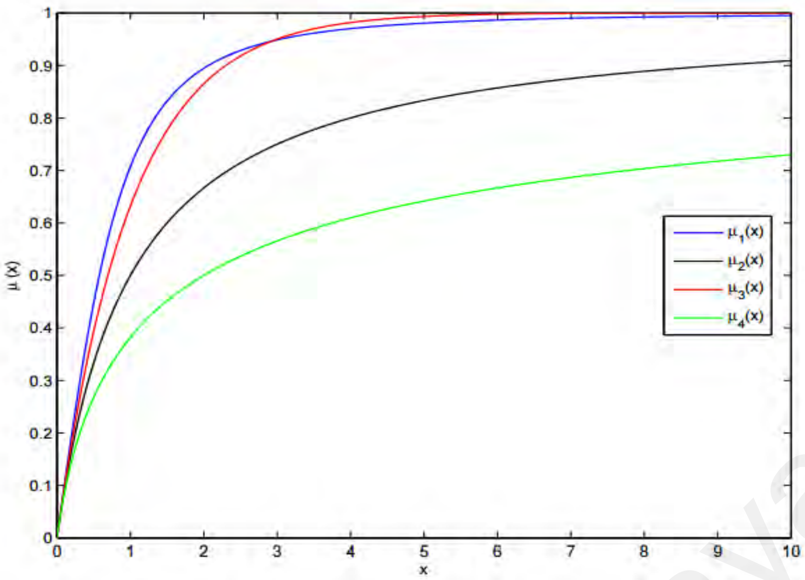

Figure 2.2: Various interpolation $\mu(x)$-function. $\mu 1(x)$=$x/(1+x)$are the most commonly used interpolation function in the Milgrom's MOND. $\mu 3(x)$= 1-e^{-x} and $\mu 4(x)$= 1+$\frac{1}{2x}$ - $\sqrt{\frac{1}{x}+\frac{1}{4x^2}}$ is the interpolation function in the Finslerian MOND (Chang et al., 2013).

function and so is refered to as the standard function (Bekenstein & Milgrom, 1984) below.

$$\mu(\frac{a}{a_0}) = \left[1 + (\frac{a_0}{a})\right]^{-1} \tag{2.5}$$

and

$$\mu(\frac{a}{a_0}) = \left[1 + (\frac{a_0}{a})^2\right]^{-1/2} \tag{2.6}$$

Owing to its simplicity, this function is cunningly called the simple function. The only serious limitation of the interpolating function is that for x when x is small and unity when x is large. Figure 2.2 presents various interpolation function (Chang et al., 2013).

CHAPTER 3: METHODOLOGY

3.1 Introduction

The current evidence for the existence of dark matter in galaxies is very strong. In particular, spiral rotation curves have revealed the presence in these objects of a dark "mass component" of the first-order approximation. Rotation curves of galaxies in the disk and outer regions have been studied based on optical and HI observations. These rotation curves have been used to calculate the mass distribution in the outermost regions. In contrast, the inner rotation curves have not yet been thoroughly investigated with sufficient accuracy, not only because of the concern on the distribution of mass in the outermost regions, but also because of the difficulty in deriving the central rotation velocities. The lack of HI gas in the central regions has resulted in the difficulty in measuring central rotation curves (Sofue, 2001). This chapter will explain the major method to estimate the dark matter in the central regions of galaxies.

3.2 Methodology

In order to derive the central rotation curves, CO molecular lines are the most convenient because of the high concentration of molecular gas in the centers of many galaxies, the high angular velocity resolutions in CO observations, and the negligible extinction even towards the dusty nuclear disk. Therefore, CO-line data from ALMA observations was used (see data collection for more details about ALMA) to obtain well-sampled inner rotation curves for nearby galaxies. The rotation curve was derived from a Position-Velocity (PV) diagram. From these observations we can construct the observed line of sight velocity of different parts of the galaxy. In the simplest sense, we can tell that a galaxy is rotating when one side of the galaxy is moving towards us and the other is moving away. In principle, from the rotation curve, it is possible then to determine the mass of galaxy, which is known as dynamical mass (M_{dyn}), including all the masses in the forms of stars, gas, dust, and the SMBH. It is expressed as follows:

$$M_{\mathrm{dyn}} = M_{\mathrm{DM}} + M_{\mathrm{gas}} + M_{*} + M_{\mathrm{HI}} + M_{\mathrm{SMBH}} + M_{\mathrm{dust}}. \tag{3.1}$$

The gas mass (M_{gas}) in this work was estimated from integrated flux via moment-0 (mom0) map and the CO-to-H_2 conversion factor (X_{CO}). The mom0 map was constructed from task 'imomments' by Common Astronomy Software Applications (CASA)[1](see Appendix A). Figure 3.1 shows the CASA window in the Ubuntu operating system. The HI line is an extremely useful tool for studying gas in the interstellar medium of external galaxies and tracing the large-scale distribution of galaxies in the universe because HI is detectable in most spiral galaxies and in some elliptical galaxies. The neutral hydrogen mass (M_{HI}) was estimated from the integrated HI flux in units of Jy km s^{-1} and D_L is the luminosity distance in unit of Mpc.

The stellar mass (M_*) and dust mass were estimated by using IR data as shown in Figure 3.2. Using the IR 2MASS data, we needed to de-project the image profile I(R) using the Image Reduction and Analysis Facility (IRAF)[2] software (see Figure 3.3) to obtain the surface brightness of the galaxies and convert the luminosity density distribution into stellar mass. For the dust mass, the IRAS and Spitzer (MIPS) data (refer to Section 3.3) were considered for the late-type galaxies based on the flux densities.

The SMBH mass was estimated from the SMBH-bulge relation and other methods such

[1]The package can process both interferometric and single dish data, and is developed by an international consortium of scientists based at the National Radio Astronomical Observatory (NRAO), the European Southern Observatory (ESO), the National Astronomical Observatory of Japan (NAOJ), the Academia Sinica Institute of Astronomy and Astrophysics (ASIAA), the CSIRO division for Astronomy and Space Science (CASS), and the Netherlands Institute for Radio Astronomy (ASTRON) under the guidance of NRAO.

[2]IRAF is distributed by the National Optical Astronomy Observatory, which are operated by the Association of Universities for Research in Astronomy, Inc., under cooperative agreement with the National Science Foundation.

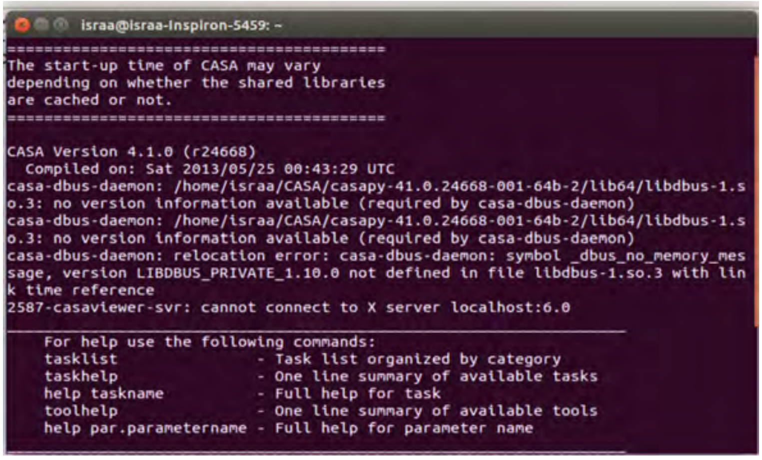

Figure 3.1: CASA software in the Ubuntu operating system.

as the fundamental plane of black hole activity, which is a plane in the space given by black hole mass and the radio/X-ray luminosities. Finally, the mass of dark matter in the central regions of the samples can be deduced from Equation 3.1. The detail of the methodology for the work was summarised in Figure 3.2.

3.3 Data Source

The estimation of dark matter in the central regions of sources was performed based on the radio and IR data.

3.3.1 Radio Data

Radio data collection was conducted by using radio telescopes, which are either used singularly or with multiple linked antennas utilising the techniques of radio interferometry and aperture synthesis. The former is a single-dish telescope and the latter is a radio interferometer. Radio interferometers achieve higher angular resolution than single-dish telescopes because the angular resolution Θ is determined by approximately λ/D, where λ is the wavelength observed and D is the diameter of the single-dish telescope or the longest baseline length. Figure 3.4 shows the difference between a single-dish telescope and an interferometer telescope.

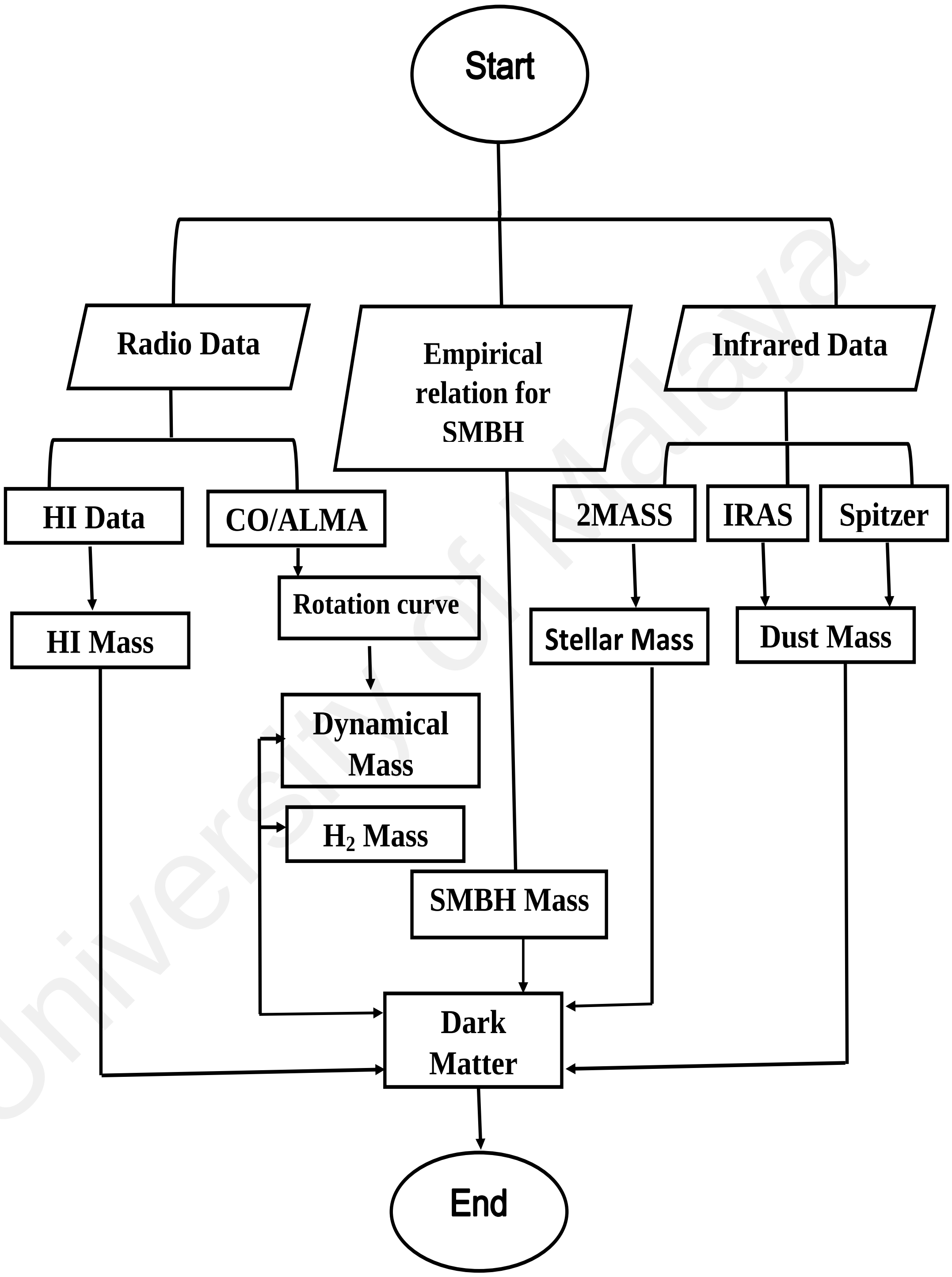

Figure 3.2: The research methodology of this work.

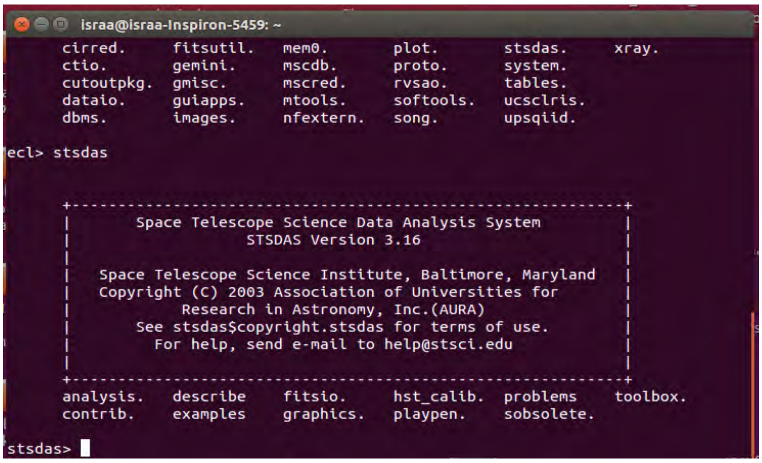

Figure 3.3: IRAF software in the Ubuntu operating system.

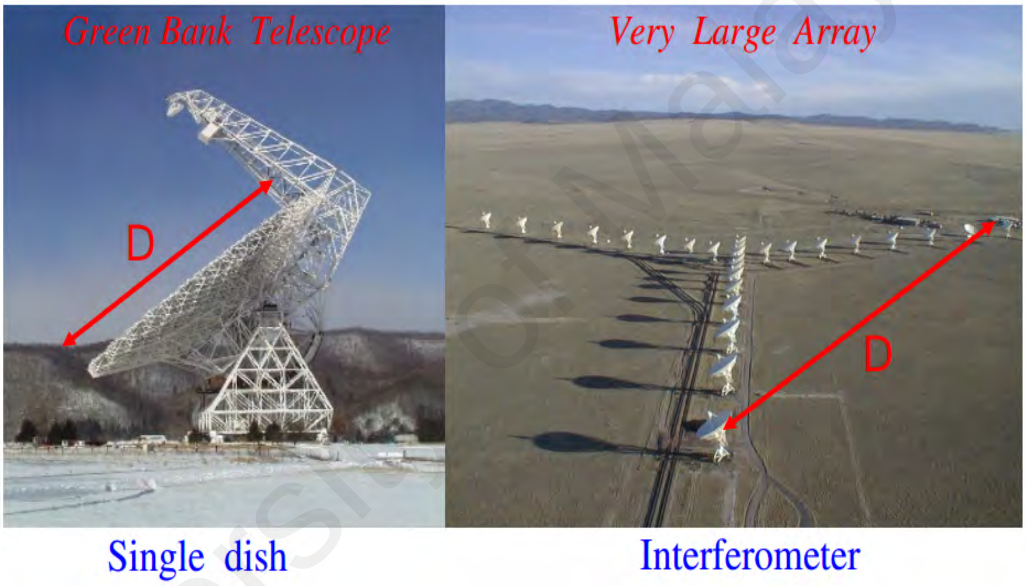

Figure 3.4: Example of single-dish telescope (left) and an interferometer telescope (right).

Interferometry has been successfully employed for many decades in radio astronomy and the ALMA is the latest, and certainly the best, venture into applying this technique at millimetre wavelengths. In the present work, the CO data was taken from ALMA. For HI data, the Very Large Array (VLA) data and previous studies were considered to estimate M_{HI}.

ALMA is a millimeter/submillimeter (mm/submm) interferometer located in the Atacama desert of northern Chile at an elevation of about 5000 m above sea level and

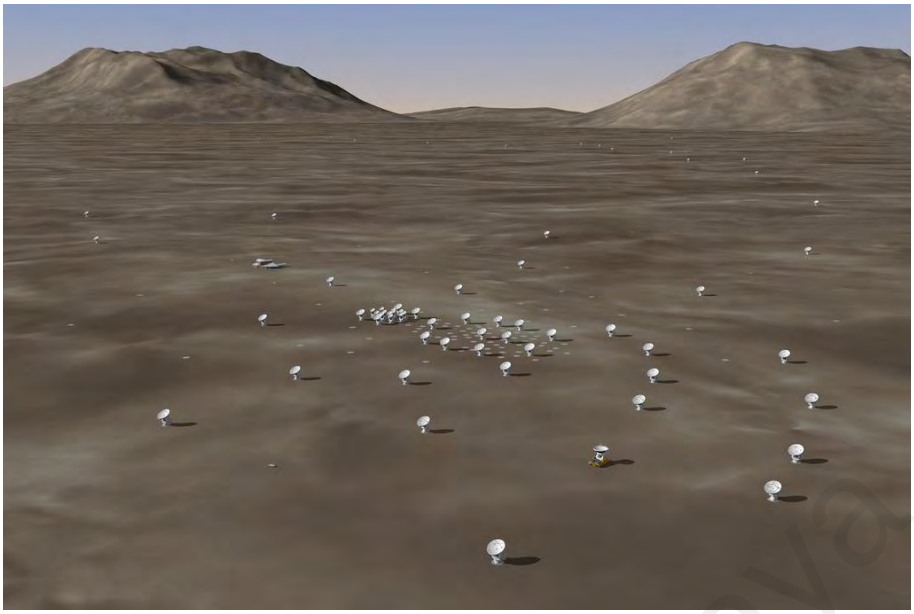

Figure 3.5: The fifty antennas of the ALMA 12-m array.

at a latitude of $-23°$ (ALMA Partnership et al., 2015). ALMA array is composed of 66 reconfigurable high-precision antennas (fifty 12 m antennas in the 12 m Array, as well as twelve 7 m antennas in the ALMA Compact Array (ACA) and four 12 m antennas forming the Total Power Array (TPA)) which covers wavelengths 0.3 to 9.6 mm. It has ten frequency bands between 30 GHz and 1 THz covering all atmospheric windows at the Chajnantor site (Chile) (Sørensen & Pontoppidan, 2010). Figure 3.5 shows the fifty antennas of the ALMA 12-m array.

VLA is a radio observatory located on the plains of San Augustin, New Mexico. It is an interferometer consisting of 27 radio antennas which are each 25 meters in diameter. The antennas are arranged on three 21 km long rail tracks resulting in a y-shaped configuration (see Figure 3.6). As the antennas can be moved along the rail tracks, the VLA can operate in four main and several hybrid configurations resulting in different baselines. The array provides diffraction-limited images of astronomical objects in all Stokes parameters, with a maximum resolution at 1.4 GHz of 1.4 arcseconds, and at 45 GHz of 0.05 arcseconds (Perley et al., 2009).

Figure 3.6: The Very Large Array. Image credit: http://www.cv.nrao.edu/~sransom/web/Ch8.html.

3.3.2 Infrared Data

Due to the dominant modes of galaxy change and growth yielding distinctive IR emission, infrared emission from galaxies is still a fundamental tracer of their evolution from the Big Bang. 2MASS, the IRAS and Spitzer (see the infrared bands for more details (Mackie, 2011)) were used in this work.

2MASS project is a ground-based survey of the entire sky in the J (1.2μ), H (1.65μ), and Ks (2.17μ) near-infrared bands (Finlator et al., 2000) (see Figure 3.7). The 2MASS project uniformly scans the whole sky using two 1.3 m equatorial telescopes. The northern one is located at the Whipple Observatory in Arizona (N $31°40'50''.8$, $W110°52'4''$), whereas the southern telescope is at Cerro Tololo Inter-American in Chile (S $30°10'3''.7$, $W70°48'18''$). Each telescope's camera is equipped with three 256×256 arrays of HgCdTe detectors. The 2MASS arrays images the sky in a drift-scan mode. Each final pixel consists of six pointings on the sky for a total integration time of 7.8^s per pixel. The final image frames have a plate scale of $1''$ per pixel. The observations of the whole sky were taken between 1997 and 2001 (Skrutskie et al., 2006; Schombert & Smith, 2012).

IRAS is a joint project between the US, UK and the Netherlands. IRAS has 62 detectors, sensitive from 8.5 μm - 120 μm, as well as a spectrometer covering the range of 8 μm - 23 μm (Mampaso et al., 2004). IRAS was revolutionary in that it was sensitive enough to detect many extra-galactic infrared sources at longer infrared wavelengths (Sanders & Mirabel, 1996). Moreover, IRAS let to numerous scientific discoveries spanning a broad range of astrophysical subjects, from comets to circumstellar disks to interacting galaxies. The first IRAS sky survey made an extremely significant impact on astronomy as a whole: it covered 95% of the sky at 12 μm, 25 μm, 60 μm and 100 μm (see Figure 3.8), detecting 250,000 point sources and thus increasing by half the total number of recorded astronomical objects in existence; until then was a mere 500,000 (Neugebauer et al., 1984).

An infrared space observatory was built: **the Spitzer Space Telescope**, launched in 2003 (Werner et al., 2004). It is performing extremely well, returning excellent scientific data from its Earth-trailing solar orbit. The Spitzer Space Telescope's three science instruments operate in the mid-to far-infrared between 3 and 160 microns as shown in Figure 3.9 (Werner et al., 2004; Elmegreen et al., 2006), which is

The Infrared Array Camera (IRAC) takes images at four fixed wavelengths ranging from 3.6 to 8.0 μm.

The Infrared Spectrograph (IRS) has four modules that break light into a spectrum of infrared colors, much like a prism. These detectors range from 5.3 to 40 μm.

The Multiband Imaging Photometer for Spitzer (MIPS) takes images at three fixed wavelengths ranging from 24 to 160 microns. MIPS can also function as a spectrograph in the range of 50 to 100 μm.

3.4 Archival Observation

The NASA/IPAC Extragalactic Database (NED) is widely used by astronomers around the world because it contains crucial astronomical information on extragalactic objects such

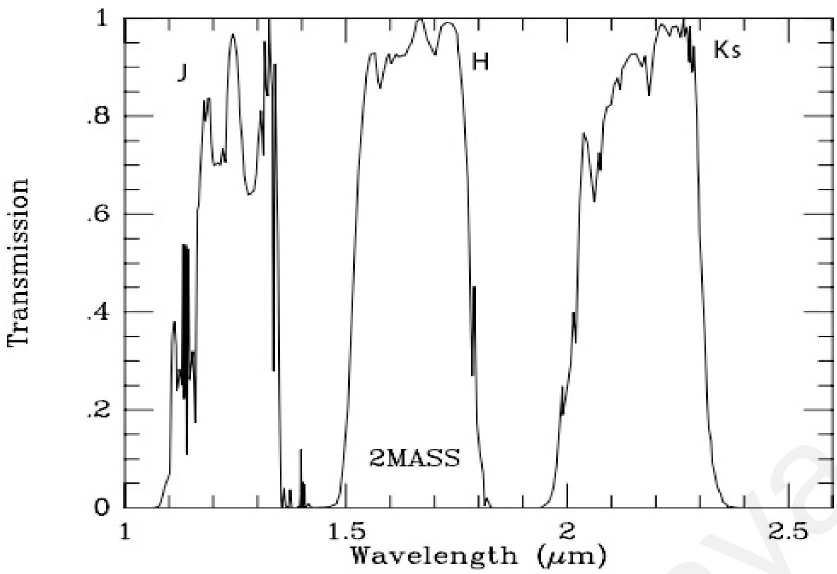

Figure 3.7: Calculated relative spectral response curves for 2MASS bands, renormalized to peak values of unity. Source: Cohen et al. (2003).

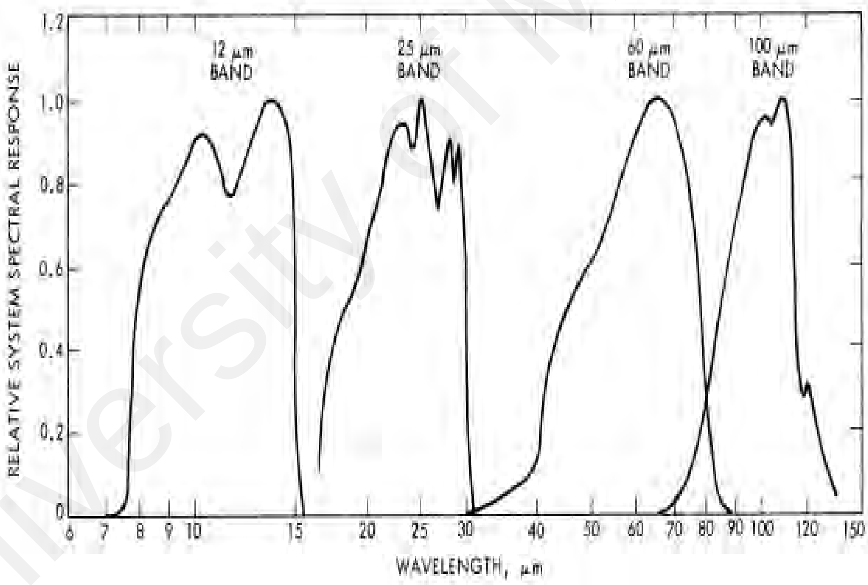

Figure 3.8: IRAS spectral response of the detector, field lens, and filter combinition of the survey array. Quoted, the flux densities have been calculated at wavelengths of 12, 25, 60, and 100 μm assuming the energy distribution of the source is flat in flux per logarithmic frequency interval. Source: Neugebauer et al. (1984).

as galaxies, active galactic nuclei (or AGN) and clusters of galaxies. It was established by astronomers Helou and Madore in the late of 1980s. NED contains millions of data entries ranging from photometric data, redshift and diameter measurements, object's classification maps as well as journal articles, notes and abstracts. Thus, this database was chosen based

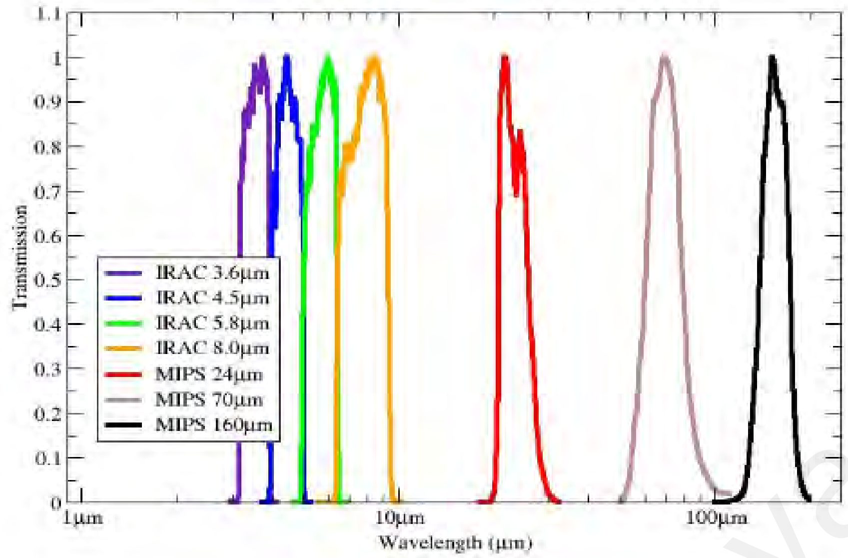

Figure 3.9: Spitzer space telescope filters. Source: http://www.astro.caltech.edu/~capak/filters/index.html.

on its powerful data mining and cited for various studies in astronomy.

CHAPTER 4: DARK MATTER IN THE CENTRAL REGION OF NGC 3256

4.1 Introduction

The universe is believed to contain a huge amount of dark matter. The existence of dark matter can be deduced from its gravitational influence on the movement of ordinary matter. Observations of spiral galaxies suggested that a significant amount of invisible (missing) mass is required in order to explain the observed rotation curves of the spiral galaxies (Einasto et al., 1974; Roberts & Whitehurst, 1975; Faber & Gallagher, 1979); the rotation curves of spiral galaxies have also been studied with different methods e.g., (Rubin et al., 1980; Bosma, 1981a). Besides, it was also found that different types of galaxies might have different distributions of dark matter; for example, dwarf galaxies might contain larger fractions of dark matter than normal galaxies (Faber & Lin, 1983; Mateo, 1998). All these studies showed that dark matter should be a common feature in galaxies. However, although the dark matter might contribute to about 80% of the material mass of the universe (Athanassoula, 2004; Bauer et al., 2015); attempts to detect the dark matter directly are still unsuccessful (e.g., Tan et al. (2016)).

An alternative theory, MOND (Milgrom, 1983a, 1983b, 1983c), has been proposed to explain the observed properties of galaxies without utilizing dark matter. The theory proposed a modification of Newton's laws to account for the observed rotation curves of galaxies and suggested that the missing mass problem in galaxies only occurs in the small acceleration regime with $a \ll a_0$, where $a_0 \approx 1.2 \times 10^{-8}$ cm s^{-2}. The MOND theory can reproduce the galactic rotation curves from the observed distribution of stellar and gaseous matter (e.g., (Bottema et al., 2002)). The MOND theory could also account for the Tully–Fisher and Faber–Jackson relations of galaxies (van den Bosch & Dalcanton, 2000) and the kinematics of small groups of galaxies (Milgrom, 1998) without dark matter.

Recently, Tian and Ko (2016) found that some elliptical galaxies seem to have a deficit of dark matter, and the dynamics of the elliptical galaxies can be well explained with the MOND theory.

Although MOND is quite successful in explaining many dark matter phenomena at the galactic scale, it is also well known that MOND has difficulty in explaining the dark matter phenomena in galaxy clusters (e.g., Aguirre et al. (2001)). It is thus very interesting to know whether the success of MOND at the galactic scale is really showing evidence for some modification of the Newtonian law, or it only happens that MOND has some similarity with dark matter by accident. To investigate these possibilities, it would be important to know whether MOND can really explain all dark matter phenomena at different galactic scales.

In the hierarchical scenario of dark-matter halo formation, i.e., galaxy formation, large halos (large galaxies) are formed from mergers of small halos (small galaxies). Luminous infrared galaxies, which were usually found to be in the process of galaxy merging, should thus also be in the processes of dark-matter halo merging and are in a very important stage of galaxy evolution. However, LIRGs were usually found to contain a huge amount of molecular gas ($\geqslant 10^9 M_\odot$), which was usually too massive to be reconciled with the observed dynamical masses (e.g., Solomon et al. (1997)). The inconsistency is usually believed to be caused by the CO-luminosity-to-H_2-mass conversion factor, which was derived from the Galaxy and might not be applicable to the LIRGs. Even adopting a lower value of conversion factor, the dynamical mass would still be dominated by the molecular mass. However, since LIRGs are usually merging galaxies, which are regulated by dark-matter halo merging, it would be interesting to ask whether a significant amount of dark matter can be observed in the centre regions of LIRGs, whose dynamical masses usually seem to be dominated by molecular masses.

The LIRG NGC 3256 is among the brightest nearby galaxies. NGC 3256 belongs to the Hydra-Centaurus clusters of galaxies at a distance $D = 35$ Mpc (Sargent et al., 1989) (see Figure 4.1 and Figure 4.2). This galaxy is descended from a merger of two gas-rich disk galaxies and has a nearly face-on orientation (Agüero & Lipari, 1991). These facts make the galaxy the best target to study the dark matter in a LIRG. NGC 3256 has two nuclei with $5''$(1 kpc) separation in the north-south direction (Moorwood & Oliva, 1994; Norris & Forbes, 1995; Alonso-Herrero et al., 2006). The southern nucleus is indeed heavily obscured; various studies argued that the southern nucleus may harbor a highly obscured AGN (Neff et al., 2003). It was also suggested that IR emission of these two nuclei is ascribed mostly to star formation process (Lira et al., 2008; Alonso-Herrero et al., 2012).

The molecular gas distributions of NGC 3256 have been studied by Sargent et al. (1989); Aalto et al. (1991); Baan et al. (2008). Submillimeter Array (SMA) CO(2-1) observations showed that there is a large molecular disk concentrated around the centre of the double nuclei using CO(2-1) (Sakamoto et al., 2006); Sakamoto et al. (2006) also discovered a high velocity component (up to around 400 km s^{-1}) of molecular gas at the center between the double nuclei. Sakamoto et al. (2014) used the Atacama Large Millimeter/submillimeter Array to study NGC 3256 and suggested that the two nuclei have their own molecular disks, and the high-velocity gas is associated with the molecular outflows from the two nuclei and could have velocity $\geqslant$ 1000 km s^{-1}.

In this chapter, this study tries to determine the mass distributions in the central region ($r \lesssim 1.7$ kpc) of NGC 3256 using the CO(1-0) observations of the ALMA data and the near-IR data of the 2MASS. The data selection is described in Section 4.2. Section 4.3 presents results and discussion of this chapter. In Subsection 4.3.6, the dark matter in the central region of NGC 3256 is looked into.

Figure 4.1: This image was taken by HST of NGC 3256 and released on the occasion of its 18th anniversary on 24th April 2008. Image Credit: NASA, ESA, the Hubble Heritage Team (STScI/AURA)-ESA/Hubble Collaboration and A. Evans (University of Virginia, Charlottesville/NRAO/Stony Brook University).

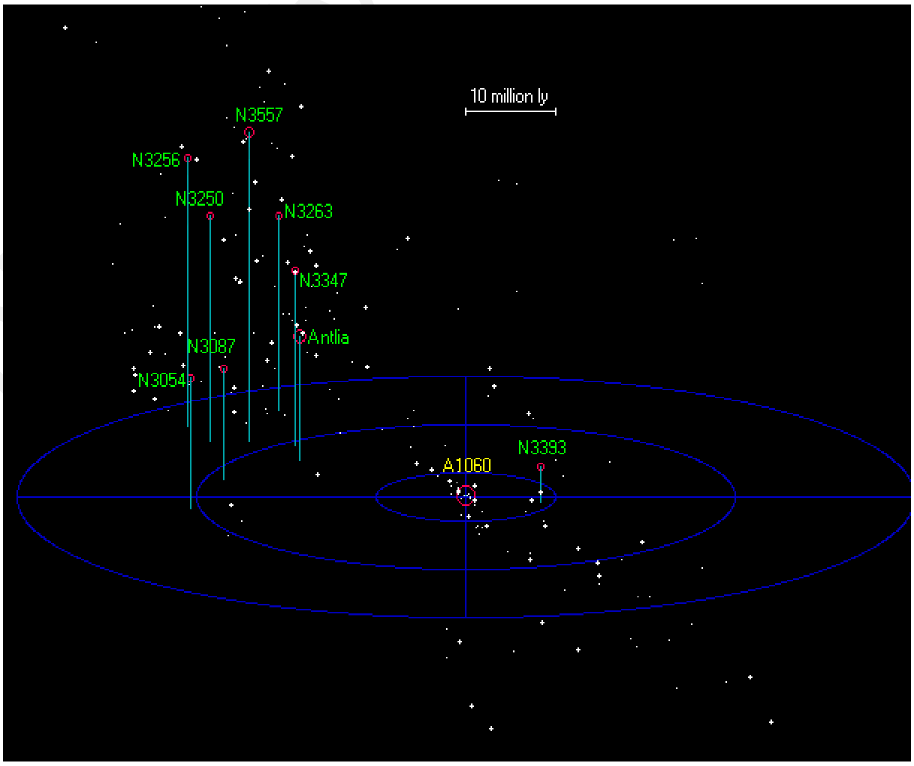

Figure 4.2: Three-dimensional map of the Hydra Supercluster. Credits: Powell, Richard. Atlas of the Universe.

Table 4.1: ALMA Observational Parameters for NGC 3256.

Parameter	Value
Target	NGC 3256
Observing date	27-Jan-2012
Total integration time	3996.53 seconds
Field center:	
R.A.(J2000)	10h27m51s.23
Dec.(J2000)	$-43°54'16.6''$
Number of antenna	17
Rest frequency	115 GHz
Restoring beam	(major, minor, P.A.)
	($3.17'' \times 1.98''$, $4.92°$)
Channel width	488.28125 kHz
Total bandwidth	1.875 GHz
Total channels	3840
Velocity resolution	20km s^{-1}

4.2 Data Collection

4.2.1 ALMA Data

The ALMA data of NGC 3256 were obtained from ALMA Cycle 0 (ID =2011.0.00525.S, PI: Sakamoto) of the CO(J=1-0) rotational transition line at 3 mm (band 3). The data was collected in 2011– 2012 using up to twenty-three 12-m antennas. The central position of the observations was at Right Ascension (R.A.)=10h 27m51.23s, Declination (Dec.)=$-43°54'16.6''$ (J2000).

The ALMA data were calibrated using the CASA reduction package version 4.1. Data reduction and image processing were also performed with CASA. The CO(1-0) data cube was obtained from the continuum subtracted visibilities using the task 'uvconsub'. The cleaned images were obtained using the multiscale clean with robust weighting. The resulted beam size of the images is $\approx 3.17'' \times 1.98''$, corresponding to the angular linear scales of 538 pc $\times$ 336 pc, and position angle (PA)=$4°.92$. The observation parameters are listed in Table 4.1.

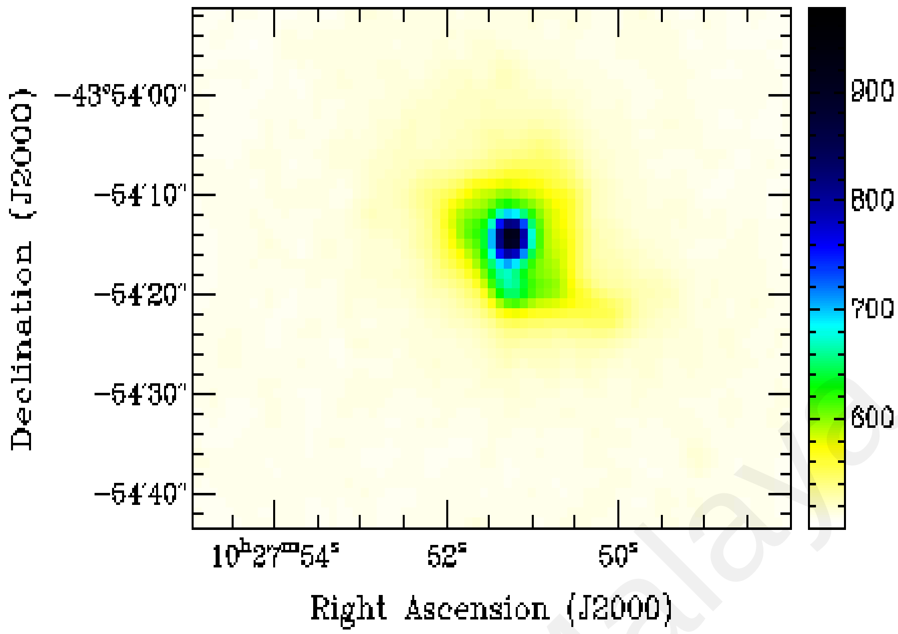

Figure 4.3: Image of NGC 3256 at the 2MASS Ks-band.

4.2.2 2MASS Data

The 2MASS image of NGC 3256 was used to estimate the stellar mass of this galaxy. The data are publicly available. To estimate the stellar mass, this study considered the Ks image of NGC 3256 from the 2MASS All-Sky Extended Source Catalog (XSC). Figure 4.3 shows the 2MASS Ks image in the centre region of NGC 3256.

4.3 Results and Discussion

4.3.1 CO Distributions of NGC 3256

Figure 4.4 shows the CO(1–0) integrated intensity map that is produced by summing all emission features in the channel map at the resolution of $3.17'' \times 1.98''$. The channel map of the CO line in the central region of NGC 3256 is shown in Figure 4.5. The rms level in a single channel map is 16 mJybeam^{-1} with the velocity channel width=20km s^{-1}. Certain basic features of the gas distribution and kinematics in NGC 3256 are immediately apparent in Figure 4.5. One can see a strong inner region of CO line. This shows up

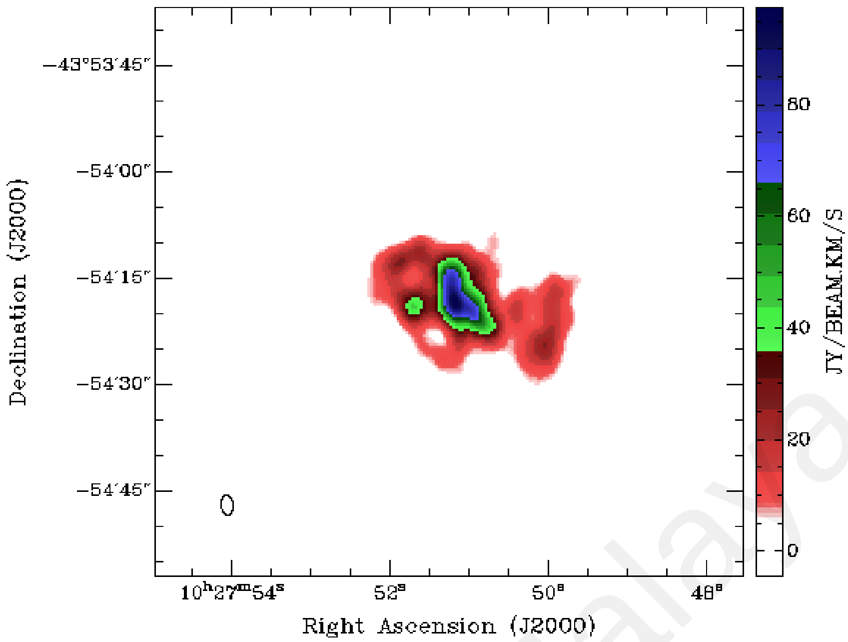

Figure 4.4: Integrated intensity map of the CO(1-0) line emission in the central region of NGC 3256. The color scale range is shown in the wedge at right in units of Jy beam^{-1}km s^{-1}. The synthesized beam is 3.17″ × 1.98″.

particularly in the middle channels, 2722 to 2782 km s^{-1}. There is also a velocity gradient in the region that runs roughly along southwest-northeast direction.

4.3.2 Central Rotation Curve of NGC 3256

The dynamical mass was determined in central region of NGC 3256 using the rotation curve of the galaxy derived from the CO line observations. To determine the rotation curve of NGC 3256, the position-velocity diagram was first considered across the N nucleus, S nucleus and the dynamic center of the galaxy along the different positions angles with a slit of 5″ width. This study adopted the position for the north nucleus to be R.A.(N)=10h27m51.23s, Dec.(N)=−43°54′14.0″ and that for the south nucleus to be R.A.(S)=10h27m51.22s, Dec.(S)=−43°54′19.2″. The center position between the two nuclei was taken to be R.A.=10h27m51.23s, Dec.=−43°54′16.6″ in J2000.0 (Norris &

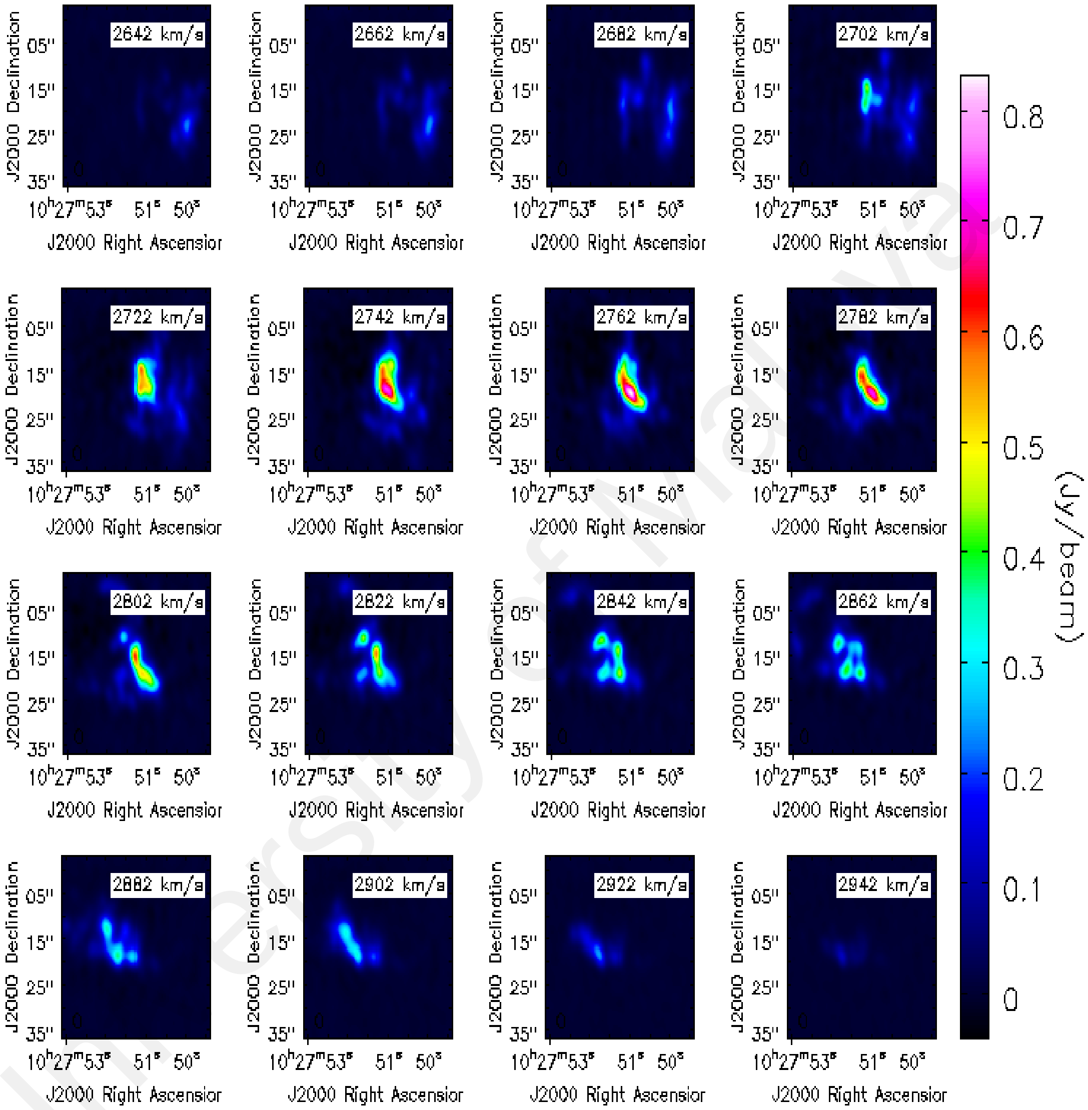

Figure 4.5: Channel maps of the CO(1-0) line emission in the central region of NGC 3256 with the velocity channel width= 20 km s^{-1}. The system velocity of NGC 3256 is 2775 km s^{-1}. The color scale range is shown in the wedge at right in units of Jy $beam^{-1}$.

Forbes, 1995; Lira et al., 2002; Sakamoto et al., 2006) (see Table 4.2). Figure 4.6 shows examples of the PV diagrams.

Note that the two nuclei of NGC 3256 are separated in the north-south direction by 5″(0.8 kpc). Therefore, the rotation velocity of the gas should be less affected by the two nuclei along the direction of PA=−90°. This study considered the velocity difference at PA≈ −90° to be mainly caused by the rotational velocity of the whole molecular distribution. The radial component of the rotation velocity on the line of sight (v_r) is related to the observed radial velocity (v_{obs}) by:

$$v_r = v_{\rm obs} - v_{\rm sys}, \tag{4.1}$$

where v_{sys} is the systemic velocity of the galaxy. v_{sys} was assumed to be 2775 km s^{-1} from previous studies for NGC 3256 (Roy et al., 2005). The rotational velocity v_c can be obtained as

$$v_c = \frac{v_r}{\sin(i)}. \tag{4.2}$$

Figure 4.7 shows the projected rotation velocity on the line of sight of the system centered at R.A.=10h27m51.23s and Dec.=−43°54′16.6″. The errorbars is standard deviation of mom1 map (see Figure 4.8). The systematic error was not taken into account, which is 5% uncertainty of the absoulte flux density calibration of band 3 in ALMA observations.

4.3.3 Dynamical and Molecular Gas Masses

The dynamical mass inside a radius r of a galaxy can be estimated with the rotation velocity v_c at r (Koda et al., 2002).

$$M_{\rm dyn} = 2.3 \times 10^5 \times (\frac{r}{\rm kpc}) \times (\frac{v_c}{\rm km\ s^{-1}})^2\ {\rm M_\odot}, \tag{4.3}$$

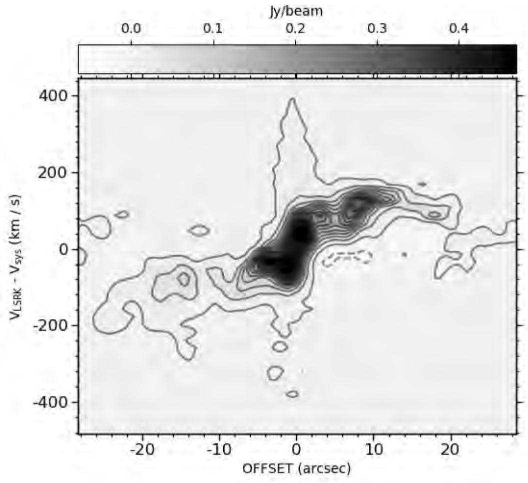

(a)

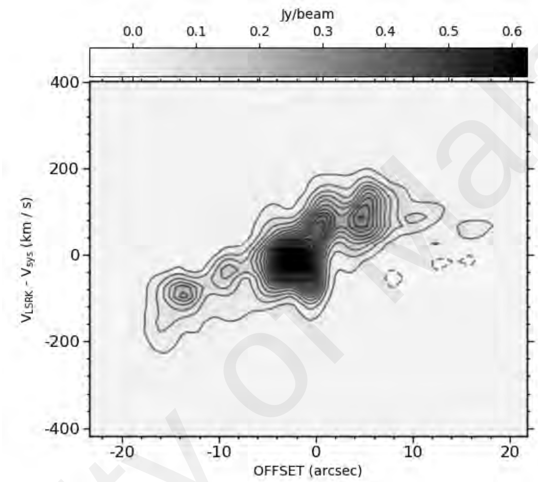

(b)

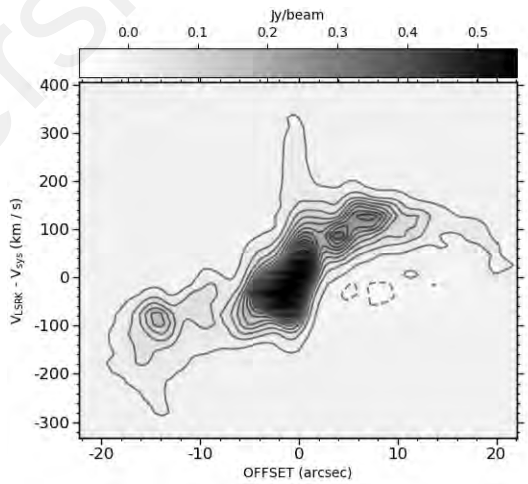

(c)

Figure 4.6: CO Position-Velocity diagrams of NGC 3256 passing through the nuclei along different PA angles. (a) PV diagram along PA= $-90°$ through N nucleus, (b) PV diagram along PA= $-90°$ through S nucleus, (c) PV diagram along PA= $-90°$ passing through the center between the two nuclei. Each PV cut has a slit width of 5″.

Table 4.2: Galaxy properties for NGC 3256.

Parameter	Value
R.A.(J2000)	10h27m51s.23
Dec.(J2000)	$-43°54'16.6''$
Adopted distance	35 Mpc
Scale. 1″in pc	170
i	30°
Systemic velocity	2775 km s^{-1}
Morphological type	Sb
z	0.009354
Luminosity Class	LIRG

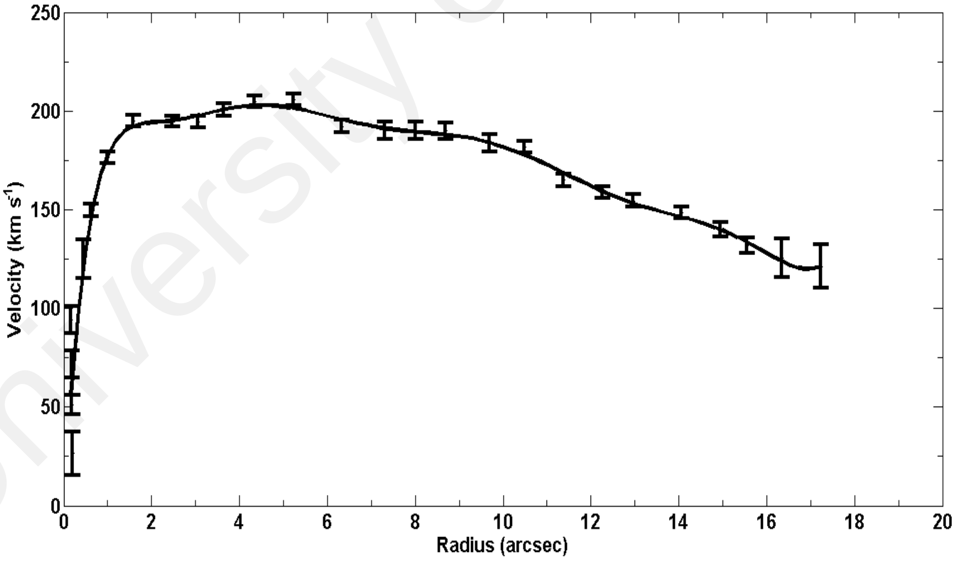

Figure 4.7: Projected rotation velocity of NGC 3256 derived from the PV diagram of Figure 4.7c assuming an inclination angle of 30°. Dots with error bars are the data points and the solid curve is the fitting. The error bars are the standard deviations of the velocity.

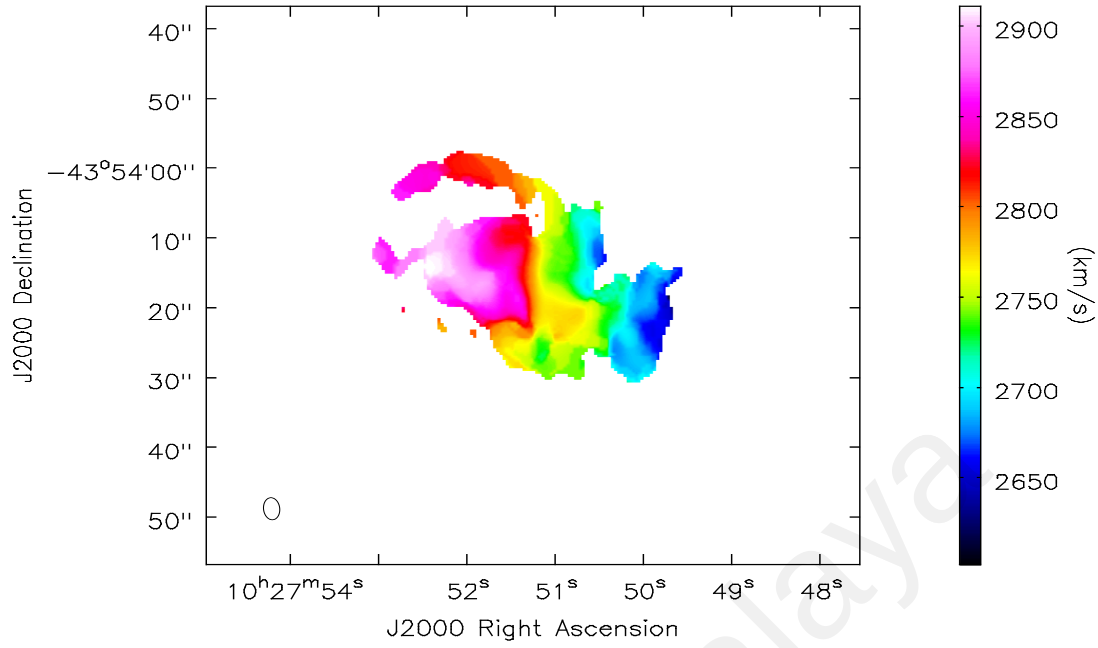

Figure 4.8: The CO(1-0) velocity field map of NGC 3256.

The central position of the system was taken to be R.A.=10h27m51.23s and Dec.=−43°54′16.6″ to estimate the dynamical mass within the central region. From Figure 4.7, the $M_{\rm dyn}$ is estimated to be $5.1 \pm 0.2 \times 10^{10}$ $M_\odot$ within $r = 10''$ from the line-of-sight rotational curve of $\sim 184 \pm 5$ km s^{-1} assuming the inclination angle $i = 30°$ from Sakamoto et al. (2014). For more information on the errors, refer to Appendix C.

The molecular hydrogen mass of NGC 3256 can be estimated using Tsai et al. (2009):

$$M_{\rm H_2} = 1.2 \times 10^4 \times D^2 \times S_{\rm CO(1-0)} \times \frac{\rm X_{CO}}{3 \times 10^{20}}, \tag{4.4}$$

where D is the distance in units of Mpc, $S_{\rm CO(1-0)}$ is the CO-line flux in units of Jy km s^{-1}, and X_{CO} is the CO-to-H_2 conversion factor. The conversion factor is usually in the range of X_{CO}= $0.3 \times 10^{20} - 3 \times 10^{20}$ cm^{-2}(K km s^{-1})$^{-1}$ with high values for normal galaxies (see (Dickman et al. 1986)), and low values for LIRGs (Bolatto et al., 2013). The total gas mass associated the molecular hydrogen is $M_{\text{gas}} \approx 1.36 \times M_{\text{H}_2}$ (Tsai et al., 2009). The total CO(1-0) flux is $\approx$ 1013 ± 23 Jy km s^{-1} within the radius 10″of NGC 2356; this region contains almost all of the CO(1-0) emission. The X_{CO} was assumed to be 0.3×10^{20} cm^{-2}(K km s^{-1})$^{-1}$ and found $M_{\text{H}_2} = 1.51 \pm 0.34 \times 10^9$ M$_\odot$ and $M_{\text{gas}} \approx 2.16 \pm 0.46 \times 10^9$ M$_\odot$ within the central region. Our results for the molecular mass are also consistent with those derived by Sakamoto et al. (2014).

Using the SEST 15 m single dish observation, Casoli et al. (1991) found that the M_{H_2} within the area 44″× 44″ is equal to 1.3×10^{10} M$_\odot$ at D =35 Mpc, which is close to our result of $M_{\text{H}_2} = 1.41 \times 10^{10}$ M$_\odot$ from ALMA observation at the same area. This result indicates that no missing flux exists.

4.3.4 Stellar Mass

The central region of NGC 3256 might also contain a significant amount of stellar mass. 2MASS Ks band images was used to derive the stellar mass of NGC 3256. To obtain the stellar mass in the central region of the galaxy, the image profile $I(R)$ needs to be de-projected to obtain the luminosity density $j(r)$ distribution of the galaxy and converted the luminosity density distribution to stellar mass. In general, if the image profile $I(R)$ is circular symmetric, the $I(R)$ can be deprojected to find the $j(r)$:

$$j(r) = -\frac{1}{\pi}\int_r^\infty \frac{dI}{dR}\frac{dR}{\sqrt{R^2 - r^2}} \tag{4.5}$$

$j(r)$ could be numerically derived using the above formula. However, it was found that the Ks image of NGC 3256 can be well fitted with reduced χ^2 (χ^2_{red}) ≈1 with the modified Hubble profile (Binney & Merrifield, 1998):

$$I(r) = \frac{I_0}{1 + (\frac{R}{r_0})^2} \tag{4.6}$$

which has a simple analytic form of $j(r)$:

$$j(r) = \frac{j_0}{\left[1 + (\frac{r}{r_0})^2\right]^{\frac{3}{2}}} \tag{4.7}$$

where I_0 is the central surface brightness, r_0 is the core radius, and r_0 and j_0 is related to the central surface brightness with $I_0 = 2r_0 j_0$. The de-projected total luminosity from the central region within a radius R can be derived as $L = \int_0^R 4\pi r^2 j(r) dr$, and the de-projected flux from the central region would be $F = L/(4\pi D^2)$. Figure 4.9 shows the brightness profile of the 2MASS Ks image of NGC 3256 and the fitted modified Hubble profile. The well fit of the Ks image with the modified Hubble profile makes it much easier to derive the luminosity density distribution of the galaxy. Besides, this study also tried to fit the stellar light profile with the de Vaucouleurs $r^{1/4}$ law but was unable to obtain a reasonable fit ($\chi^2_{red} \approx 20$). Note that the modified Hubble profile is an approximation of the King model, which is derived by assuming that the stellar system is in a quasi-relaxation state (King, 1966); the well fit of the Ks image with the modified Hubble profile thus suggests that the system should be very close to be dynamically relaxed.

To obtain the stellar mass of NGC 3256, the de-projected flux within the selected galactic region was first converted to apparent magnitude:

$$m = 19.93 - 2.5log(F) \tag{4.8}$$

where 19.93 is the zero point magnitude of the Ks band (Jarrett et al., 2000b; Mineo et al., 2012; Zhang et al., 2012). The apparent magnitude was converted to absolute

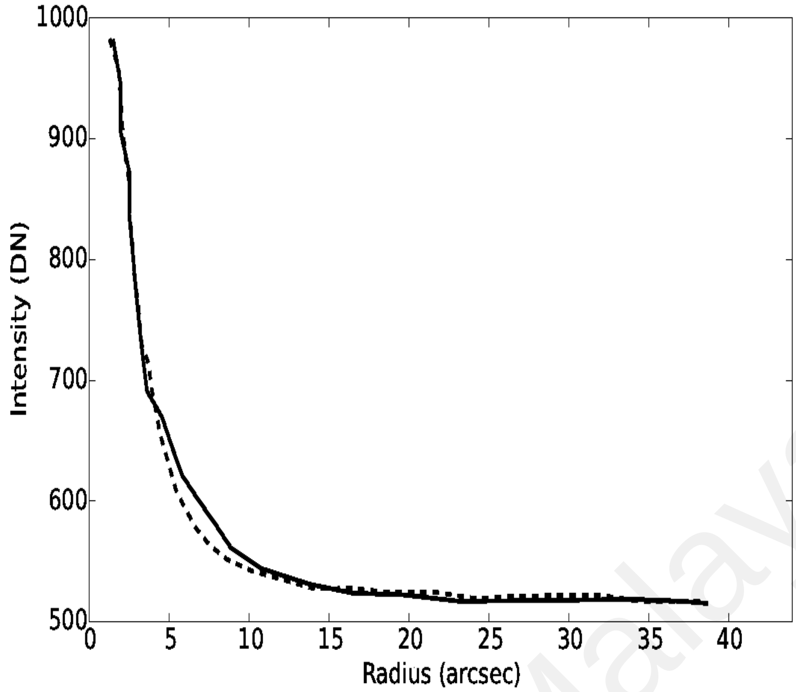

Figure 4.9: Surface brightness profile of NGC 3256 in 2MASS Ks image. The solid line is the radial profile of the Ks image of NGC 3256, and the dashed line is the fitting modified Hubble law with r_0 = 2.44″ and I_0 = 412.5 data number (DN).

magnitude using Kochanek et al. (2003).

$$M_K = m - 25 - 5log(D_L) - k_z, \tag{4.9}$$

D_L is the luminosity distance in Mpc, and k_z=-6.0log(1+z) is the k-correction (Domingue et al., 2009; Kochanek et al., 2001). The derived absolute magnitudes is about -20.45. It was assumed that the absolute magnitude of the Sun at the Ks band is 3.39 (Mulroy et al., 2014; Johnson, 1966), and it was then found that the Ks luminosities are about $4.38 \times 10^9 L_\odot$ within $r = 10''$ of the central region of NGC 3256. The mass-to-light ratio at the 2MASS Ks band is about M/L =0.73 (Bell et al., 2003). The stellar mass in the central region of NGC 3256 is then estimated to be about $M_* = 3.06 \pm 0.27 \times 10^9$ $M_\odot$ within $r = 10''$.

4.3.5 Other Masses

The SMBH mass of NGC 3256 is expected to be only around $10^7 - 10^8$ M$_\odot$ based on the SMBH-bulge relation (Alonso-Herrero et al., 2013) and is around 1.7×10^7 M$_\odot$ estimated from the X-ray and radio luminosities (Merloni et al., 2003), defined as follows:

$$L_R = (0.6^{+0.11}_{-0.11}) log L_X + (0.78^{+0.11}_{-0.09}) log M + 7.33^{+4.05}_{-4.07} \tag{4.10}$$

The unit of luminosities is ergs^{-1} and the mass of black holes in solar mass.

The dust mass of NGC 3256 is around 5×10^6 M$_\odot$, estimated from the IRAS flux densities at 60μm and 100μm obtained from the NED and the relation derived by Riffel et al. (2015).

$$\mathrm{M_{dust}} = 0.959 S_{100} D^2 \left[\left(9.96 \frac{S_{100}}{S_{60}} \right)^{1.5} - 1 \right] \mathrm{M_\odot} \tag{4.11}$$

where S_{100} and S_{60} are the IRAS flux densities in Jy at 60μm and 100μm respectively, and D is the distance to the galaxy in Mpc. The dust mass and the SMBH mass are thus negligible compared with the molecular mass in the central region of NGC 3256.

The HI observations of NGC 3256 shows absorption features in the central regions (English et al., 2003). The HI mass was estimated by English et al. (2003) to be around $0.4 - 2 \times 10^9$M$_\odot$ within the synthesized beam of their observation (23$''$ in diameter).

4.3.6 Dark Matter in the Central Region of NGC 3256

Based on equation 3.1, the dark matter mass can be estimated by:

$$M_{\mathrm{DM}} = M_{\mathrm{dyn}} - M_{\mathrm{gas}} - M_* - M_{\mathrm{HI}} - M_{\mathrm{SMBH}} - M_{\mathrm{dust}} \tag{4.12}$$

The mass of the SMBH, dust, and HI gas can be estimated from previous observations with well-established empirical relations. The baryonic mass within the 10″ central region of NGC 3256 is thus about $M_{\rm baryon} \approx M_{\rm gas} + M_{*} + M_{\rm HI} \approx 7.22 \pm 0.73 \times 10^{9}$ $M_{\odot}$. Please note that most baryon mass is from molecular mass and stellar mass and the HI mass contributes very little. Comparing with the dynamical mass derived, it was found that there is about $4.38 \pm 0.53 \times 10^{10}$ $M_{\odot}$ invisible mass in the central region. The fraction of the invisible mass is about 80% of the dynamical mass. Note that Sakamoto et al. (2014) found the gas-to-dynamical mass ratio to be around 9%; this difference is mainly caused by the fact that they adopted a different CO-to-H_2 conversion factor and they did not consider the stellar mass and HI mass. Similar results would be obtained if we had adopted the same parameters; however, the most conservative parameters was used to ensure the posibility of the existence of invisible mass. In any case, the existance of a significant amount of invisible mass in the central region of the galaxy is unavoidable. The observed rotation velocity might have been influenced by the merging process of NGC 3256. However, since the velocity of the molecular gas was used to derive the dynamical mass, the dynamical mass would have been overestimated only if the molecular gas was unbounded to the galaxy. Some of the molecular outflows from the nuclei of NGC 3256 might be unbounded; but the outflow velocities are distinguishable from the rotation velocity and would not be confused (Sakamoto et al., 2014), and the regions of nuclei are avoided in deriving the rotation velocity. Therefore, the rotation velocity should not be affected by the molecular outflows. Random velocity of the molecular gas associated with stellar/AGN feedback may lead to some uncertainties in the estimate of the dynamical mass. However, the derived rotation velocity showed a smooth rotation curve with small fluctuations, indicating that the influence of the random velocity should be negligible.

It is clear from Figure 4.10 that the normalization for the baryonic component in galaxies is very much lower, reflecting the fact that galaxy masses are dominated by dark matter,

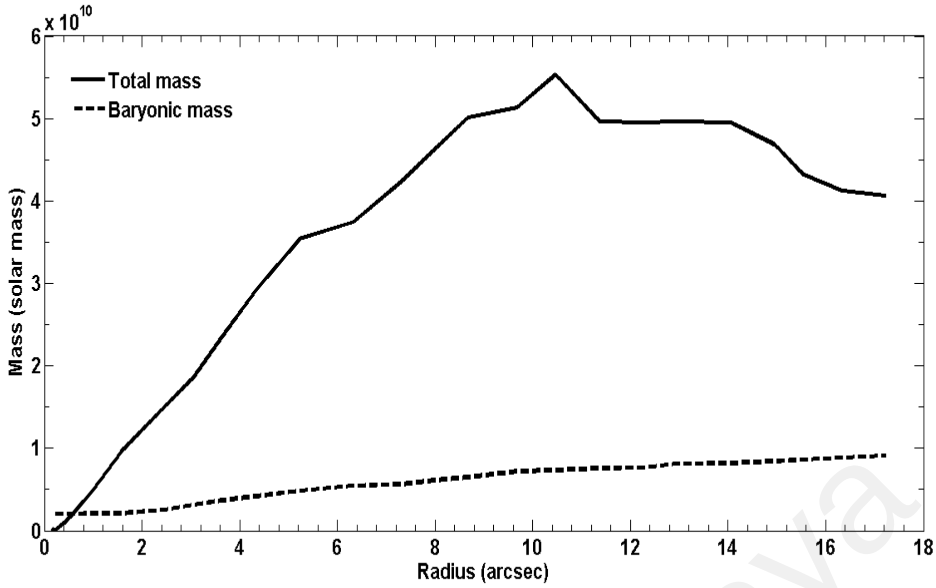

Figure 4.10: Total mass and baryonic mass of NGC 3256 as a function of radius.

not baryons. The only explanation for this is dark matter surrounding the NGC 3256 and pulling the baryonic matter around faster than they would otherwise orbit. Table 4.3 reveals the values of mass components (total and baryonic mass) of NGC 3256.

Most of the invisible mass should be in the form of dark matter. The amount of dark matter is about $4.38 \pm 0.53 \times 10^{10}$ $M_{\odot}$, which is significantly larger than the stellar mass. Dark matter is the dominant mass component for most galaxies and is the fundamental ingredient in determining the properties and evolution of the galaxies. However, dark matter usually dominates in the outer regions of galaxies (refer to Subsection 4.3.8) but is not considered as an important mass component in the central region of galaxies. The discovery of a significant amount of dark matter in the central region of a galaxy might have a significant impact on the MOND theories, which were proposed to explain the "missing mass problem" without using dark matter. In the next section I present the MOND theory.

4.3.7 MOND in the Central Region of NGC 3256

An implication of the MOND theory is that the dark matter phenomena is not expected to be observed in the region of high accelerations where the dynamics should be well described by the normal Newtonian law. However, it was found that the acceleration in the central region of NGC 3256 is about $a = v^2/r \approx 2.45 \times 10^{-7}$ cm s^{-2} at $r = 1.7$ kpc (see Figure 4.7). The derived $\mu(x)$ are ≈ 0.95 and 0.99 for both interpolating functions respectively.

In both cases, the value of $\mu(x)$ are too large to account for the missing mass. Therefore, it might be impossible to explain the mass discrepancy in the centre region of NGC 3256 with the traditional MOND theory. However, it was well known that the standard X_{CO}, which was derived from molecular clouds in the Galactic plane, might over-estimate the molecular mass in the central regions of LIRGs (Hinz & Rieke, 2006). It was suggested that the true conversion factor in LIRGs might be a factor of 5 lower than the standard value. Since NGC 3256 is an LIRG, it might be more accurate to adopt a smaller conversion factor for the molecular gas in the central region of the galaxy. Sakamoto et al. (2014) argued that they did not know the true X_{CO} in NGC 3256 and did not have a strong reason to believe that X_{CO} is constant across the galaxy; therefore Sakamoto used X_{CO}= 3×10^{20} cm^{-2}(K km s^{-1})$^{-1}$ to derive the molecular mass of NGC 3256. It was emphasized that different conversion factors do not affect the findings because X_{CO}= 0.3×10^{20} cm^{-2}(K km s^{-1})$^{-1}$ was used, which is the smallest possible value of X_{CO}. If a different choice of X_{CO} was used X_{CO}= 3×10^{20} cm^{-2}(K km s^{-1})$^{-1}$, the dark matter could be as massive as 75% of the dynamical mass. This also makes it difficult to account for the invisible mass with the MOND theory.

Table 4.3: Radius, total mass, gas mass, stellar mass and baryonic mass. The explanation of the columns: (1) radius; (2) total mass of NGC3256; (3) gas mass; (4) stellar mass and (5) baryonic mass.

Radius (arcsec) (1)	$M_{\rm dyn}\times10^{10}$ ($M_\odot$) **(2)**	$M_{\rm gas}\times10^{9}$ ($M_\odot$) **(3)**	$M_{*}\times10^{9}$ ($M_\odot$) **(4)**	$M_{\rm baryon}\times10^{9}$ ($M_\odot$) **(5)**
0.160	0.023	0.004	0.001	2.005
0.175	0.014	0.004	0.001	2.005
0.189	0.008	0.004	0.001	2.005
0.205	0.002	0.004	0.006	2.010
0.436	0.109	0.012	0.006	2.018
0.618	0.222	0.014	0.017	2.031
0.995	0.496	0.064	0.046	2.110
1.576	0.958	0.078	0.046	2.124
2.465	1.497	0.230	0.271	2.501
3.075	1.856	0.512	0.637	3.149
3.646	2.354	0.642	1.050	3.692
4.334	2.913	0.740	1.456	4.196
5.226	3.539	1.026	1.837	4.862
6.318	3.742	1.255	2.187	5.442
7.318	4.231	1.471	2.187	5.658
7.999	4.628	1.633	2.507	6.140
8.690	5.024	1.655	2.800	6.455
9.988	5.130	2.054	3.069	7.220
10.473	5.531	2.027	3.318	7.345
11.373	4.962	2.031	3.548	7.579
12.266	4.954	2.091	3.548	7.639
12.960	4.962	2.159	3.963	8.122
14.051	4.952	2.249	3.963	8.212
14.945	4.693	2.299	4.151	8.450
15.543	4.321	2.301	4.327	8.628
16.337	4.121	2.383	4.494	8.877
17.229	4.060	2.429	4.652	9.081

4.3.8 The Dark Matter Distribution of NGC 5921

The dark matter distribution has also been studied in the outer region of the spiral galaxy as mentioned previously. So, in this part, this study presents NGC 5921 as an example for this study. NGC 5921 is a barred spiral galaxy (Sbc) with z= 0.0049 at the distance of 22.4 Mpc in the constellation Serpens Caput. Pogge (1989a) has classified it as a LINER, located at position (RA:15h21m56.4s, Dec:+05d04m14s (J2000)) (Hernandez et al., 2005; Saburova et al., 2011). Many previous studies used NGC 5921 as a sample to investigate the physical properties of galaxies with different domains. This study investigates the existence of dark matter in NGC5921 as well as the density profile. Here the data, results and discussion of this work and summary are presented.

4.3.8.1 Data Collection

VLA data. The data of NGC 5921 were obtained from the public archive of the VLA. The source was observed on 13 April 1995 with total integration time of 5280 seconds. The observations were carried out with the D configuration of 27 antennas at the L band, and the spectra were centered at the HI 21-cm line with 63 independent channels in two polarizations (LL and RR) and with a total bandwidth of 1.55 MHz. The data were calibrated and reduced using the CASA software. The continuum data was subtracted from the visibility data using the CASA task "uvcontsub". Image processing was also performed with the CASA Software using the task "clean" with the Briggs weighting. The restoring beam is $51.76'' \times 47.21''$.

2MASS. In this work, the J image of NGC 5921 was only taken from the 2MASS Large Galaxy Atlas Catalog to estimate the radial surface brightness of this galaxy.

4.3.8.2 Results and Discussion

In this work, the observed PV diagram of this galaxy was derived along the major axis of the position angle, which was assumed from Erroz-Ferrer et al. (2015) with $15''$slit width (see Figure 4.11(a)) from the cube image of NGC 5921. To determine the observed rotation curve of NGC 5921 by HI observations, this study adopted the Tiled-Ring Method because the rotation curve cannot be determined straight from the PV diagram.

The inclination angle was estimated from i = $\cos^{-1}(\frac{\text{minor axis}}{\text{major axis}})$ using a 2D/Gaussian fit with CASA 4.1. The results of the inclination angle and other fitting parameters are listed in Table 4.4. The inclination angle (43°) is in good agreement with that determined by

Table 4.4: Properties of NGC 5921.

Property	**Value**
R.A. (J2000)	15h21m56.4s
Dec. (J2000)	+05d04m14s
Morphology	Sbc
Redshift	0.0049
Luminosity distance, D_L	22.6 Mpc
Linear scale	1arcsec= 109.5pc
v_{sys}	1480
Major axis	141.564 arcsec
Minor axis	192.221 arcsec
i	43°

Saburova et al. (2011). The systemic velocity $V_{\rm sys}$ was assumed as 1480 km s^{-1} taken from HI observation by Nordgren et al. (1998). Figure 4.11(b) displays the errorbar plot of the rotation curve of NGC 5921 from HI observation. The rotation curve can be presented as a model of Equation 4.13 which is the sum of the contribution from the disc, halo and gas component (Randriamampandry & Carignan, 2014).

$$V_{total}^2 = V_{disc}^2 + V_{gas}^2 + V_{halo}^2, \tag{4.13}$$

where V_{disk}^2 is the rotation curve of a galaxy from the disc contribution (Distefano et al., 1990), which can be obtained from the equation below.

$$V_{disc}^2 = \sqrt{\frac{0.5GM_D(3.2x)^2(I_oK_o - I_oK_o)}{h}}. \tag{4.14}$$

The modified Bessel functions are evaluated at 1.6x, where x=$\frac{r}{R_{opt}}$ (R_{opt} =3.2 h). Here, h is the scale length of disc and M_D is the disc mass (free parameter). In order to estimate the scale length of disc from the surface brightness profile, the exponential law (Freeman, 1970; Carignan, 1985) was used, expressed as

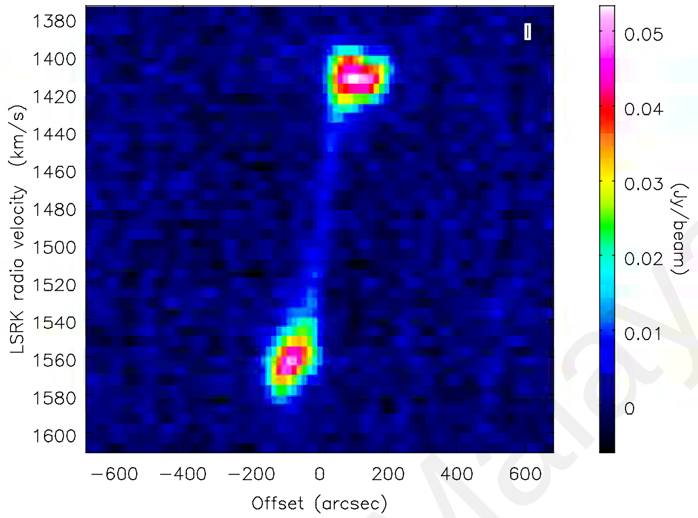

(a)

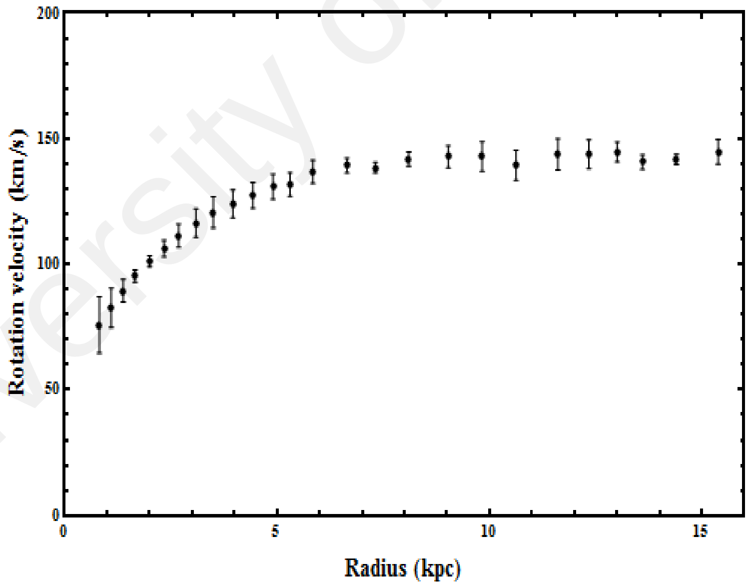

(b)

Figure 4.11: (a) HI Position-Velocity diagram made from the cube map along the major axis. (b)The errorbar plot of the rotation curve of NGC 5921 from HI observation.

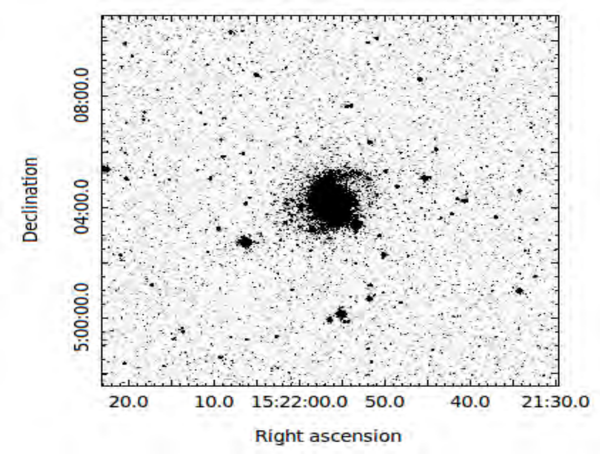

(a)

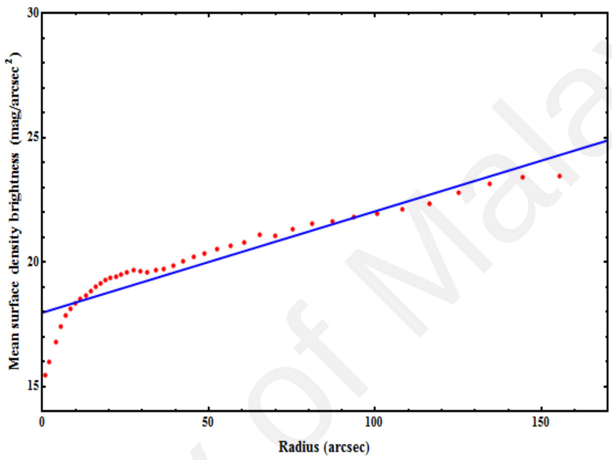

(b)

Figure 4.12: (a) 2MASS image of NGC 5921 at J band.(b)Surface brightness profile of NGC 5921 in J 2MASS image. The solid line represents the fitting line.

$$\mu(r) = \mu_0 + 1.085 \left(\frac{\mathrm{r}}{\mathrm{h}}\right), \tag{4.15}$$

where μ_0 is the central surface brightness of the disc. Measurements of radial profile and scale length give important information on the light density and physical size of galaxies. In this work, the radial profile of NGC 5921 was obtained from 2MASS J band image (Figure 4.12(a)) to derive the luminosity profile. Figure 4.12(b) shows the brightness profile of the 2MASS J band and the fitted exponential law of Equation 4.15. It is a good match to the disc light profile $h \approx 2.9$ kpc (26.67 arcsec) and μ_0 which is approximately 17.96 mag/arcsec.

The gas contribution, V_{gas}, was obtained from $V_{gas} = \sqrt{\frac{GM_{HI}(r)}{r}}$. The total HI mass, M_{HI}, of NGC 5921 was obtained from the equation below (Davies et al., 2001).

$$M_{HI} = 2.4 \times 10^5 D^2 \int S_v dv. \tag{4.16}$$

M_{HI} is in $M_\odot$. D is the distance of the galaxy in Mpc and $\int S_v dv$ is the total integrated flux in units of Jy km s^{-1} from Figure 4.13. Hence, the obtained M_{HI} is about 2×10^9 $M_\odot$ within 16 kpc, which is close to the results of $M_{HI} \approx 1.57 \times 10^9 M_\odot$ from Arecibo and Parkes Observatories (Nordgren et al., 1998). To estimate V_{gas} of NGC 5921, the average HI integrated intensity was first obtained from moment 0 map within concentric elliptical rings at different radii with the task 'IRING' of the Astronomical Image Processing System (AIPS) software. Then, it was converted to HI surface density, $\sigma(r)$, and estimated $M_{HI}(r)$ (and hence, V_{gas}) from $M_{HI}(r) = 2\pi \int_0^r r\sigma(r)dr$.

V_{halo}^2 is the contribution of the dark matter component. In this work, two models of halo were considered, namely, cored and cuspy halos. The cored halo by Burkert (Burkert, 1995) defined the dark component as

$$V_{halo}^2 = 6.4G\frac{\rho_o r_o^3}{r}\left\{ln\left(1 + \frac{r}{r_o}\right) - arctan\left(\frac{r}{r_o}\right) + \frac{1}{2}ln\left(1 + \left(\frac{r}{r_o}\right)^2\right)\right\}, \tag{4.17}$$

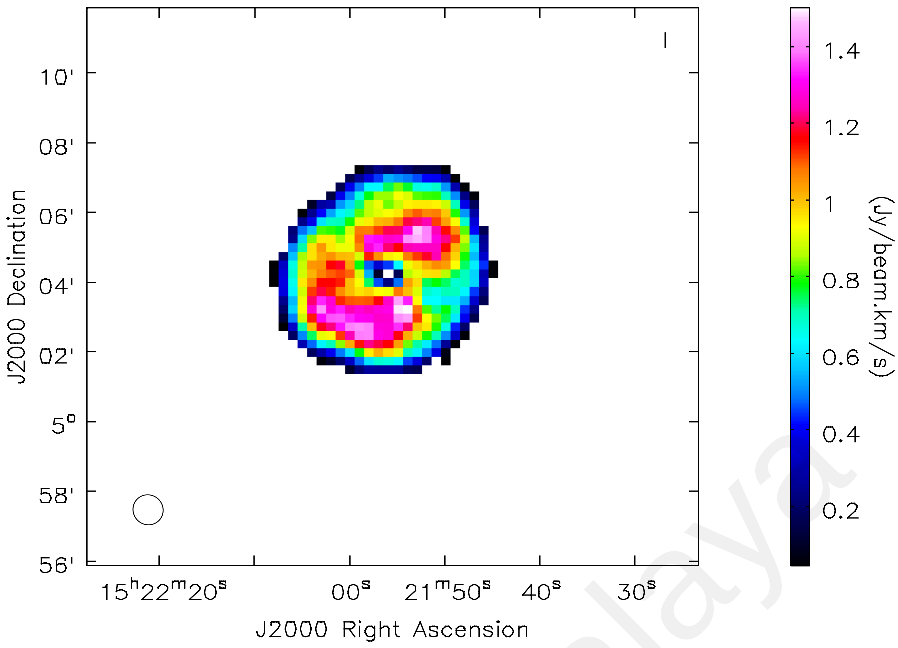

Figure 4.13: HI integrated intensity map of NGC 5921.The synthesized beam is 51.77″x 47.22″(5.62 x 5.12 kpc^2).

with empirical density profile,

$$\rho_{burk}(r) = \frac{\rho_o r_o^2}{(r + r_o)(r^2 + r_o^2)}, \tag{4.18}$$

where the central dark matter density ρ_o and the core radius r_o are free parameters. The dark matter mass of the Burkert halo is expressed by

$$M_{burk}(r) = 6.4G\rho_o r_o^3 \left\{ ln\left(1 + \frac{r}{r_o}\right) - arctan\left(\frac{r}{r_o}\right) + \frac{1}{2} ln\left(1 + \left(\frac{r}{r_o}\right)^2\right)\right\}. \tag{4.19}$$

The cuspy halo was adopted from the NFW dark halo profile, which is known as the universal density profile (Navarro et al., 1997);

$$\rho_{NFW}(r) = \frac{\rho_o}{\left(\frac{r}{r_s}\right)\left(1+\frac{r}{r_s}\right)^2}, \tag{4.20}$$

where r_s is the scale radius. The NFW profile has an inner cuspy form with the density $\rho \propto r^{-1}$ and an outer envelope of the form $\rho \propto r^{-3}$. The corresponding velocity contribution is given by Equation 4.21 and the mass within a sphere can be obtained from the Equation 4.22. Both equations are given below.

$$V^2_{halo} = \frac{4\pi G\rho_o r_s^3}{r}\left\{ln\left(1+\frac{r}{r_s}\right) - \frac{\frac{r}{r_s}}{\left(\frac{r}{r_s}\right)+1}\right\}. \tag{4.21}$$

$$M_{NFW}(r) = 4\pi\rho_o r_s^3\left\{ln\left(1+\frac{r}{r_s}\right) - \frac{\frac{r}{r_s}}{1+\left(\frac{r}{r_s}\right)}\right\}. \tag{4.22}$$

The nonlinear least square method was used in this study to fit the observed data with Equation 4.13 by considering either the Burkert (refer Equation 4.17) or NFW models (refer Equation 4.21). The Mathematica software was used to facilitate our fitting. For model assessment, it is customary to measure how good is the fit between the observed data and the expected data from model. Hence, this work used the chi-square test to minimize the sum of the weighted residuals (see Appendix B).

It is clear from Table 4.5 that the NFW profile provides the best fitting values of the observed data with $\chi^2_{red} \approx 1$, whereas the Burkert halo model gave the value of χ^2_{red} as 3.72. Figure 4.14 illustrates the curve fitting results of the NFW profile. This result shows that the NFW model is able to reproduce the observed rotation curve, and NGC 5921 has a cuspy dark matter distribution (see Figure 4.15). The $M_{NFW}(r)$ was also derived from Equation 4.22 with value around 5.44×10^{10} $M_\odot$. It was found that the value of $M_{NFW}(r)$ is higher than the total luminous mass (i.e. disk and gas) of the whole galaxy. The value of the halo mass provides good information on the efficiency of star formation and stellar

Table 4.5: The free parameters of Burket and NFW models with χ^2_{red} of the fitting.

Model	$M_D[M_\odot]$	$\rho_o[M_\odot \mathrm{kpc}^{-3}]$	r_o[kpc]	r_s[kpc]	χ^2_{red}
Burket	$(9.99 \pm 8.79)\times10^9$	$(1.84 \pm 0.93)\times10^8$	(2.67 ± 0.33)	-	3.72
NFW	$(1.5 \pm 0.29) \times 10^{10}$	$(1.35\pm0.51)\times10^7$	-	(9.57 ± 1.58)	≈ 1

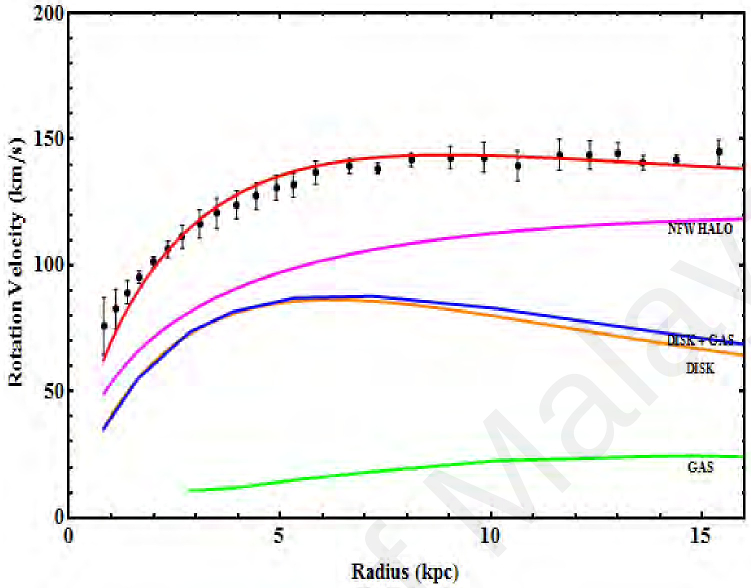

Figure 4.14: Rotation curves of NGC 5921 and NFW halo model. Also shown are the disc, gas and baryonic contributions.

mass assembly in galaxies, in addition to, dominating the total mass. It was found that the expected total mass from the NFW model was in accord with the total mass of NGC 5921 (i.e. $M_{dyn} \sim 8.3 \times 10^{10}$ M$_\odot$) with 86 % accuracy. Rotation curve fitting can be used to constrain the disc mass-to-light ratio of NGC 5921 by $(\frac{M}{L}) = \frac{M_D}{Luminosity}$. Using the total absolute magnitude in the B band (M_B= 20.41) from (Erroz-Ferrer et al., 2015), luminosity, L_B, was estimated to be 2.26$\times$ 10^{10} $L_\odot$. The ratio between the disc mass M_D from the fitting and luminosity of NGC 5921 is ~ 0.66. It is well in agreement with a typical mass-to-light ratio of 0.5 – 2.0.

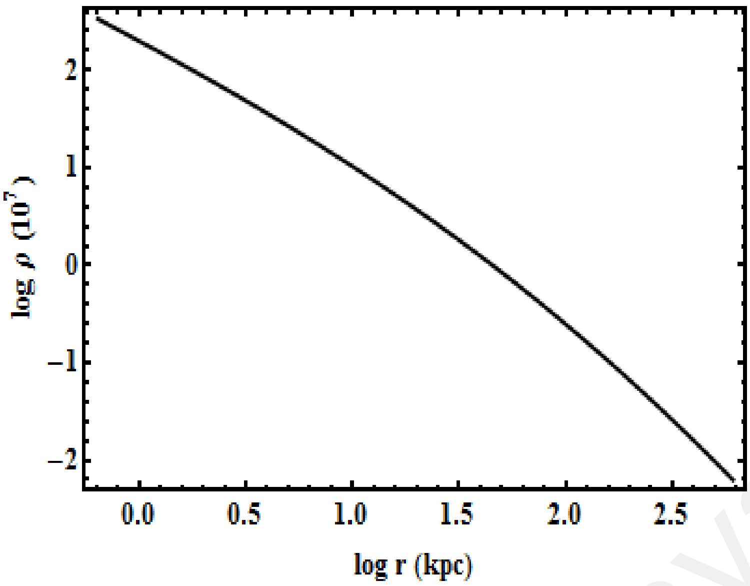

Figure 4.15: NFW density halo profile of NGC 5921.

4.3.8.3 MOND

The MOND formalism shows that the observed rotation curves can be interpreted from the contributions of stellar and gas components (as a function of a_o (Gentile, 2008)), obtained from the following equation

$$V^2_{MOND} = V^2_{bar}(r) + V^2_{bar}(r)\left(\frac{\sqrt{1+\frac{4a_o r}{V^2_{bar}}}-1}{2}\right), \tag{4.23}$$

where $V_{bar} = \sqrt{V^2_{stars} + V^2_{gas}}$.

To estimate the rotation curve of the MOND model, the best value of M_D was considered from the previous section (see Figure 4.16(a)), added the factor k (range from 0.6 to 1.4) to the velocity of baryonic matter, and increased the value of M_D. Figure 4.16(b) displays the observed rotation curve of NGC 5921 and the MOND model with additional factor κ=1 and disc mass range from 1.5×10^{10} $M_\odot$ to 2.3×10^{10} $M_\odot$. It can be seen that the observed data does not fitt well with the MOND profile as illustrated in Table 4.6. Figure 4.16(c) shows the value of M_D =1.5×10^{10} $M_\odot$ and κ=1 produced the best result

Table 4.6: The comparison of the additional factor κ and M_D with χ^2_{red} of the fitting.

Model	$M_D[M_\odot]$	κ	χ^2_{red}
MOND1	1.5×10^{10}	0.6	8.62
		0.8	2.47
		1	0.60
		1.2	7.70
		1.4	21.12
MOND2	1.7×10^{10}	0.6	10.60
		0.8	0.17
		1	3.97
		1.2	16.85
		1.4	36.02
MOND3	1.9×10^{10}	0.6	5.23
		0.8	0.43
		1	9.96
		1.2	28.58
		1.4	53.49
MOND4	2.1×10^{10}	0.6	1.88
		0.8	2.79
		1	18.05
		1.2	42.41
		1.4	73.07
MOND5	2.3×10^{10}	0.6	2.30
		0.8	0.25
		1	6.88
		12	27.88
		1.4	57.88

for the MOND prediction. Generally, the values of χ^2_{red} reveals that the MOND results were incompatible with the observed data of NGC 5921. In other words, the model totally fails to match the observations. If we vary the distance of the galaxy and let the disc mass to be 1.5×10^{10} $M_\odot$ (see Table 4.7), the fits are still unable to reproduce the rotation curve of NGC 5921 (even at all distances) as shown in Figure 4.16(d). The amount of baryonic matter and the distance are the most crucial parameters in estimating the prediction of rotation curve according to the MOND theory. Therefore, both factors are not acceptable for predicting the rotation curve of NGC 5921.

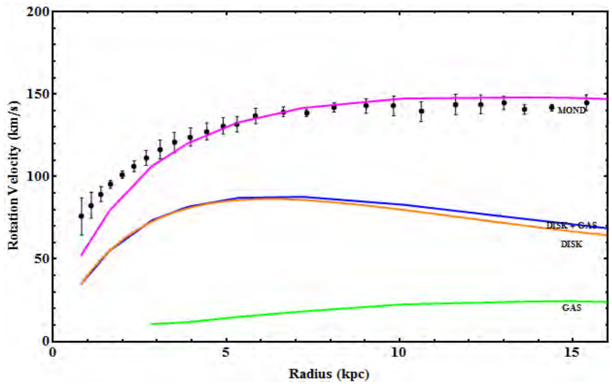

(a)

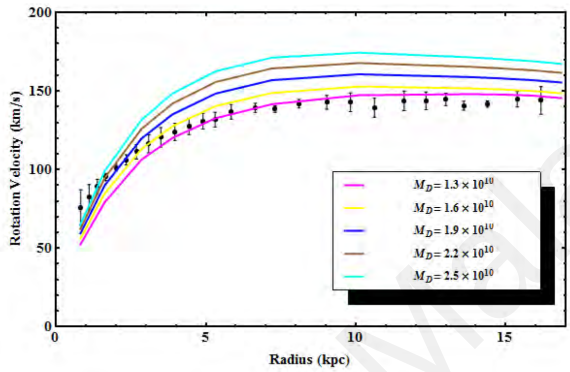

(b)

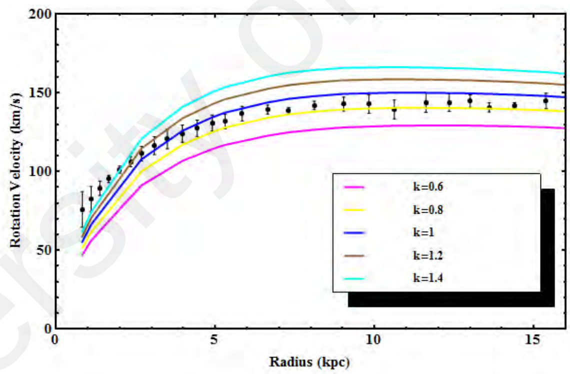

(c)

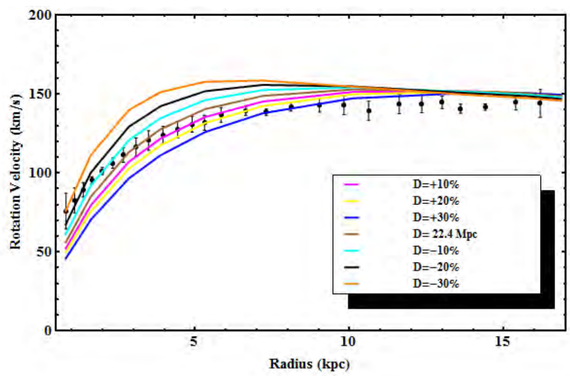

(d)

Figure 4.16: (a) The observed data of NGC 5921 and MOND profile with the disc, HI as well as the total baryonic contributions. (b) The observed data and MOND prediction with disc mass from 1.5×10^{10} to 2.3×10^{10} $M_{\odot}$ and κ=1. (c) The MOND model of NGC 5921 with κ=1 and M_D =1.5 $\times 10^{10}$ $M_{\odot}$. (d) The MOND profile of NGC 5921 for a distance from the galaxy.

Table 4.7: The MOND fit with various value of distance and χ^2_{red}.

Model	$M_D[M_\odot]$	D	χ^2_{red}
MOND	1.5×10^{10}	+10%	0.73
		+20%	0.81
		+30%	0.78
		22.4	0.55
		-10%	0.30
		-20%	0.10
		-30%	0.30

4.3.8.4 Summary

Using the HI data of the spiral galaxy NGG 5921 with various models in this work, it was found that the Burkert model fails to fit the observational data of NGC 5921. Then, this study tried to model our source by assuming a cuspy distribution. The NFW halo produces a good match with the observed rotation curve. This result discloses the existence of dark matter in the outskirt regions of NGC 5921. It was also found that the MOND formalism is not in agreement with the kinematic data even if this study adopts the additional factor k to the baryonic contribution. The rotation curve cannot be reproduced in the MOND model even when the distance of galaxy was changed to be within a certain limit.

CHAPTER 5: DARK MATTER IN THE CENTRAL REGION OF THE SPIRAL GALAXY NGC 4321

5.1 Background

Current cosmology has placed galaxies inside a much larger dark halo. The dynamics of the outer regions of the galaxy is mainly dominated by the dark matter halo. However, the dynamics of the inner regions of the galaxy is much more complicated because the dynamics is also affected by the dark matter distribution, the central super massive black holes, and the stellar bulges in the central regions of the galaxy. Besides, the acceleration in the inner regions of a galaxy is expected to be rather strong because of its relatively small size and mass concentration. Therefore, the inner regions of galaxies might provide us a platform to distinguish the influence of dark matter from that of MOND.

As mentioned in the previous chapter, the discrepancies between the total mass and the baryonic mass can be explained the dark component. This component may be found in the NGC 4321 galaxy as well. Therefore, in this chapter we will investigate the dark matter in this late-type galaxy. M100 (=NGC 4321) is one of the brightest spiral galaxy (SAB(s)bc galaxy) in the Virgo cluster (see Figure 5.1). M100 is tilted nearly face-on as observed from Earth with relative proximity (16.1 Mpc; Ferrarese et al. (1996)). M100 has two symmetric and well-defined spiral arms. The nucleus of the galaxy is bright and compact; the galaxy was also classified as an HII/LINER (Ho et al., 1997). M100 has received a lot of observational and theoretical attention because its moderate inclination and proximity, which make it easier to investigate the content, distribution, and kinematics of its interstellar medium and stellar components of this galaxy; the circumnuclear region of NGC 4321 has also been observed with various wavebands (e.g., (Sérsic & Pastoriza, 1967; Pogge, 1989b; Knapen, 1998)).

The study of the DM for this object need to be complemented by the CO(1-0) observations

Figure 5.1: ESO image of NGC 4321 galaxy with size:1800 $\times$ 1802 px. Image credit: ESO.

of ALMA and the photometry data obtained by the 2MASS database. In detail, the structure of this chapter is in the ensuing sections as follows: data selection will be revealed in Section 5.2; the results and discussion of NGC 4321 galaxy will be conducted in Section 5.3; the mass distribution in the central region ($r \lesssim 0.7$ kpc) of NGC 4321 will be performed in Subsection 5.3.7.

5.2 Data Collection

5.2.1 CO Data

The ALMA data of NGC 4321 were obtained from the ALMA science verification (SV) data. The galaxy was mapped at the CO (J=1–0) transition within the Band 3 receiver of the ALMA. There are three sets of observations of ALMA data; the first set was observed with the 12-m array on August 10 and September 10, 2011. The observation formed of 47 pointing mosaics centered at RA= 12h22m54.6s, Dec=+15°48′56.5″ with four spectral windows. The beam size of the 12-m alone observation was 3.46″× 2.37″. The second one, the data taken for NGC 4321 with 7-m array on March 17–18, April 14 and May 11, 2013, consisted of 23 pointing mosaics centered at RA= 12h22m54.3s, Dec= +15°48′51.4″ with either two or four central windows with the beam size 12.72″× 10.12″. The third one is the single dish data for NGC 4321, which was taken on July 1, 5, 7 and 17, 2014, with a total power array with a beam size 56.9″× 56.9″. The full description of the data reduction and the combination of the three observing modes can be found in the CASA 4.1 guide for this specific data set[1].

The resulting beam size of the CO image of NGC 4321 is ≈ 3.87″ × 2.53″. The angular-to-linear scale is ∼ 78 pc at 16.1 Mpc. The Image analysis was done using the CASA software.

5.2.2 HI Data

The HI data of NGC 4321 was obtained from the public archive of the VLA. The source was observed on 25-30 March 2003 with total integration time of 451560 seconds The observations were carried with the D configuration of 28 antennas at the L band, and the spectra were centered at the HI 21-cm line with 63 independent channels in two polarizations (LL and RR) and with a total bandwidth of 2.71 MHz. The observation parameters are listed in Table 5.1. Image processing was also performed with the CASA software using the task "clean" with briggs weighting. The restoring beam is 31.11″ × 28.10″ with PA=−26°.

[1]https://casaguides.nrao.edu/index.php/M100_Band3.

Table 5.1: VLA Observational Parameters of NGC 4321.

Parameter	Value
Target	NGC 34321
Observing date	25-30-March-2003
Total integration time	451560 seconds
Field center:	
R.A.(J2000)	12h22m54.89s
Dec.(J2000)	$+15°49'20.7''$
Number of antenna	28
Rest frequency	1420.40575 MHz
Restoring beam	(major, minor, P.A.)
	$(31.11'', 28.10'', -26°.$
Channel width	43.015 kHz
Total bandwidth	2710 kHz
Total channels	63
Velocity resolution	10 km s^{-1}

5.3 The Results and Discussion

5.3.1 Line Emission Distribution

The integrated intensity (i.e., mom0) map of the CO line of NGC 4321 is shown in Figure 5.2. High resolution CO (J=1–0) observations show two spiral arms and gas in the nucleus as well as faint emission bridging the arms. Figure 5.3 shows an integrated-intensity image of the the HI gas, which is derived from the Briggs weighted channel map. The spiral arm could not be detected because of poor resolution of these data.

Figure 5.4 shows the channel maps of the CO Line in the central region of NGC 4321. The channel width is 5 km s^{-1}, and the channel noise is about 16 mJybeam^{-1}.

5.3.2 The Total Mass of NGC 4321

The total mass in disk galaxies is typically determined from resolved rotation curves, depending on the distribution of the mass in the galaxy. Spiral galaxies are generally thought to consist of the superposition of a flat disk and spherical components (a central bulge and a massive halo) (Lequeux, 1983). For the observed velocity, the actual mass is intermidate between the assumption of a pure spherical mass distribution and that of a pure

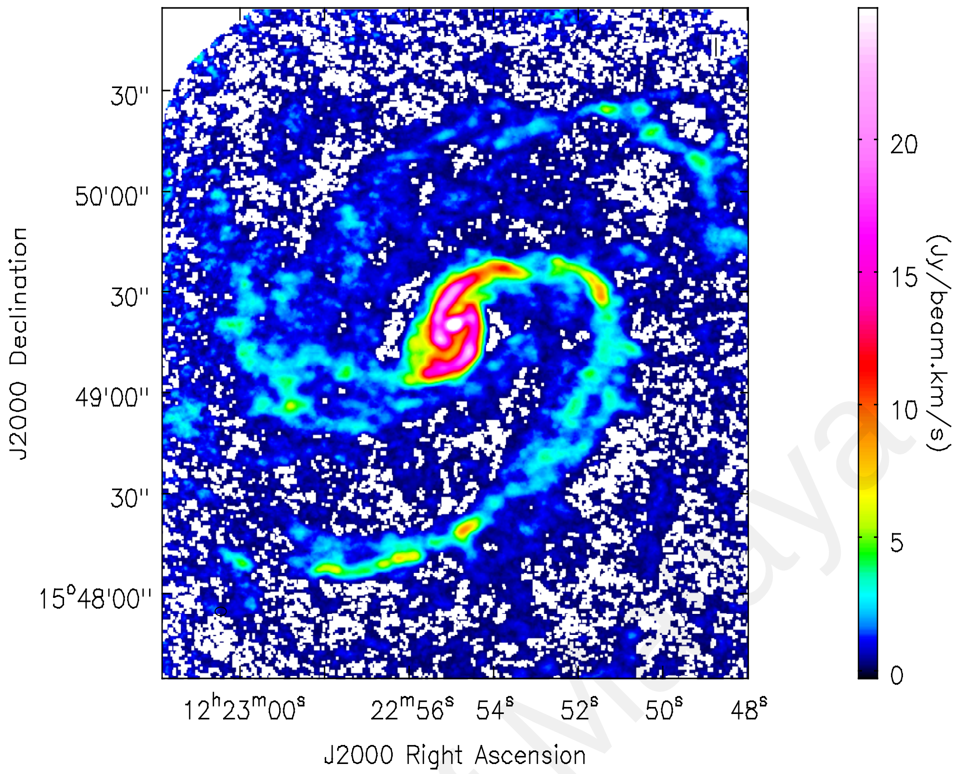

Figure 5.2: Integrated intensity map of the CO(1-0) line emission of NGC 4321. The color scale range is shown in the wedge at right in units of Jy beam^{-1}km s^{-1}. The synthesized beam is 3.87″ × 2.53″.

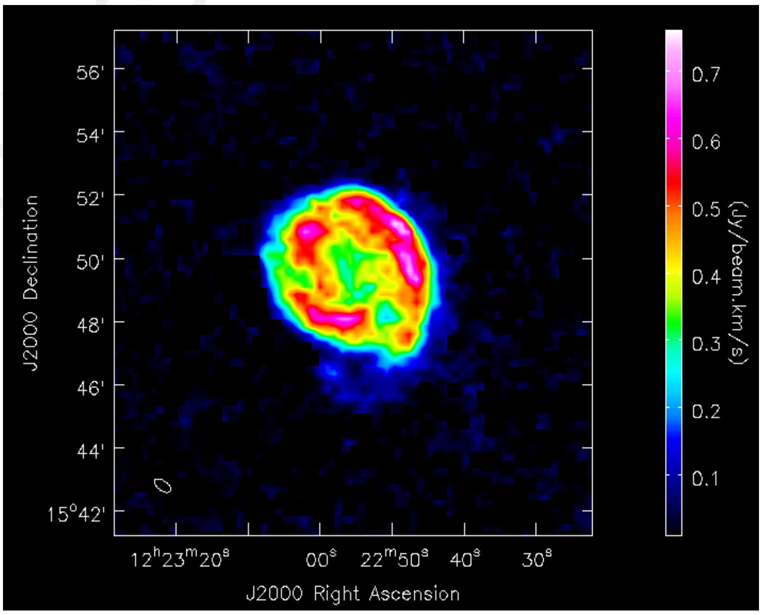

Figure 5.3: mom0 map of HI observatins of NGC 4321. The color scale range is shown in the wedge at right in units of Jy beam^{-1}km s^{-1}. The synthesized beam is 31.11″× 28.10″.

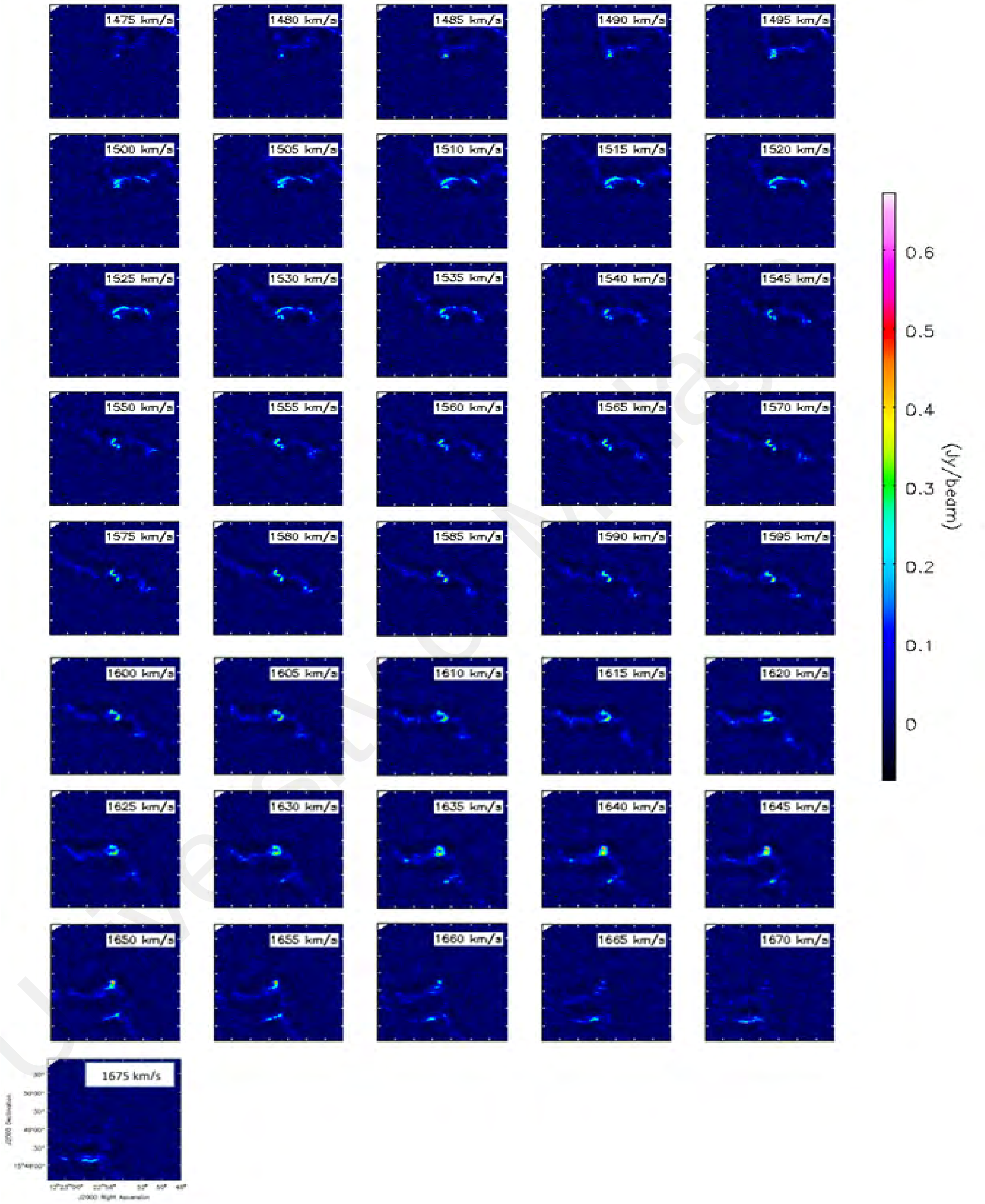

Figure 5.4: Channel maps of the CO(1-0) line emission in the central region of NGC 4321. The color scale range is shown in the wedge at right in units of Jybeam^{-1}.

flat distribution because the gravitaional potential is a linear function of mass. Therefore, the total mass inside a given radius r can be measured by the speed at that radius, following the Kepler formula (Equation 4.3)

The central rotation curve of NGC 4321 was constructed using the PV diagrams generated from the CO line emission. This diagram displays how the gas velocity change with position along line-of-sight. Figure 5.5 shows examples of the PV diagrams of the CO line emission, where the spectra have been smoothed to a velocity resolution of 5 km s^{-1}.

Figure 5.5(d) shows the PV diagram along the major axis of the galaxy (PA= 151°); it is obvious that the galaxy tend to show a linear increasing of the rotation velocity in the most inner central regions and becomes nearly constant in the outer regions. Note that the "outer" region here is still within the central 1 kpc of the galaxy. The colors indicate the intensity of the emission distributed along the line-of-sight.

Further, as in Subsection 4.3.2, the rotation curve of the galaxy in Equation 4.2 will be obtained from the observed line-of-sight velocities by correcting the inclination angle of the disk plane with the systemic velocity of the galaxy. In this work, the inclination angle was assumed to be 30° (Castillo-Morales et al., 2007) and V_{sys} of 1575 km s^{-1} from Knapen et al. (1997) (see Table 5.2). Figure 5.6 shows the rotation curve of NGC 4321 derived from the CO(1-0) PV diagram along the major axis of the galaxy (PA = 151°). The errorbars are standard deviation of velocity field (mom1) map (see Figure 5.7), which is represented poisson uncertainties. The dynamic mass M_{tot} is estimated to be around $1.02 \pm 0.04 \times 10^{10}$ $M_{\odot}$ within the central radius of 0.7 kpc (9″).

5.3.3 The Gas Mass

The gas mass can be obtained from the following formula (Rahmani et al., 2016):

$$M_{\mathrm{gas}} = 1.36[M_{\mathrm{HI}} + M_{\mathrm{H_2}}]\ \mathrm{M}_{\odot}, \tag{5.1}$$

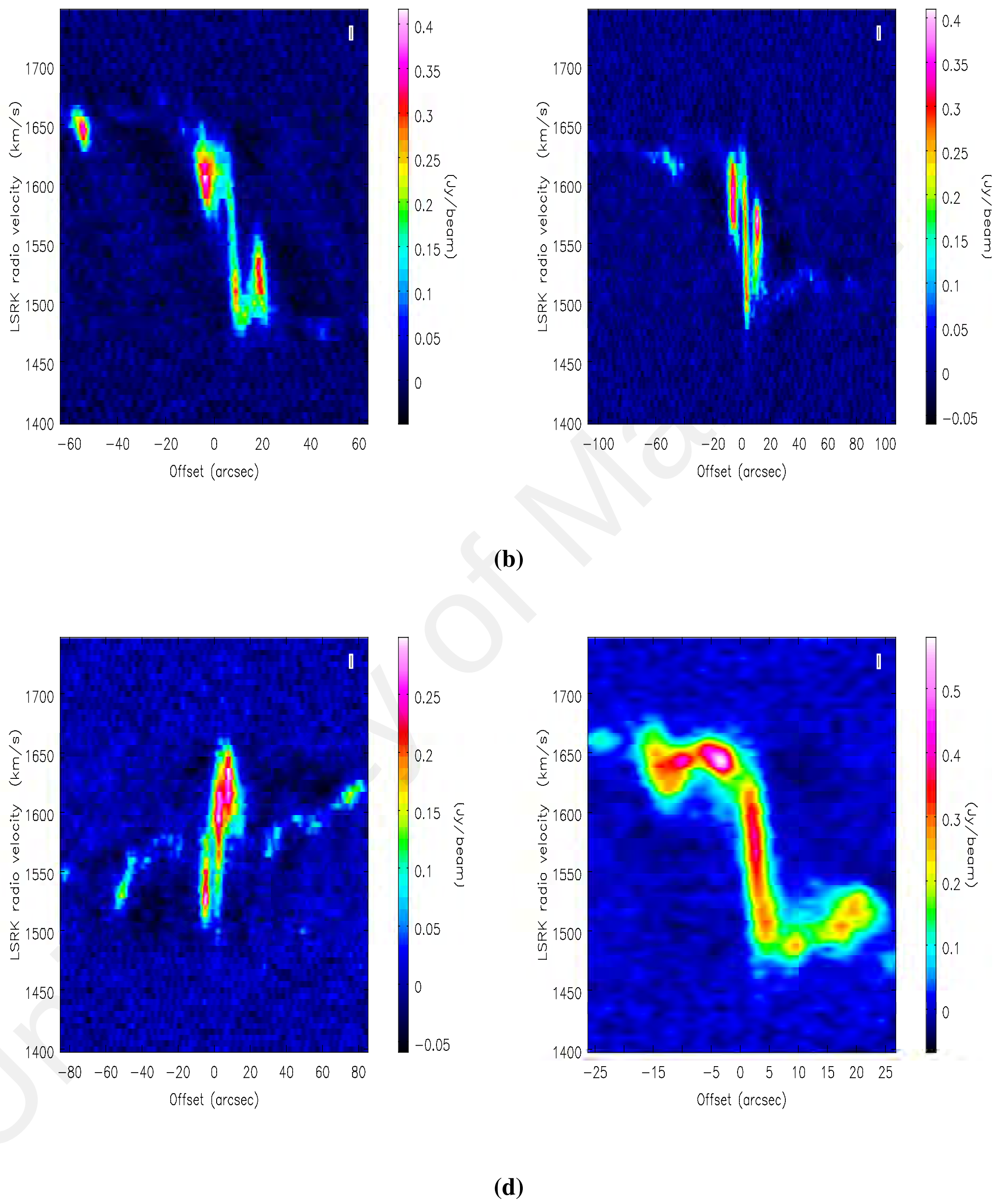

Figure 5.5: CO Position-Velocity diagrams of NGC 4321 passing the nucleus along different PA angles. (a) PV diagram along PA= 0°, (b) PV diagram along PA= 30°, (c) PV diagram along PA= 90° and (d) PV diagram along PA= 151°. Each PV cut has a slit width of 1″.

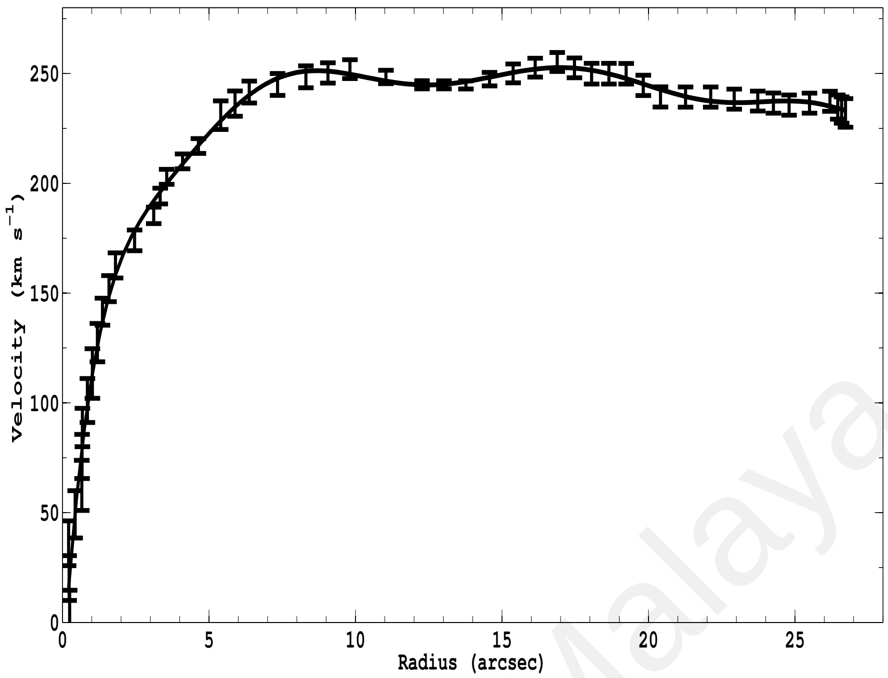

Figure 5.6: The rotation curve of NGC 4321 obtained from PV diagram of Figure 2d. Dots with errorbars are the observed data and the solid curve is the fitting. The error bars are the standared deviations from the (mom1) map.

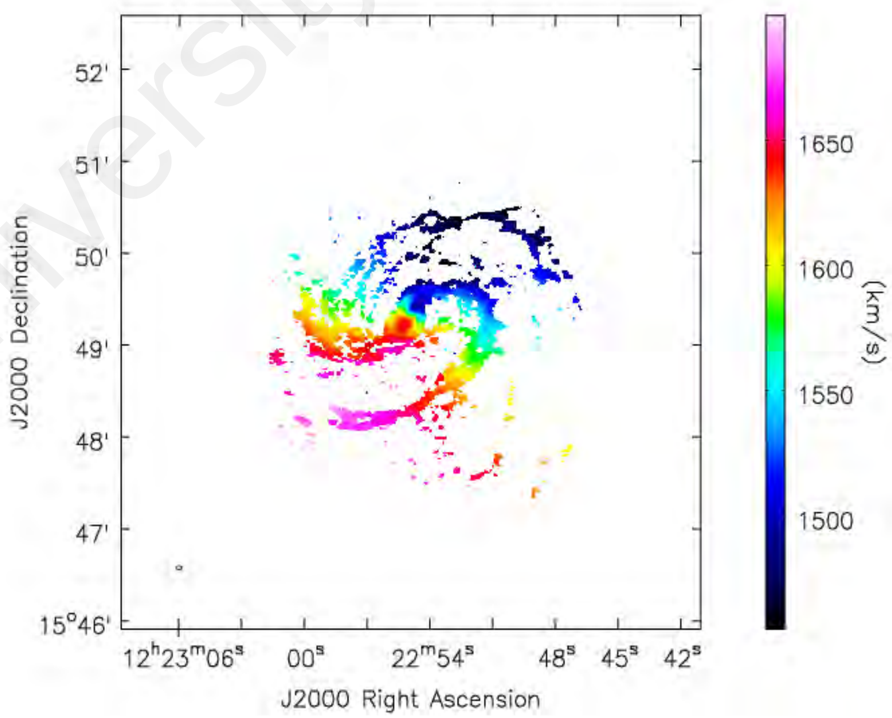

Figure 5.7: The CO(1-0) velocity field map of NGC 4321.

Table 5.2: Galaxy properties for NGC 4321.

Parameter	Value
R.A.(2000)	12h22m54.8s
Dec.(2000)	$15°49'19''$
Adopted distance	16.1 Mpc
Inclination	30°
PA	151°
Systemic velocity	1575 km s^{-1}

where the factor 1.36 is a constant to include the contributions of He and the other heavier elements to the gas mass.

The mass of atomic neutral hydrogen was obtained from the HI 21 cm emission line (see Figure 5.3). The HI mass can be derived from the HI flux using the Equation 4.16 (Davies et al., 2001; Liu et al., 2015). Since the resolution of the HI image is about $30''$, the HI flux was estimated within the central $1'$ region of the galaxy. The flux was found to be around 2.36 ± 0.12 Jy km s^{-1}, which corresponds to an HI mass of $1.4 \pm 0.07 \times 10^8$ $M_\odot$. This is the total HI mass within the central $1'$ region and is the upper limit of the HI mass within the central region of our investigation.

The molecular gas mass, M_{H_2} was derived from the observed ALMA CO flux (Tsai et al., 2009). This study adopted $X_{CO} = 2.2 \times 10^{20}$ cm^{-2} (K km s^{-1})$^{-1}$ from García-Burillo et al. (2005). The total flux is 408 ± 6 Jy km s^{-1} within the central $18'' \times 18''$ region of NGC 4321; and the M_{H_2} is estimated to be $9 \pm 0.13 \times 10^8$ $M_\odot$. If the region was extended to include the CO flux within a $30''$ (2.4 kpc) radius, it was found that the molecular mass becomes $M_{H_2} \approx 3 \times 10^9$ $M_\odot$, which is close to the values obtained with single-dish observations (Garcıa-Burillo et al., 1998). This suggests that the missing flux of the ALMA observations is negligible.

It can be seen that moelcular gas mass is higher than atomic gas mass in centre region of galaxy. The reason that M_{H_2} seeks galaxy centers, and HI avoids them (Israel, 2008).

The central kiloparsec is usually completely dominated by H_2. This dominance decreases when going outward, and the outermost parts of spiral galaxies contain atomic gas almost exclusively (Sofue, 1996; Sofue, 2001; Israel, 2008). However, the total gas mass of NGC 4321 within the central 0.7 kpc radius, including atomic gas, molecular gas, and metal contributions, is thus about $1.4 \pm 0.21 \times 10^9\ M_\odot$.

5.3.4 The stellar Mass

Surface photometry and the examination of radial surface brightness profile are the first step towards identifying the various components of a galaxy and determing their masses. The radial surface brightness profile of NGC 4321 has been extracted from surface photometry data to derive the luminositu profile. The data was taken from 2MASS database at Ks band of the 2MASS All-Sky XSC as shown in Figure 5.8. Such luminosity profile was fitted well with a modified Hubble law (Equation 4.6). Figure 5.9 shows the brightness profile of the 2MASSS Ks image of NGC 4321 and the fitted modified Hubble profile. The de-projected flux was converted to apparent magnitude within the selected galactic region. Then the Equation 4.9 was used to estimate the $M_K \approx$ -18.79 of NGC 4321. It was assumed that the absolute magnitude of the Sun at the Ks band is 3.39 (Mulroy et al., 2014; Johnson, 1966), and the mass-to-luminosity relation is $M/L = 0.45$ (Wada et al., 1998). The derived stellar mass is about $(3.3 \pm 0.03) \times 10^8 M_\odot$ within the central 0.7 kpc of NGC 4321.

$$M_* = 0.45 \times 10^{-0.4(M_K - 3.39)}\ M_\odot \tag{5.2}$$

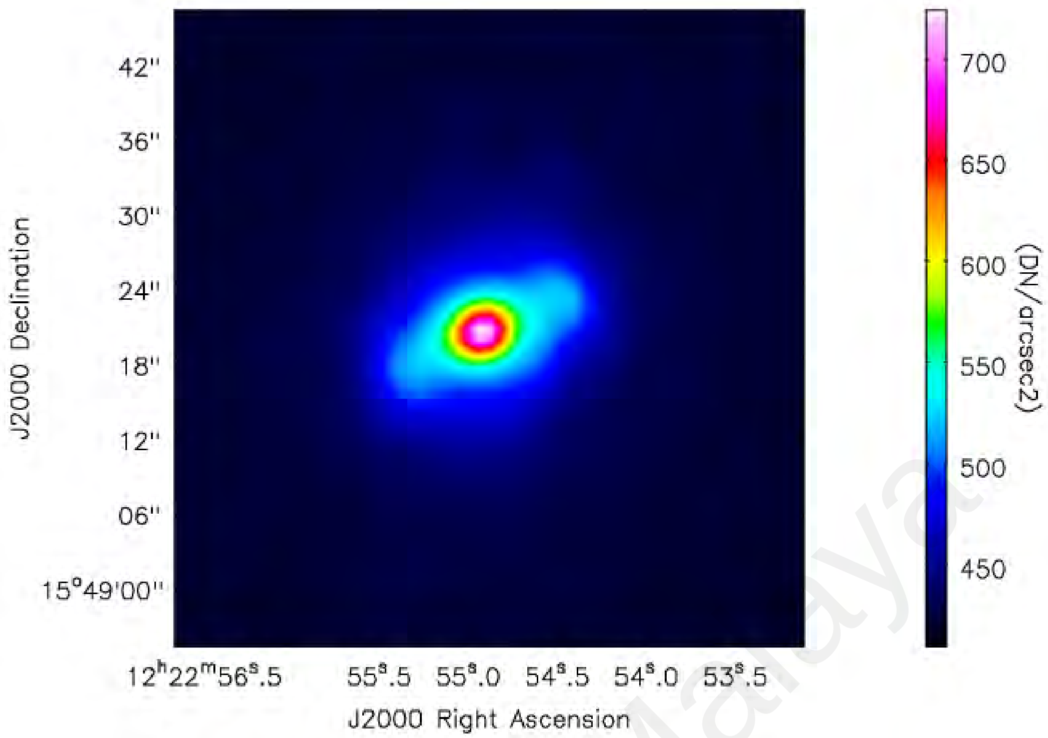

Figure 5.8: Near-IR image of NGC 4321 in the 2MASS Ks-band.

5.3.5 Dust Mass

The dust mass of NGC 4321 was obtained by using the integrated MIPS data at 24 μm, 70 μm, and 160 μm using the following relation given by Muñoz-Mateos et al. (2009), i.e.,

$$\frac{M_{dust}}{M_\odot} = \frac{4\pi}{1.616 \times 10^{-13}} \left(\frac{D}{Mpc}\right)^2 \left(\frac{\langle \nu F_\nu \rangle_{70}}{\langle \nu F_\nu \rangle_{160}}\right)^{-1.801}$$
$$\times (1.559\langle \nu F_\nu \rangle_{24} + 0.7686\langle \nu F_\nu \rangle_{70} + 1.347\langle \nu F_\nu \rangle_{160}), \quad (5.3)$$

where $\langle \nu F_\nu \rangle_{24}$, $\langle \nu F_\nu \rangle_{70}$ and $\langle \nu F_\nu \rangle_{160}$ are the MIPS flux densities (in erg s^{-1}cm^{-2}) at 24μm, 70μm and 160μm, respectively. Thus, it was found the dust mass to be approximately 3×10^6 $M_\odot$. Using the IRAS flux densities at 60μm and 100μm (Equation 4.11), the dust mass is similar to the result of M_{dust} from the MIPS flux densities.

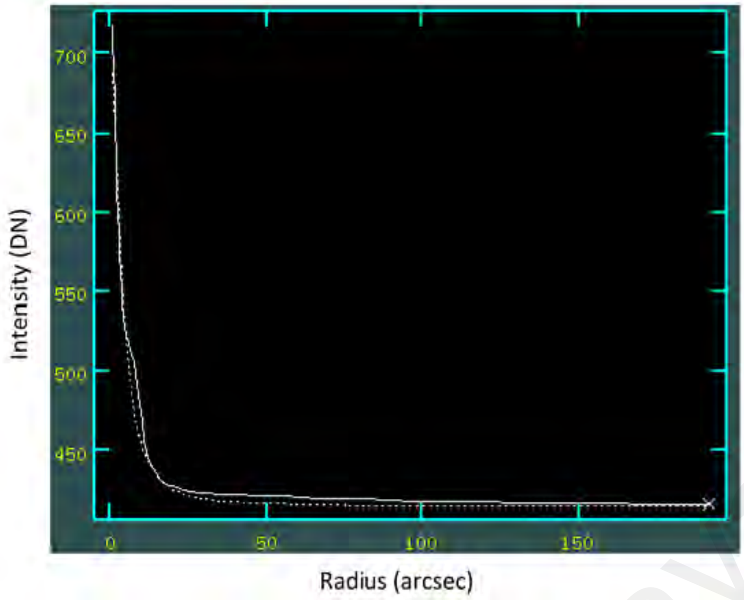

Figure 5.9: Surface brightness profile of NGC 4321 in 2MASS Ks image. The dashed line (fitting plot) is the modified Hubble law match with r_0 = 3.99 arcsec and I_0 = 250 Data Number, DN, within central raduis of 9″.

5.3.6 Supermassive Black Hole Mass

The relation of central black hole mass and bulge luminosity implies that there is a correlation between the black hole and bulge masses for nearby galaxies (Magorrian et al., 1998; Ho & Chakrabarti, 1999; Wu & Han, 2001). In order to estiamte the mass of the SMBH in NGC 4321 by the Luminosity relation, the total absolute B magnitude M_B^{total} of NGC 4321 was evaluated about -20.98 from total apparent magnitude of 10.05, m_b (Sarzi et al., 2002). The absolute bulge B magnitude M_B^{bulge} was estimated based on the relation between M_B^{bulge} and M_B^{total} (Simien & De Vaucouleurs, 1986) and the Hubble stages (defined in de Vaucouleurs et al. (1976)) to be -19. Then M_B^{bulge} of NGC 4321 was translated to the absolute bulge V magnitude, M_V^{bulge} by using the relation $B-V = 0.8$. This study obtained the bulge luminosity in units of $L_\odot$ using the standard relation (Gültekin et al., 2009).

$$\mathrm{Log}(L_{bulge}/L_\odot) = 0.4\ (-M_V^{bulge} + 4.83) \tag{5.4}$$

To find the bulge mass, the relation between the bulge mass and luminosity was used

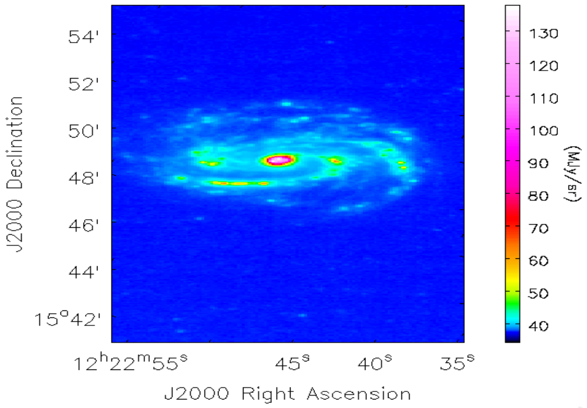

(a)

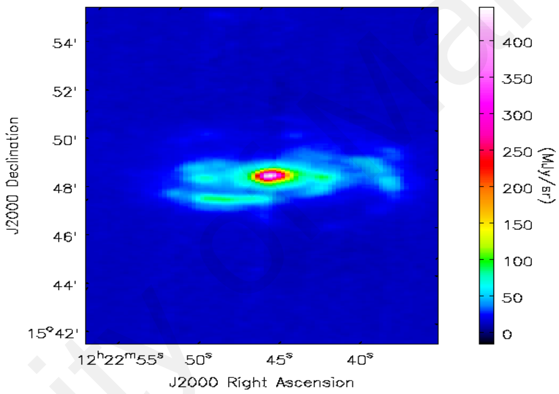

(b)

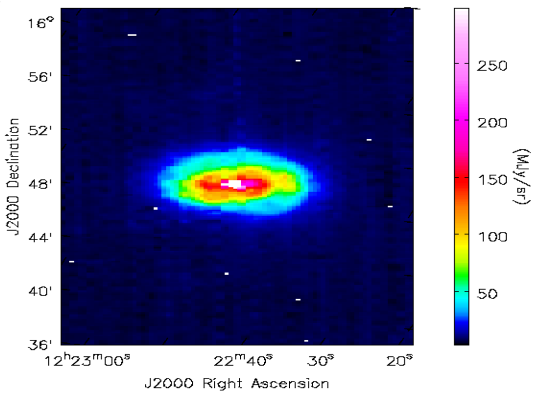

(c)

Figure 5.10: MIPS image of NGC 4321 at (a) 24μm, (b) 70μm and (c) at 160 μm respectively.

(Magorrian et al., 1998; Wandel, 2002),

$$\mathrm{Log}(\mathrm{M_{bulge}}/\mathrm{M_{\odot}}) = 1.18\ log\ (\mathrm{L_{bulge}}/L_{\odot}) - 1.11 \tag{5.5}$$

Then the SMBH mass for NGC 4321 can be obtained from (Wu & Han, 2001)

$$\mathrm{Log}(\mathrm{M_{BH}}/\mathrm{M_{bulge}}) = (-11.06 \pm 1.11)+(0.74 \pm 0.14)\ \log(\mathrm{M_{bulge}}/M_{\odot}) \tag{5.6}$$

Where -11.06 ± 1.11 *and* 0.74 ± 0.14 are cofficients of the linear fit, thus Log $\mathrm{M_{BH}}$ is about 7.1 $M_{\odot}$ for NGC 4321. From Figure 5.11, NGC 4321 is still within the intrinsic scatter, which is located slightly above the $\mathrm{M_v}$(bulge)- Log $\mathrm{M_{BH}}$ relation. This result of the $\mathrm{M_v}$(bulge) relation is close to the results of Sarzi et al. (2002), who derived upper limits of Log $\mathrm{M_{BH}}$ to be 7.3 from the modeling of the central emission-line widths.

5.3.7 Dark Matter in the Central Region of NGC 4321

In comparison to all the mass components derived, it was found that the invisible mass in the central region of NGC 4321 is about $8.5\pm0.2\times 10^9$ $\mathrm{M_{\odot}}$. Most of the invisible mass should be the dark matter, with the fraction of the dark matter being about 83% of the dynamical mass within the central 0.7 kpc radius of NGC 4321. It turns out from Figure 5.12 that the total mass extends further than the baryonic matter. From the discrepancy between the total mass and the baryonic one from the stars and gas, the existence of a dark halo is inferred. The values presented in Table 5.3 are the total and the baryonic masses of NGC 4321.

The mass distribution in the centre of such systems is the key to understanding galaxy

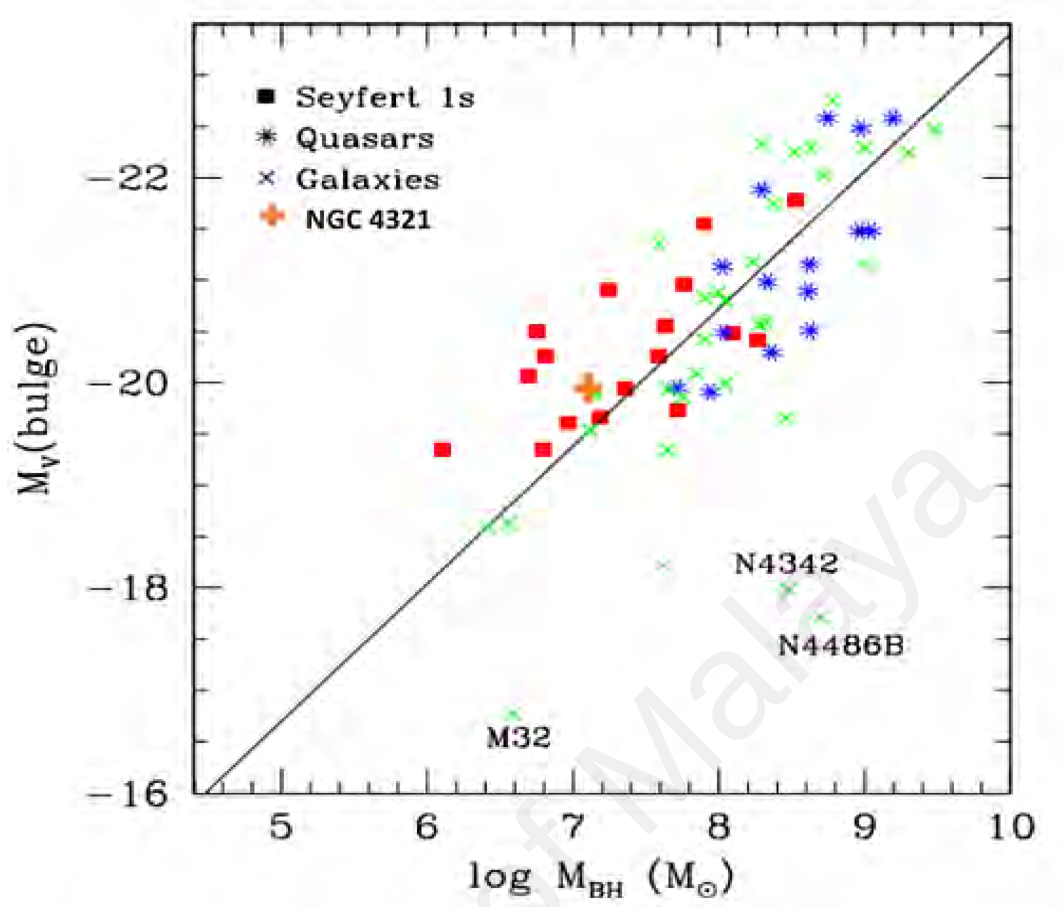

Figure 5.11: M_v(bulge)- Log M_{BH} diagram. NGC 4321 is plotted as a + along with the sampling data of Wu & Han (2001).

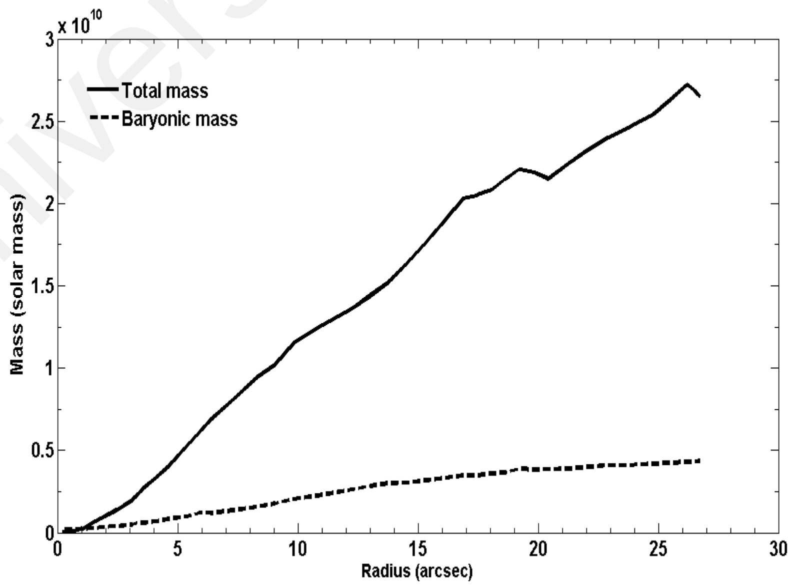

Figure 5.12: Discrepancy between the total mass and the baryonic mass of NGC 4321 galaxy.

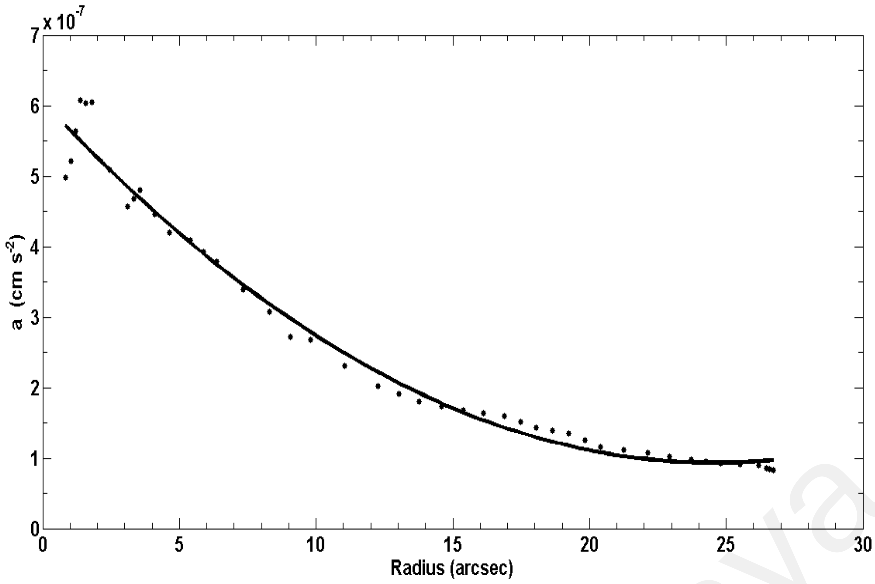

Figure 5.13: Accelerations of NGC 4321 galaxy as a function of radius. Solid line represents a second order polynomial fit. Note that higher accelerations occur at smaller radii.

formation. New studies are providing evidence for the presence of dark matter in the innermost part of galaxies (e.g. Milky Way). They claimed that large amounts of dark matter exist in the inner region of Milky Way (Iocco et al., 2015). In this chapter, I also applied the MOND theory to know whether MOND can explain the dark matter in the central region (r=0.7 kpc) of NGC 4321.

For NGC 4321, $a = v^2/r \approx 29.2 \times 10^{-8}$ cm s^{-2} is found at approximately 0.7 kpc, and v is about 250 km s^{-1} (see Figure 5.6). The obtained $\mu(x)$ are $\approx$ 0.96 and 0.99 for both interpolating functions. The $\mu(x)$ values indicate that it might be impossible to interpret the unseen matter using the MOND theory in the central region of NGC 4321 because of the relatively strong acceleration in the central region of (see Figure 5.13).

Table 5.3: Radius, total mass, gas mass, stellar mass and baryonic mass. The explanation of the columns: (1) radius; (2) total mass of NGC3256; (3) gas mass; (4) stellar mass and (5) baryonic mass.

Radius (arcsec) (1)	$M_{dyn}\times10^{10}$ ($M_\odot$) (2)	$M_{gas}\times10^{9}$ ($M_\odot$) (3)	$M_{*}\times10^{8}$ ($M_\odot$) (4)	$M_{baryon}\times10^{9}$ ($M_\odot$) (5)
0.434	0.002	0.200	0.012	0.201
0.658	0.005	0.200	0.012	0.201
0.669	0.007	0.200	0.012	0.201
0.680	0.010	0.200	0.027	0.203
0.850	0.016	0.215	0.051	0.220
1.021	0.024	0.218	0.051	0.223
1.193	0.036	0.218	0.051	0.223
1.588	0.068	0.254	0.158	0.270
1.810	0.088	0.290	0.338	0.324
2.462	0.137	0.343	0.585	0.401
3.114	0.197	0.403	0.886	0.492
3.336	0.232	0.468	1.227	0.591
3.557	0.270	0.474	1.227	0.597
4.098	0.333	0.541	1.593	0.700
5.401	0.531	0.700	2.745	0.974
5.887	0.606	0.874	3.127	1.186
6.374	0.685	0.874	3.127	1.186
7.341	0.812	1.063	3.146	1.377
8.308	0.945	1.255	3.245	1.579
9.059	1.023	1.431	3.332	1.764
9.811	1.148	1.606	4.403	2.046
11.040	1.255	1.770	5.403	2.311
12.269	1.355	1.929	6.939	2.623
13.019	1.438	2.078	7.682	2.846
14.575	1.644	2.216	8.141	3.030
15.381	1.772	2.338	8.361	3.174
16.133	1.897	2.447	8.782	3.326
16.885	2.027	2.548	9.182	3.466
17.472	2.054	2.548	9.374	3.485
18.059	2.079	2.646	9.561	3.602
18.648	2.146	2.670	9.744	3.644
19.238	2.214	2.883	9.922	3.876
19.823	2.185	2.801	10.266	3.828
20.408	2.153	2.801	10.595	3.861
21.265	2.243	2.813	10.754	3.889
22.122	2.333	2.914	10.910	4.005
22.925	2.399	2.963	11.212	4.084
23.728	2.465	2.963	11.358	4.099
24.263	2.501	3.008	11.502	4.159
24.798	2.537	3.008	11.780	4.186
25.495	2.627	3.048	11.916	4.240
26.192	2.719	3.082	12.049	4.287
26.590	2.668	3.112	12.149	4.327

CHAPTER 6: CONCLUSIONS AND SUMMARY

6.1 Conclusions

Undoubtedly, the dark matter problem in galaxies is one of the interesting and important problems of modern astrophysics. The distribution of luminous and dark matter in galaxies shows interesting properties and behavior systematics that make it one of the frontier issues in cosmology. The following describes the main results that have been obtained from the studies of spiral galaxies of different Hubble type, mass and luminosities. These results clearly show that there is mass distribution in the central regions of spiral galaxies.

This study reported the mass distributions of late-type galaxies, i.e, NGC 3256 and NGC 4321 using ALMA observations and the NIR data of 2MASS. The PV diagram was first considered to estimate the projected rotation curves of NGC 3256 and NGC 4321. This study found that the projected rotation curves are 184±5 km s^{-1} at 10″and 125±4.63 km s^{-1} at 9″ for NGC 3256 and NGC 4321 respectively. The projected rotation curves of these objects are shown in Figure 6.1. Each object is representative of a different structural type: Sb(pec) and SAB(s)bc, respectively. The total mass for each object, as derived, is $5.1 \pm 0.2 \times 10^{10}$ $M_\odot$ and $1.02 \pm 0.04 \times 10^{10}$ $M_\odot$ (see Table 6.1). NGC 4321 contains around 20% of the dynamical mass of NGC 3256, and has a lower maximum rotation speed of 250±4.63 km s^{-1}, in comparison to 368±5 km s^{-1} for NGC 3256.

Using the observed ALMA CO flux and X_{CO}, the molecular gas mass has been estimated to be $(1.51 \pm 0.34) \times 10^9$ $M_\odot$ within within the central region (r~1.7 kpc) of NGC 2356, where the X_{CO} is 0.3×10^{20} $cm^{-2}(K\ km\ s^{-1})^{-1}$. This result for the molecular mass is in agreement with with those derived by Sakamoto et al. (2014). For NGC 4321, M_{H_2} is estimated to be $(9 \pm 0.13) \times 10^8$ $M_\odot$ at the radius of 0.7 kpc and assuming $X_{CO} \approx 2.2 \times 10^{20}$ $cm^{-2}(K\ km\ s^{-1})^{-1}$.

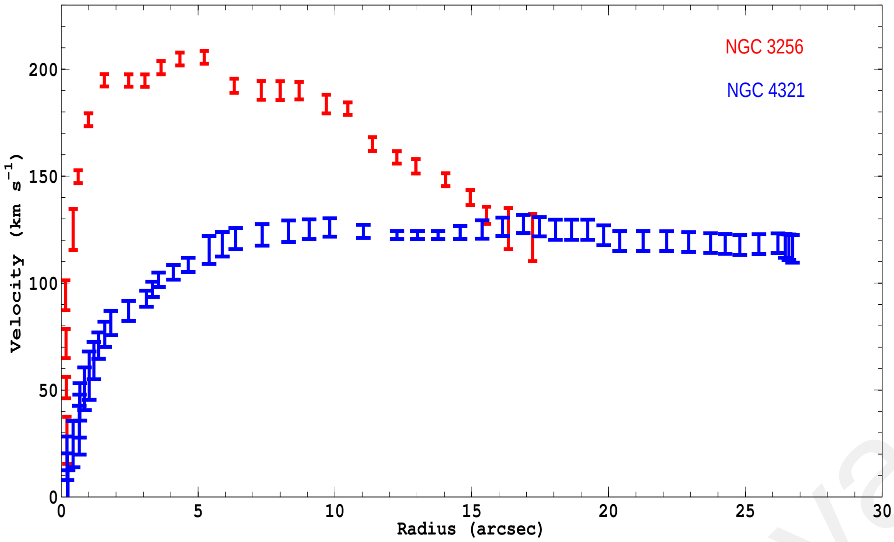

Figure 6.1: Projected rotation velocity of NGC 3256 (red) and NGC 4321 galaxy (blue).

Table 6.1: Properties of galaxies.

Parameter	NGC3256	NGC4321
Type	Sb(pec)	SAB(s)bc
Adopted Distance	16 Mpc	35 Mpc
Inclination	30°	30°
Projected rotation curve	184±5 km s^{-1}	125±4.63 km s^{-1}
Total mass	5.1±0.2 × 10^{10} $M_{\odot}$	1.02±0.04 × 10^{10} $M_{\odot}$
Molecular gas mass	1.51±0.34× 10^{9} $M_{\odot}$	9±0.13× 10^{8} $M_{\odot}$
Stellar mass	3.06±0.27× 10^{9} $M_{\odot}$	3.3±0.03× 10^{8} $M_{\odot}$

In order to obtain the stellar mass using the NIR data of 2MASS image at Ks band, the image profile I(R) first needs to be de-projected to obtain the luminosity density j(r) distribution of the galaxy. The de Vaucouleurs law and modified Hubble law are used to fit the central region of the galaxy. This study finds that the Ks image of NGC 3256 and NGC 4321 can be well fitted with a modified Hubble law (see Table 6.2). Hence, the obtained stellar mass was ~ (3.06±0.27)× 10^{9} $M_{\odot}$ and (3.3±0.03)× 10^{8} $M_{\odot}$ within the same assumed radius of NGC 3256 and NGC 4321, respectively. It is clear that the stellar and molecular gas masses are smaller than total mass of NGC 3256 and NGC 4321.

This work shows that within the central region of the galaxy, there is a significant amount of invisible mass, which cannot be explained by the molecular mass and the stellar mass within this region. This study suggests that there might be a significant amount of dark matter in the central region of the galaxy. This thesis also takes a look at a possible solution by introducing the "MOND theory". The central idea is that there exists a new fundamental constant of acceleration, a_0, below which the laws of inertia or of attraction takes on a specific non-Newtonian form. However, it is important to note that this missing mass problem cannot be explained with a traditional MOND theory because of the strong acceleration in the central region of the galaxy. Most observed phenomena at galaxy scales can usually be explained by the MOND theory very well. However, the findings pose here a significant challenge to the traditional MOND models.

To summarize this:

- There is vast amount of unseen mass ($4.38 \pm 0.53 \times 10^{10} M_{\odot}$) in the central region of NGC 3256. Most of the unseen mass should be the dark matter, therefore, the dark matter makes up about 75% of the dynamical mass at the radius of 1.7 kpc of this galaxy. The acceleration is about 2.45×10^{-7} cm s^{-2}, which is much larger than the critical acceleration, $a_0 \approx 1.2 \times 10^{-8}$ cm s^{-2} in the MOND theory.

- More than 80% of the dynamical mass within the central 0.7 kpc radius of NGC 4321 is provided by dark matter, which is about $8.5 \pm 0.2 \times 10^{9} M_{\odot}$. The acceleration (2.7 $\times 10^{-7}$ cm s^{-2}) at the central region of this galaxy is relatively high.

This thesis has managed to study and give an estimation to the dark matter mass in the central region of a galaxy, something that has not been done in any previous studies. It would be very interesting to see how this method could be applied to other galaxies as well. The new information about the dark matter study and theoretical understanding will enhance our understanding of the structure, origin, and evolution of the Universe as a whole.

Table 6.2: Modified Hubble fitting.

Galaxy	modified Hubble profile		χ^2_{red}
	$\mathbf{r_0}$	$\mathbf{I_0}$	
NGC 3256	2.44″	412.5 DN	≈1
NGC 4321	3.99″	270 DN	≈1

The results were obtained from observations, not from theoretical considerations as done in previous studies. Thus, in this section, the work in progress and also future works on dark matter searches will be covered. Currently, work is being done on other objects including spirals and other different morphologies.

In the future, it is proposed that:

- One possibility is that another alternative may be found to infer the existence of dark matter.
- The correlation between dark matter in the central region of galaxies with star formation rate in that region can be studied.
- Another possibility is to expand the study by looking for new data with ALMA observations to study dark matter.
- Looking for more modified theory of gravity that can explain dark matter in the central regions of galaxies.

REFERENCES

Aalto, S., Booth, R. S., Johansson, L. E. B., & Black, J. H. (1991). Peculiar molecular clouds in NGC 3256? *Astronomy & Astrophysics*, *247*, 291-302.

Agüero, E., & Lipari, S. (1991). Physical considerations of the nuclear region of NGC 3256. *Astrophysics & Space Science*, *175*(2), 253–260.

Aguirre, A., Schaye, J., & Quataert, E. (2001). Problems for modified newtonian dynamics in clusters and the Lyα forest? *The Astrophysical Journal*, *561*, 550-558.

ALMA Partnership, Fomalont, E. B., Vlahakis, C., Corder, S., Remijan, A., Barkats, D., ... Wood, S. J. (2015). The 2014 ALMA long baseline campaign: an overview. *The Astrophysical Journal, Letters*, *808*, L1.

Alonso-Herrero, A., Colina, L., Packham, C., Díaz-Santos, T., Rieke, G. H., Radomski, J. T., & Telesco, C. M. (2006). High spatial resolution T-ReCS mid-infrared imaging of luminous infrared galaxies. *The Astrophysical Journal, Letters*, *652*, L83-L87.

Alonso-Herrero, A., Pereira-Santaella, M., Rieke, G. H., Diamond-Stanic, A. M., Wang, Y., Hernán-Caballero, A., & Rigopoulou, D. (2013). Local luminous infrared galaxies. III. Co-evolution of black hole growth and star formation activity? *The Astrophysical Journal*, *765*, 78.

Alonso-Herrero, A., Pereira-Santaella, M., Rieke, G. H., & Rigopoulou, D. (2012). Local luminous infrared galaxies. II. Active galactic nucleus activity from spitzer/infrared spectrograph spectra. *The Astrophysical Journal*, *744*, 2.

Anderson, R. W. (2015). *The cosmic compendium: black holes*. North Carolina: Lulu Press.

Athanassoula, E. (2004). Bars and the connection between dark and visible matter. In *Symposium-international astronomical union* (pp. 255–264). San Francisco: Astronomical Society of the Pacific.

Athanassoula, E., Bosma, A., & Papaioannou, S. (1987). Halo parameters of spiral galaxies. *Astronomy & Astrophysics*, *179*, 23-40.

Baan, W. A., Henkel, C., Loenen, A. F., Baudry, A., & Wiklind, T. (2008). Dense gas in luminous infrared galaxies. *Astronomy & Astrophysics*, *477*, 747-762.

Babcock, H. W. (1939). The rotation of the Andromeda nebula. *Lick Observatory Bulletin*, *19*, 41-51.

Bartelmann, M., & Schneider, P. (2001). Weak gravitational lensing. *Physics Reports*, *340*, 291-472.

Bauer, D., Buckley, J., Cahill-Rowley, M., Cotta, R., Drlica-Wagner, A., Feng, J. L., . . . Wood, M. (2015). Dark matter in the coming decade: complementary paths to discovery and beyond. *Physics of the Dark Universe*, *7*, 16-23.

Bekenstein, J., & Milgrom, M. (1984). Does the missing mass problem signal the breakdown of Newtonian gravity? *Astrophysical Journal*, *286*, 7-14.

Bell, E. F., McIntosh, D. H., Katz, N., & Weinberg, M. D. (2003). The optical and near-infrared properties of galaxies. I. Luminosity and stellar mass functions. *The Astrophysical Journal, Supplement*, *149*, 289-312.

Bennett, J. O., Donahue, M., Schneider, N., & Voit, M. (2014). *The cosmic perspective*. New York: Pearson.

Bergvall, N., Laurikainen, E., & Aalto, S. (2003). Galaxy interactions–poor starburst triggers-III. a study of a complete sample of interacting galaxies. *Astronomy & Astrophysics*, *405*(1), 31–52.

Bevington, P. R., Robinson, D. K., Blair, J. M., Mallinckrodt, A. J., & McKay, S. (1993). Data reduction and error analysis for the physical sciences. *Computers in Physics*, *7*(4), 415–416.

Binney, J., & Merrifield, M. (1998). *Galactic astronomy*. Princeton: Princeton University Press.

Binney, J., & Tremaine, S. (1998). *Galactic dynamics (2nd ed.)*. Princeton: Princeton University Press.

Bolatto, A. D., Wolfire, M., & Leroy, A. K. (2013). The CO-to-H_2 conversion factor.

Annual Review of Astronomy & Astrophysics, *51*, 207-268.

Borne, K., Bushouse, H., Colina, L., Lucas, R., Baker, A., Clements, D., . . . Rowan-Robinson, M. (1999). A morphological classification scheme for ULIRGs. *Astrophysics and Space Science*, *266*(1), 137–142.

Borriello, A., & Salucci, P. (2001). The dark matter distribution in disc galaxies. *Monthly Notices of the Royal Astronomical Society*, *323*(2), 285–292.

Bosma, A. (1981a). 21-cm line studies of spiral galaxies. II. The distribution and kinematics of neutral hydrogen in spiral galaxies of various morphological types. *The Astronomical Journal*, *86*, 1825-1846.

Bosma, A. (1981b). 21-cm line studies of spiral galaxies. I-Observations of the galaxies NGC 5033, 3198, 5055, 2841, and 7331. II-The distribution and kinematics of neutral hydrogen in spiral galaxies of various morphological types. *The Astronomical Journal*, *86*, 1791–1846.

Bottema, R., Pestaña, J. L. G., Rothberg, B., & Sanders, R. H. (2002). MOND rotation curves for spiral galaxies with Cepheid-based distances. *Astronomy & Astrophysics*, *393*, 453-460.

Breddels, M. A., & Helmi, A. (2013). Model comparison of the dark matter profiles of fornax, sculptor, carina and sextans. *Astronomy & Astrophysics*, *558*, A35.

Burkert, A. (1995). The structure of dark matter halos in dwarf galaxies. *The Astrophysical Journal, Letters*, *447*(1), L25.

Carignan, C. (1985, May). Surface photometry of the sculptor group galaxies - NGC 7793, NGC 247, and NGC 300. *The Astrophysical Journal, Supplement*, *58*, 107-124.

Carroll, B. W., & Ostlie, D. A. (2007). *An introduction to modern galactic astrophysics and cosmology (2nd ed.).* San Francisco: Pearson Addison Education.

Castillo-Morales, A., Jiménez-Vicente, J., Mediavilla, E., & Battaner, E. (2007). Non-circular motion evidence in the circumnuclear region of M100 (NGC 4321). *Monthly Notices of the Royal Astronomical Society*, *380*(2), 489–498.

Cattaneo, A., Salucci, P., & Papastergis, E. (2014). Galaxy luminosity function and Tully-Fisher relation: reconciled through rotation-curve studies. *The Astrophysical Journal*, *783*, 66.

Chang, Z., Li, M.-H., Li, X., Lin, H.-N., & Wang, S. (2013). Effects of spacetime anisotropy on the galaxy rotation curves. *The European Physical Journal C*, *73*(5), 2447.

Clowe, D., Bradač, M., Gonzalez, A. H., Markevitch, M., Randall, S. W., Jones, C., & Zaritsky, D. (2006). A direct empirical proof of the existence of dark matter. *Astrophysical Journal Letters*, *648*(2), L109.

Cohen, M., Wheaton, W. A., & Megeath, S. (2003). Spectral irradiance calibration in the infrared. XIV. The absolute calibration of 2MASS. *Astronomical Journal*, *126*(2), 1090.

Colless, M., & Dunn, A. M. (1996). Structure and dynamics of the coma cluster. *The Astrophysical Journal*, *458*, 435.

Condon, J. J., Huang, Z.-P., Yin, Q. F., & Thuan, T. X. (1991). Compact starbursts in ultraluminous infrared galaxies. *The Astronomical Journal*, *378*, 65-76.

Cowsik, R., & McClelland, J. (1973). Gravity of neutrinos of nonzero mass in astrophysics. *Astrophysical Journal*, *180*, 7–10.

Davies, J. I., De Blok, W., Smith, R., Kambas, A., Sabatini, S., Linder, S. M., & Salehi-Reyhani, S. (2001). Gas-rich galaxies and the HI mass function. *Monthly Notices of the Royal Astronomical Society*, *328*(4), 1151–1160.

De Blok, W., & Bosma, A. (2002). High-resolution rotation curves of low surface brightness galaxies. *Astronomy & Astrophysics*, *385*(3), 816–846.

De Blok, W., & McGaugh, S. (1998). Testing modified newtonian dynamics with low surface brightness galaxies: rotation curve fits. *The Astrophysical Journal*, *508*(1), 132.

Dekel, A., & Shlosman, I. (1983). Galactic warps in tilted halos. In *Symposium-international astronomical union* (p. 187). Dordrecht: Springer.

De Naray, R. K., McGaugh, S. S., & De Blok, W. (2008). Mass models for low surface brightness galaxies with high-resolution optical velocity fields. *Astrophysical Journal*, *676*(2), 920.

de Vaucouleurs, G., de Vaucouleurs, A., & Corwin, J. (1976). *Second reference catalogue of bright galaxies*. Austin: University of Texas Press.

Distefano, A., Rampazzo, R., Chincarini, G., & De Souza, R. (1990). Optical studies of galaxies in clusters. II-Observations of spirals in Virgo. *The Astrophysical Journal, Supplement*, *86*, 7–43.

Dodelson, S., Gates, E. I., & Turner, M. S. (1996). Cold dark matter. *Science*, *274*, 69-75.

Domingue, D. L., Xu, C., Jarrett, T., & Cheng, Y. (2009). 2MASS/SDSS close major-merger galaxy pairs: luminosity functions and merger mass dependence. *The Astrophysical Journal*, *695*(2), 1559.

Drexler, J. (2006). *Comprehending and decoding the cosmos: discovering solutions to over a dozen cosmic mysteries by utilizing dark matter relationism, cosmology, and astrophysics*. Florida: Universal-Publishers.

Einasto, J., Kaasik, A., & Saar, E. (1974). Dynamic evidence on massive coronas of galaxies. *Nature*, *250*, 309-310.

Ellis, J. (2003). Dark matter and dark energy: summary and future directions. *Philosophical Transactions of the Royal Society of London Series A*, *361*, 2607-2627.

Elmegreen, D. M., Elmegreen, B. G., Kaufman, M., Sheth, K., Struck, C., Thomasson, M., & Brinks, E. (2006). Spitzer space telescope irac and mips observations of the interacting galaxies IC 2163 and NGC 2207: clumpy emission. *The Astrophysical Journal*, *642*(1), 158.

English, J., Norris, R. P., Freeman, K. C., & Booth, R. S. (2003). NGC 3256: Kinematic anatomy of a merger. *The Astronomical Journal*, *125*(3), 1134.

Erroz-Ferrer, S., Knapen, J. H., Leaman, R., Cisternas, M., Font, J., Beckman, J. E., . . . Bosma, A. (2015). Hα kinematics of *S4G* spiral galaxies–II. Data description and non-circular motions. *Monthly Notices of the Royal Astronomical Society*, *451*(1), 1004–1024.

Faber, S. M., & Gallagher, J. S. (1979). Masses and mass-to-light ratios of galaxies. *Annual Review of Astronomy & Astrophysics*, *17*, 135-187.

Faber, S. M., & Lin, D. N. C. (1983). Is there nonluminous matter in dwarf spheroidal galaxies. *Astrophysical Journal, Letters*, *266*, L17-L20.

Ferrarese, L., Freedman, W. L., Hill, R. J., Saha, A., Madore, B. F., Kennicutt Jr, R. C., . . . Hoessel, J. G. (1996). The extragalactic distance scale key project. IV. the discovery of cepheids and a new distance to M100 using the hubble space telescope. *The Astrophysical Journal*, *464*, 568.

Field, G. B. (1972). Intergalactic matter. *Annual Review of Astronomy and Astrophysics*, *10*, 227.

Finlator, K., Ivezić, Ž., Fan, X., Strauss, M. A., Knapp, G. R., Lupton, R. H., . . . Csabai, I. (2000). Optical and infrared colors of stars observed by the two micron all sky survey and the sloan digital sky survey. *The Astrophysical Journal*, *120*(5), 2615.

Fraser, H. J., McCoustra, M. R., & Williams, D. A. (2002). The molecular universe. *Astronomy & Geophysics*, *43*(2), 2–10.

Freeman, K. C. (1970). On the disks of spiral and so galaxies. *Astrophysical Journal*, *160*, 811.

Gan, Z.-M., Wang, D.-X., & Lei, W.-H. (2009). A model of magnetically induced disc–corona for black hole binaries. *Monthly Notices of the Royal Astronomical Society*, *394*(4), 2310–2320.

García-Burillo, S., Combes, F., Schinnerer, E., Boone, F., & Hunt, L. (2005). Molecular gas in nuclei of galaxies (NUGA)-IV. Gravitational torques and AGN feeding. *Astronomy & Astrophysics*, *441*(3), 1011–1030.

Garcıa-Burillo, S., Sempere, M., Combes, F., & Neri, R. (1998). Molecular gas in the barred spiral M100. *Astronomy & Astrophysics*, *333*, 864–876.

Gentile, G. (2008). Mond and the universal rotation curve: similar phenomenologies. *The Astronomical Journal*, *684*(2), 1018.

Gentile, G., Burkert, A., Salucci, P., Klein, U., & Walter, F. (2005). The dwarf galaxy ddo 47 as a dark matter laboratory: testing cusps hiding in triaxial halos. *The Astrophysical Journal Letters*, *634*(2), L145.

Gentile, G., Salucci, P., Klein, U., Vergani, D., & Kalberla, P. (2004). The cored distribution of dark matter in spiral galaxies. *Monthly Notices of the Royal Astronomical Society*, *351*(3), 903–922.

Gültekin, K., Richstone, D. O., Gebhardt, K., Lauer, T. R., Tremaine, S., Aller, M., . . . Filippenko, A. V. (2009). The M-σ and $M - L$ relations in galactic bulges, and determinations of their intrinsic scatter. *Astrophysical Journal*, *698*(1), 198.

Harvey, D., Massey, R., Kitching, T., Taylor, A., & Tittley, E. (2015). The nongravitational interactions of dark matter in colliding galaxy clusters. *Science*, *347*, 1462-1465.

Hashim, N., Abidin, Z., Ibrahim, U., Hassan, M., Hamidi, Z., Umar, R., & Ibrahim, Z. (2015). The nonlinear least square fitting for rotation curve of orion dwarf spiral. *Sains Malaysiana*, *44*(3), 457–462.

Hernandez, O., Carignan, C., Amram, P., Chemin, L., & Daigle, O. (2005, July). BHαBAR: big Hα kinematical sample of barred spiral galaxies - I. fabry-perot observations of 21 galaxies. *Monthly Notices of the Royal Astronomical Society*, *360*, 1201-1230.

Hinz, J. L., & Rieke, G. H. (2006). Dynamical masses in luminous infrared galaxies. *The Astrophysical Journal*, *646*(2), 872.

Ho, L., & Chakrabarti, S. (1999). Observational evidence for black holes in the universe. *Astrophysics and Space Science Library*, *157*, 234.

Ho, L., Filippenko, A. V., & Sargent, S. W. L. (1997). A search for dwarf seyfert nuclei. III. Spectroscopic parameters and properties of the host galaxies. *Astrophysical Journal Supplement Series*, *112*(2), 315.

Hubble, E. (1926). Extragalactic nebulae. *Astrophysical Journal*, *64*, 321-369.

Hubble, E. (1936). *Realm of the nebulae*. New Haven: Yale University Press.

Hughes, I., & Hase, T. (2010). *Measurements and their uncertainties: a practical guide to* *modern error analysis*. New York: Oxford University Press.

Iocco, F., Pato, M., & Bertone, G. (2015). Evidence for dark matter in the inner Milky Way. *Nature Physics*, *11*(3), 245–248.

Israel, F. (2008). Physical conditions of molecular gas in spiral galaxy centers. *Memorie della Societa Astronomica Italiana*, *79*, 1136.

Jarrett, T. H., Chester, T., Cutri, R., Schneider, S., Skrutskie, M., & Huchra, J. P. (2000b). 2MASS extended source catalog: overview and algorithms. *The Astronomical Journal*, *119*, 2498-2531.

Johnson, H. L. (1966). Astronomical measurements in the infrared. *Annual Review of Astronomy & Astrophysics*, *4*, 193.

Kahn, F., & Woltjer, L. (1959). Intergalactic matter and the galaxy. *Astrophysical Journal*, *130*, 705.

Kalinova Dimitrova, V. (2014). *Dark matter indirect detection and subhalosmass distributions of galaxies from sauron and califa stellar kinematic maps* (Doctoral dissertation). University of Heidelberg, Heidelberg, Germany.

Kapteyn, J. C. (1922). First attempt at a theory of the arrangement and motion of the sidereal system. *The Astrophysical Journal*, *55*, 302.

Karachentsev, I. (1966). The virial mass-luminosity ratio and the instability of different galactic systems. *Astrophysics*, *2*(1), 39–49.

Kent, S. M. (1986). Dark matter in spiral galaxies. I-Galaxies with optical rotation curves. *Astronomical Journal*, *91*, 1301–1327.

Kent, S. M. (1990). Dark matter in elliptical galaxies. In *Evolution of the universe of galaxies* (Vol. 10, p. 109-118). San Francisco: Astronomical Society of the Pacific.

Khachikian, E. Y., & Weedman, D. W. (1974). An atlas of seyfert galaxies. *The Astrophysical Journal*, *192*, 581–589.

Kim, D.-C., Sanders, D. B., Veilleux, S., Mazzarella, J. M., & Soifer, B. T. (1995). Optical spectroscopy of luminous infrared galaxies. I. Nuclear data. *The Astrophysical Journal, Supplement*, *98*, 129.

Kim, D.-C., Veilleux, S., & Sanders, D. B. (2002). Optical and near-infrared imaging of the IRAS 1 Jy sample of ultraluminous infrared galaxies. I. The atlas. *The Astrophysical Journal, Supplement*, *143*, 277-314.

King, I. R. (1966). The structure of star clusters. III. Some simple dynamical models. *The Astrophysical Journal*, *71*, 64.

Knapen, J. (1998). Statistical properties of HII regions in the disc of M100. *Monthly Notices of the Royal Astronomical Society*, *297*(1), 255–264.

Knapen, J., Shlosman, I., Rand, R., Beckman, J., Nadeau, D., & Doyon, R. (1997). Circumnuclear starbursts in barred galaxies. In *The impact of large scale near-IR sky surveys* (pp. 253–256). Dordrecht: Springer.

Kochanek, C., White, M., Huchra, J., Macri, L., Jarrett, T., Schneider, S., & Mader, J. (2003). Clusters of galaxies in the local universe. *The Astrophysical Journal*, *585*(1), 161.

Kochanek, C. S., Pahre, M. A., Falco, E. E., Huchra, J. P., Mader, J., Jarrett, T. H., ... Schneider, S. E. (2001). The K-band galaxy luminosity function. *The Astrophysical Journal*, *560*, 566-579.

Koda, J., Sofue, Y., Kohno, K., Nakanishi, H., Onodera, S., Okumura, S. K., & Irwin, J. A. (2002). Nobeyama millimeter array CO (J=1-0) observations of the Hα/radio lobe galaxy NGC 3079: gas dynamics in a weak bar potential and central massive core. *The Astrophysical Journal*, *573*, 105-121.

Lequeux, J. (1983). Rotation curves and masses of galaxies. *Astronomy and Astrophysics*, *125*, 394.

Lira, P., Gonzalez-Corvalan, V., Ward, M., & Hoyer, S. (2008). An infrared study of the double nucleus in NGC 3256. *Monthly Notices of the Royal Astronomical Society*, *384*(1), 316–322.

Lira, P., Ward, M., Zezas, A., Alonso-Herrero, A., & Ueno, S. (2002). Chandra observations of the luminous infrared galaxy NGC 3256. *Monthly Notices of the Royal Astronomical Society*, *330*, 259-278.

Liu, L., Gao, Y., & Greve, T. R. (2015). The global star formation laws of galaxies from a radio continuum perspective. *Astrophysical Journal*, *805*(1), 31.

Macchetto, F. D. (2000). Supermassive black holes and galaxy morphology. In *Toward a new millennium in galaxy morphology* (pp. 269–291). Dordrecht: Springer.

Mackie, G. (2011). *The multiwavelength atlas of galaxies*. New York: Cambridge University Press.

Magorrian, J., Tremaine, S., Richstone, D., Bender, R., Bower, G., Dressler, A., ... Grillmair, C. (1998). The demography of massive dark objects in galaxy centers. *Astrophysical Journal*, *115*(6), 2285.

Mampaso, A., Prieto, M., & Sánchez, F. (2004). *Infrared astronomy (1st ed.)*. Cambridge: Cambridge University Press.

Martig, M., & Bournaud, F. (2008). Triggering of merger-induced starbursts by the tidal field of galaxy groups and clusters. *Monthly Notices of the Royal Astronomical Society*, *385*, L38-L42.

Mashian, N., Sternberg, A., & Loeb, A. (2013). The ratio of CO to total gas mass in high-redshift galaxies. *Monthly Notices of the Royal Astronomical Society*, *435*(3), 2407–2415.

Mateo, M. L. (1998). Dwarf galaxies of the local group. *Annual Review of Astronomy & Astrophysics*, *36*, 435-506.

Merloni, A., Heinz, S., & di Matteo, T. (2003). A fundamental plane of black hole activity. *Monthly Notices of the Royal Astronomical Society*, *345*, 1057-1076.

Milgrom, M. (1983a). A modification of the newtonian dynamics as a possible alternative to the hidden mass hypothesis. *Astrophysical Journal*, *270*, 365-370.

Milgrom, M. (1983b). A modification of the newtonian dynamics - implications for galaxies. *Astrophysical Journal*, *270*, 371-389.

Milgrom, M. (1983c). A modification of the newtonian dynamics - implications for galaxy systems. *The Astrophysical Journal*, *270*, 384.

Milgrom, M. (1998). Galaxy groups and modified dynamics. *The Astrophysical Journal, Letters*, *496*, L89-L91.

Mineo, S., Gilfanov, M., & Sunyaev, R. (2012). X-ray emission from star-forming galaxies - I. High-mass X-ray binaries. *Monthly Notices of the Royal Astronomical Society*, *419*, 2095-2115.

Moorwood, A. F. M., & Oliva, E. (1994). Extended infrared line emission excited by starburst and Seyfert activity in NGC 3256 and NGC 4945. *The Astrophysical Journal*, *429*, 602-611.

Mulroy, S. L., Smith, G. P., Haines, C. P., Marrone, D. P., Okabe, N., Pereira, M. J., … Martino, R. (2014). LoCuSS: the near-infrared luminosity and weak-lensing mass scaling relation of galaxy clusters. *Monthly Notices of the Royal Astronomical Society*, *443*, 3309-3317.

Muñoz-Mateos, J., de Paz, A. G., Boissier, S., Zamorano, J., Dale, D., Pérez-González, P. G., … Thornley, M. (2009). Radial distribution of stars, gas, and dust in sings galaxies. ii. derived dust properties. *The Astrophysical Journal*, *701*(2), 1965.

Napier, W. M., & Guthrie, B. (1975). Black dwarf stars as missing mass in clusters of galaxies. *Monthly Notices of the Royal Astronomical Society*, *170*(1), 7–14.

Navarro, J. F., Frenk, C. S., & White, S. D. (1997). A universal density profile from hierarchical clustering. *The Astrophysical Journal*, *490*(2), 493.

Navarro, J. F., Hayashi, E., Power, C., Jenkins, A., Frenk, C. S., White, S. D., … Quinn, T. R. (2004). The inner structure of ΛCDM haloes–III. universality and asymptotic slopes. *Monthly Notices of the Royal Astronomical Society*, *349*(3), 1039–1051.

Neff, S. G., Ulvestad, J. S., & Campion, S. D. (2003). Radio emission associated with ultraluminous x-ray sources in the galaxy merger NGC 3256. *The Astrophysical Journal*, *599*, 1043-1048.

Neugebauer, G., Habing, H., Van Duinen, R., Aumann, H., Baud, B., Beichman, C., … De Jong, T. (1984). The infrared astronomical satellite (IRAS) mission.

Astrophysical Journal, *278*, L1–L6.

Noordermeer, E. (2006). *The distribution of gas, stars and dark matter in early-type disk galaxies* (Doctoral dissertation). University of Groningen, Groningen, Netherlands.

Nordgren, T. E., Chengalur, J. N., Salpeter, E., & Terzian, Y. (1998). Very wide galaxy pairs of the northern and southern sky. *The Astrophysical Journal Supplement Series*, *115*(1), 43.

Norris, R. P., & Forbes, D. A. (1995). Radio detection of a double nucleus in the merging galaxy NGC 3256. *The Astrophysical Journal*, *446*, 594.

Oh, S.-H., De Blok, W., Walter, F., Brinks, E., & Kennicutt Jr, R. C. (2008). High-resolution dark matter density profiles of things dwarf galaxies: correcting for noncircular motions. *The Astronomical Journal*, *136*(6), 2761.

Oh, S.-H., Hunter, D. A., Brinks, E., Elmegreen, B. G., Schruba, A., Walter, F., ... Johnson, M. C. (2015). High-resolution mass models of dwarf galaxies from little things. *Astronomical Journal*, *149*(6), 180.

Oort, J. H. (1932). The force exerted by the stellar system in the direction perpendicular to the galactic plane and some related problems. *Bulletin of the Astronomical Institutes of the Netherlands*, *6*, 249.

Oort, J. H. (1940). Some Problems concerning the structure and dynamics of the galactic system and the elliptical nebulae NGC3115 and 4494. *Astrophysical Journal*, *91*, 273.

Ostriker, J. P. (1999). Discovery of" dark matter" in clusters of galaxies. *Astrophysical Journal*, *525*, 297.

Ostriker, J. P., & Peebles, P. J. (1973). A numerical study of the stability of flattened galaxies: or, can cold galaxies survive? *Astrophysical Journal*, *186*, 467–480.

Palunas, P., & Williams, T. (2000). Maximum disk mass models for spiral galaxies. *Astronomical Journal*, *120*(6), 2884.

Perley, R., Napier, P., Jackson, J., Butler, B., Carlson, B., Fort, D., ... Durand, S. (2009).

The expanded very large array. *Proceedings of the Institute of Electrical and Electronics Engineers*, *97*(8), 1448–1462.

Pogge, R. W. (1989a). Ionized gas in the nuclear regions of nearby non-seyfert spiral galaxies. *The Astrophysical Journal, Supplement*, *71*, 433–453.

Pogge, R. W. (1989b). Ionized gas in the nuclear regions of nearby non-seyfert spiral galaxies. *Astrophysical Journal Supplement Series*, *71*, 433–453.

Primack, J. R., & Gross, M. A. (2001). Hot dark matter in cosmology. In *Current aspects of neutrino physics* (pp. 287–308). Berlin: Springer.

Rahmani, S., Lianou, S., & Barmby, P. (2016). Star formation laws in the andromeda galaxy: gas, stars, metals and the surface density of star formation. *Monthly Notices of the Royal Astronomical Society*, *456*(4), 4128–4144.

Randriamampandry, T. H., & Carignan, C. (2014). Galaxy mass models: mond versus dark matter haloes. *Monthly Notices of the Royal Astronomical Society*, *439*(2), 2132–2145.

Reiprich, T. H. (2006). The galaxy cluster X-ray luminosity-gravitational mass relation in the light of the WMAP 3rd year data. *Astronomy & Astrophysics*, *453*, L39-L42.

Riffel, R. A., Ho, L. C., Mason, R., Rodríguez-Ardila, A., Martins, L., Riffel, R., . . . Perlman, E. (2015). Differences between CO- and calcium triplet-derived velocity dispersions in spiral galaxies: evidence for central star formation? *Monthly Notices of the Royal Astronomical Society*, *446*, 2823-2836.

Roberts, M. S. (1966). A high-resolution 21-cm hydrogen-line survey of the andromeda nebula. *Astrophysical Journal*, *144*, 639.

Roberts, M. S., & Whitehurst, R. N. (1975). The rotation curve and geometry of M31 at large galactocentric distances. *Publications of the Astronomical Society of Japan*, *201*, 327-346.

Roy, A. L., Goss, W. M., Mohan, N. R., & Anantharamaiah, K. R. (2005). Radio recombination lines from the starburst galaxy NGC 3256. *Astronomy & Astrophysics*, *435*, 831-837.

Rubin, V. C., & Ford, W. K., Jr. (1970). Rotation of the Andromeda nebula from a spectroscopic survey of emission regions. *Astronomical Journal*, *159*, 379.

Rubin, V. C., Ford, W. K. J., & . Thonnard, N. (1980). Rotational properties of 21 SC galaxies with a large range of luminosities and radii, from NGC 4605 /R = 4kpc/ to UGC 2885 /R = 122 kpc/. *The Astrophysical Journal*, *238*, 471-487.

Rubin, V. C., Thonnard, N., & Ford Jr, W. (1978). Extended rotation curves of high-luminosity spiral galaxies. IV-systematic dynamical properties, SA through SC. *Astrophysical Journal*, *225*, L107–L111.

Saburova, A., Bizyaev, D., & Zasov, A. (2011). Do disk galaxies with abnormally low mass-to-light ratios exist? *Astronomy letters*, *37*(11), 751–765.

Sakamoto, K., Aalto, S., Combes, F., Evans, A., & Peck, A. (2014). An infrared-luminous merger with two bipolar molecular outflows: ALMA and SMA observations of NGC 3256. *The Astrophysical Journal*, *797*, 90.

Sakamoto, K., Ho, P. T. P., & Peck, A. B. (2006). Imaging molecular gas in the luminous merger NGC 3256: detection of high-velocity gas and twin gas peaks in the double nucleus. *Astrophysical Journal*, *644*, 862-878.

Sánchez-Blázquez, P., Forbes, D. A., Strader, J., Brodie, J., & Proctor, R. (2007). Spatially resolved spectroscopy of early-type galaxies over a range in mass. *Monthly Notices of the Royal Astronomical Society*, *377*(2), 759–786.

Sandage, A., & Bedke, J. (1994). The carnegie atlas of galaxies. *Carnegie Institution of Washington publication*, *1*, 638.

Sanders, D., & Mirabel, I. (1996). Luminous infrared galaxies. *Annual Review of Astronomy and Astrophysics*, *34*(1), 749–792.

Sanders, D. B., Soifer, B. T., Elias, J. H., Neugebauer, G., & Matthews, K. (1988). Warm ultraluminous galaxies in the IRAS survey - The transition from galaxy to quasar? *Astrophysical Journal, Letters*, *328*, L35-L39.

Sanders, R. (2003). Clusters of galaxies with modified newtonian dynamics. *Monthly Notices of the Royal Astronomical Society*, *342*(3), 901–908.

Sanders, R., & Noordermeer, E. (2007). Confrontation of modified newtonian dynamics with the rotation curves of early-type disc galaxies. *Monthly Notices of the Royal Astronomical Society*, *379*(2), 702–710.

Sanders, R. H., & McGaugh, S. S. (2002). Modified newtonian dynamics as an alternative to dark matter. *Annual Review of Astron and Astrophys*, *40*, 263-317.

Sargent, A. I., Sanders, D. B., & Phillips, T. G. (1989). CO(2-1) emission from the interacting galaxy pair NGC 3256. *The Astrophysical Journal, Letters*, *346*, L9-L11.

Sarzi, M., Rix, H.-W., Shields, J. C., McIntosh, D. H., Ho, L. C., Rudnick, G., . . . Barth, A. J. (2002). Limits on the mass of the central black hole in 16 nearby bulges. *The Astrophysical Journal*, *567*, 237-246.

Scarpa, R., Almeida, J. B., & Lerner, E. J. (2006). Modified newtonian dynamics, an introductory review. In *First Crisis in Cosmology Conference* (pp. 253–265). New York: American Institute of Physics.

Schneider, P. (2014). *Extragalactic astronomy and cosmology: an introduction (2nd ed.)*. New York: Springer.

Schombert, J., & Smith, A. K. (2012). The structure of galaxies I: Surface photometry techniques. *Publications of the Astronomical Society of Australia*, *29*, 174-192.

Scoville, N., & Sanders, D. (1987). H_2 in the galaxy. In *Interstellar processes* (pp. 21–50). Netherlands: Springer.

Sérsic, J., & Pastoriza, M. (1967). Properties of galaxies with peculiar nuclei. *Publications of the Astronomical Society of the Pacific*, *79*(467), 152–155.

Seyfert, C. K. (1943). Nuclear emission in spiral nebulae. *The Astrophysical Journal*, *97*, 28.

Shakura, N. I., & Sunyaev, R. A. (1973). Black holes in binary systems. observational appearance. *Astronomy and Astrophysics*, *24*, 337–355.

Shapley, H. (1943). *Galaxies (1st ed.)*. Harvard: Blakiston Company.

Simien, F., & De Vaucouleurs, G. (1986). Systematics of bulge-to-disk ratios. *Astrophysical Journal*, *302*, 564–578.

Singh, R. A. (2015). *The true nature of LINER galaxies, weak AGN or strong stars* (Doctoral dissertation). University of Heidelberg, Heidelberg, Germany.

Skrutskie, M. F., Cutri, R. M., Stiening, R., Weinberg, M. D., Schneider, S., Carpenter, J. M., . . . Wheelock, S. (2006). The two micron all sky survey (2MASS). *The Astronomical Journal*, *131*, 1163-1183.

Sofue, Y. (1996). The most completely sampled rotation curves for galaxies. *Astrophysical Journal*, *458*, 120.

Sofue, Y. (2001). Central rotation curves of galaxies. In *Galaxy disks and disk galaxies* (pp. 263–266). San Francisco: Astronomical Society of the Pacific Conference Series.

Solomon, P., Downes, D., Radford, S., & Barrett, J. (1997). The molecular interstellar medium in ultraluminous infrared galaxies. *The Astrophysical Journal*, *478*(1), 144.

Sørensen, S., & Pontoppidan, K. (2010). Analysis of the alma telescope and front-ends. In *Twenty-first international symposium on space terahertz technology* (pp. 121–127). Oxford: National Radio Astronomy Observatory.

Springel, V., White, S. D., Jenkins, A., Frenk, C. S., Yoshida, N., Gao, L., . . . Helly, J. (2005). Simulations of the formation, evolution and clustering of galaxies and quasars. *Nature*, *435*(7042), 629–636.

Swaters, R. A., Madore, B. F., van den Bosch, F. C., & Balcells, M. (2003). The central mass distribution in dwarf and low surface brightness galaxies. *The Astronomical Journal*, *583*, 732-751.

Tan, A., Xiao, M., Cui, X., Chen, X., Chen, Y., Fang, D., . . . Gong, H. (2016). Dark matter results from first 98.7 days of data from the PandaX-II experiment. *Physical Review Letters*, *117*(12), 121303.

Thorstensen, J. R., & Partridge, R. (1975). Can collapsed stars close the universe. *Astrophysical Journal*, *200*, 527–534.

Tian, Y., & Ko, C.-M. (2016). Dynamics of elliptical galaxies with planetary nebulae in modified newtonian dynamics. *Monthly Notices of the Royal Astronomical Society*, *462*(1), 1092–1100.

Tsai, A.-L., Matsushita, S., Nakanishi, K., Kohno, K., Kawabe, R., Inui, T., . . . Tarchi, A. (2009). Molecular superbubbles and outflows from the starburst galaxy NGC 2146. *Publications of the Astronomical Society of Japan*, *61*, 237-250.

Urry, C. M., & Padovani, P. (1995). Unified schemes for radio-loud active galactic nuclei. *Publications of the Astronomical Society of the Pacific*, 803–845.

van den Bosch, F. C., & Dalcanton, J. J. (2000). Semianalytical models for the formation of disk Galaxies. II. Dark matter versus modified newtonian dynamics. *The Astrophysical Journal*, *534*, 146-164.

Wada, K., Sakamoto, K., & Minezaki, T. (1998). Numerical modeling for the gaseous and stellar structure of the central region of NGC 4321. *Astrophysical Journal*, *494*(1), 236.

Wandel, A. (2002). Black holes of active and quiescent galaxies. I. The black hole-bulge relation revisited. *Astrophysical Journal*, *565*(2), 762.

Werner, M., Roellig, T., Low, F., Rieke, G., Rieke, M., Hoffmann, W., . . . Fazio, G. (2004). The spitzer space telescope mission. *The Astrophysical Journal Supplement Series*, *154*(1), 1.

White, S. D., & Rees, M. (1978). Core condensation in heavy halos: a two-stage theory for galaxy formation and clustering. *Monthly Notices of the Royal Astronomical Society*, *183*(3), 341–358.

Wu, X.-B., & Han, J. (2001). On black hole masses, radio-loudness and bulge luminosities of seyfert galaxies. *Astronomy & Astrophysics*, *380*(1), 31–39.

Xie, F.-G., & Yuan, F. (2008). The influences of outflow on the dynamics of inflow. *Astrophysical Journal*, *681*(1), 499.

Zhang, Z., Gilfanov, M., & Bogdán, Á. (2012). Dependence of the low-mass X-ray binary population on stellar age. *Astronomy & Astrophysics*, *546*, A36.

Zwicky, F. (1933). Die rotverschiebung von extragalaktischen nebeln. *Helvetica Physica Acta*, *6*, 110–127.

LIST OF PUBLICATIONS AND PAPERS PRESENTED

1. **Ali, I. A. M.**, Abidin, Z. Z., & Hwang, C.-Y. (2015). Physical properties of NGC 3256 in radio and infrared domain. In *Space Science and Communication (IconSpace) International Conference* (pp. 306–309). Langkawi, Malysia.

2. **Ali, I. A. M.**, Abidin, Z. Z., & Hwang, C.-Y. (2016). Dynamical mass of merger galaxy by radio observations. In *Proceeding of the 2016 National Physics Conference (PERFIK 2016).* Pullman Kuala Lumpur Bangsar, Kuala Lumpur, Malaysia.

3. **Ali, I. A. M.**, Hashim, N., & Abidin, Z. Z. (2017). The dark matter distribution of NGC 5921. *Indian Journal of Physics*, 1–7. doi: https://doi.org/10.1007/s12648-017-1119-7.

4. **Ali, I. A. M.**, Hwang, C.-Y., & Abidin, Z. Z. (2017). Dark matter in the central region of the late-type galaxies. In *Asia-Pacific Regional IAU Meeting (APRIM 2017).* Taipei, Taiwan, Oral presentation.

5. **Ali, I. A. M.**, Hwang, C.-Y., & Abidin, Z. Z. (2017). Observations in radio astronomy. In *2nd National School on Space and Earth Electromagnetism (2nd NSoSEE2017).* UITM, Pasir Gudang, Johor, Malaysia, Poster presentation.